Recovery of base metals from a sulphate-based bioleach solution using commercially available chelating ion exchange resins and adsorbents

by

Cornelius Johannes Liebenberg

Thesis presented in partial fulfillment
of the requirements for the Degree

of

MASTER OF SCIENCE IN ENGINEERING
(EXTRACTIVE METALLURGICAL ENGINEERING)

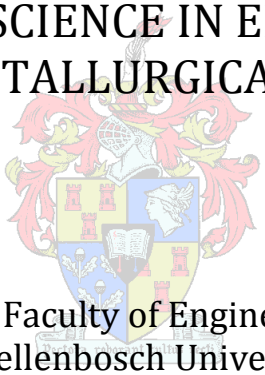

in the Faculty of Engineering
at Stellenbosch University

Supervisor
Dr C Dorfling

Co-Supervisors
Prof G Akdogan
Prof SM Bradshaw

December 2012

Declaration

By submitting this thesis electronically, I declare that the entirety of the work contained therein is my own, original work, that I am the sole author thereof (save to the extent explicitly otherwise stated), that reproduction and publication thereof by Stellenbosch University will not infringe any third party rights and that I have not previously in its entirety or in part submitted it for obtaining any qualification.

C.J. Liebenberg

……
Signature

23 November 2012

…… ……..
Date

Abstract

Lonmin Plc. is currently investigating a hydrometallurgical process route for the recovery of base metals (BMs) and platinum group metals (PGMs) from a low grade PGM bearing ore originating from the Platreef deposit in the northern limb of the Bushveld Complex. The front-end of the flow sheet entails recovering the BM values from the ore in a heap bioleach carried out at a temperature of 65°C after which the PGMs are recovered from the solid residue of the bioleach in a second stage heap cyanide leach (Mwase *et al.*, 2012; Mwase, 2009).

Commercially available chelating ion exchange resins and chelating adsorbents, Dow M4195 (bispicolylamine functionality), Dow XUS43605 (hydroxypropylpicolylamine functionality), Amberlite IRC748 and Purolite S930 (iminodiacetic acid functionality), and Purolite S991 (mixed amine and carboxylic functionality), were investigated in this thesis for the recovery of copper, nickel and cobalt (metals of interest, or MOI) from the bioleach solution. Screening tests indicated that Dow M4195 and Dow XUS43605 were able to selectively adsorb copper to the preference of all other metals in the solution at pH 3 and 4, while the other resins only succeeded in this purpose at pH 4 in the presence of little ferric iron. Only Dow M4195 proved to be able to selectively recover nickel over other metals in the solution at pH 4. Dow M4195, Dow XUS43605 and Amberlite IRC748 were selected for further investigation. Batch kinetic and equilibrium studies were performed on these resins and they were compared on the basis of their metals uptake rate and equilibrium concentrations of the MOI. The rate of metal uptake equilibrium attainment was found to be the fastest for Dow XUS43605, followed by Amberlite IRC748 and Dow M4195. Langmuir and Freundlich isotherm models were fitted to equilibrium data for copper adsorption with Dow XUS43605 and nickel adsorption

with Dow M4195, and copper and nickel capacities of these two resins at pH 4 were found to be 26 g/L and g/L 30.86 g/L, respectively.

Column adsorption experiments revealed that flow rate and temperature were the parameters that had the most significant effects on the copper loading achieved on Dow XUS43605 at copper breakthrough. A 36% increase in copper loading on Dow XUS43605 at copper breakthrough was observed when the temperature increased from 25 to 60°C, and the co-loaded nickel decreased proportionally. This increase was ascribed to the faster kinetics of copper adsorption at 60°C than at 25°C. Regarding nickel and cobalt recovery, the same trends were observed for increasing the flow rate and temperature. In addition to flow rate and temperature, an increase in initial solution pH also significantly increased metal adsorption, as would be expected.

Elution studies revealed that a split elution could be performed to remove the majority of the nickel from the resin with 2 bed volumes (BV) of 20 g/L sulfuric acid to remove the majority of the co-loaded nickel, followed by 2-3 BV of 100 or 200 g/L sulfuric acid to elute the copper, thus a purer copper-rich eluate fraction could be obtained. The same was true for nickel and cobalt elution from Dow M4195. The effect of flow rate in the range of 2 to 10 BV/h did not significantly influence metal elution from either Dow XUS43605 or Dow M4195, whereas temperature was found to increase the rate of metal elution.

Finally, two flow sheets were proposed for the recovery of the MOI. The overall recoveries of copper, nickel, cobalt and zinc for both flow sheets were 100%, but 14% nickel was lost to the copper eluate for both flow sheets, while the nickel lost to the cobalt rich effluent of the lag column was reduced from 8.3% for flow sheet option 1 to 5.6% for flow sheet option 2. By reducing the flow rate at which the process is carried out, these losses could be reduced. Also, by modifying flow sheet 2 and carrying out the copper recovery with Dow XUS43605 at a lower pH (pH 2 or 3), nickel losses to the copper eluate could be minimized as the resin's selectivity towards nickel is lower at lower solution pH values. It was further concluded that additional processing of the cobalt-rich eluate fraction of the lag column (in the lead-lag configuration of Dow M4195) is necessary to recover cobalt in a pure form.

Opsomming

Lonmin Plc. is tans besig met die ontwikkeling van 'n hidrometallurgiese proses om basismetale (BMe) en Platinum Groep Metale (PGMe) te herwin vanuit 'n laegraad erts afkomstig van die Platinumrifneerslag in die Bosveldkompleks. Aan die voorent van die proses word die BMe in 'n hoopbiologingsproses, waarna die PGMe uit die soliede oorskot van die biologingsproses geloog word met 'n sianiedoplossing. Hierdie tesis ondersoek kommersieël-beskikbare chelerende ioonuitruilingsharse asook chelerende adsorbente om koper, nikkel en kobalt uit die oplossing mee te herwin.

Die harse wat ondersoek word in hierdie studie, Dow M4195 (bispikolielamien funksionaliteit), Dow XUS43605 (hidroksiepropielpikolielamien funksionaliteit), Amberlite IRC748 (iminodiasetaatsuur funksionaliteit), en Purolite S991 (gemengde amien en karboksieliese funksionaliteit) is ondersoek in hierdie tesis vir die herwinning van koper, nikkel en kobalt vanuit die biologingsoplossing. Die harse was onderwerp aan 'n siftingsproses en resultate het getoon dat Dow M4195 en Dow XUS43605 die enigste harse was wat koper selektief bo yster kon adsorbeer by pH 3 en 4, terwyl die ander drie harse slegs in hierdie doel kon slaag by 'n oplossing pH van 4 (in die teenwoordigheid van min Fe^{3+}). Slegs Dow M4195 was in staat om nikkel en kobalt selektief bo ander metale in die oplossing te adsorbeer. Dow M4195, Dow XUS43605 en Amberlite IRC748 is gekies om onderwerp te word aan verdere kinetiese en ekwilibrium toetse. Die tempo waarteen metaaladsorpsie met Dow XUS43605 ekwilibrium bereik het was die vinnigste, gevolg deur Amberlite IRC748 en Dow M4195. Langmuir en Freundlich isoterme is gepas op die ekwilibriumdata van koperadsorpsie met Dow XUS43605 en nikkeladsorpsie met Dow M4195, en die koper- en nikkelkapasiteite van hierdie twee harse was bevind om 26 g/L en 30 g/L, onderskeidelik, gewees.

Kolomladingstoetse het aan die lig gebring dat vloeitempo en temperatuur die parameters was wat die grootste invloed op die koperlading op Dow XUS43605 by koper deurbraak gehad het. 'n 36% toename in koperlading op die hars was waargeneem toe die temperatuur verhoog was van 25 to 60°C, en die ooreenstemmende nikkellading het proporsioneel afgeneem. Die toename in koperlading by koper deurbraak was toegeskryf aan die vinniger kinetika van die hars by 60°C as by 25°C. Dieselfde neigings is waargeneem vir nikkel en kobalt herwinning met Dow M4195 as vir koper herwinning met Dow XUS43605; toenemende vloeitempo het gelei tot 'n laer konsentrasie van teikenmetale op die hars, terwyl verhoogde temperatuur die teenoorgestelde effek gehad het. Verder het 'n verhoging in die oplossing pH ook daartoe gelei dat meer kobalt en nikkel geadsorbeer word deur Dow M4195.

Dit was bepaal dat 'n twee-stadium eluering uitgevoer kan word deur die nikkel eerste van die hars te verwyder met 2 bed volumes 2% swawelsuur, gevolg deur die eluering van koper met 10-20% suur binne 2-3 bed volumes. Sodoende kan die koper-ryk fraksie meer suiwer wees. Dieselfde beginsel geld vir die eluering van nikkel en kobalt vanaf Dow M4195. Verdere bevindings sluit in dat vloeitempo's tussen 2 en 10 bed volumes per uur van die elueringsmiddel nie 'n merkwaardige invloed het op metaaleluering vanaf enige van die twee harse nie, maar dat 'n toename in temperatuur wel die tempo van metaaleluering laat toeneem het.

Ten slotte was twee vloeiskemas voorgestel vir die herwinning van koper, nikkel en kobalt met ioonuitruiling. Die algehele herwinning van koper, nikkel en kobalt vir beide vloeiskemas was 100%, alhoewel 14% van die nikkel verloor was na die koperelueaat in beide vloeiskemas, terwyl die nikkel verlies na die kobalt-ryke eluaat van die volg-kolom afgeneem het vanaf 8.3% in die eerste vloeiskema na 5.6% in die tweede vloeiskema. Die bogenoemde verliese kan verminder word deur die vloeitempo waarby die proses uitgevoer word te verlaag. Verder kan die tweede vloeiskema só aangepas word dat die herwinning van koper met Dow XUS43605 by 'n laer pH geskied (pH 2 of 3) aangesien die affiniteit van hierdie hars merkbaar laer is vir nikkel by hierdie pH's en sy affiniteit vir koper byna onveranderd bly. Die gevolgtrekking was ook gemaak dat die kobalt-ryke eluaat van die volg-kolom verder geprosesseer moet word om kobalt in 'n suiwer vorm te herwin.

Acknowledgements

First, I would like to express my gratitude to my supervisors, Christie Dorfling, Prof. Guven Akdogan and Prof. S.M. Bradshaw who guided me with their expertise and knowledge during this project, as well as for reviewing this thesis. Your valuable comments and corrections have contributed significantly to the improvement of the quality of this document. I would also like to thank Neil Snyders for his assistance and administrative contributions over the past two years.

I am also grateful to Ms Hanlie Botha for her skillful assistance with the analytical work.

I would further like to thank Dow Chemical Company and Purolite, in particular Mr Jaco Bester and Ms Johanna van Deventer, for their outstanding quality of service and for supplying the resins that were investigated in this project.

Finally, I express my greatest gratitude to Lonmin for their financial support and for providing me with the opportunity to explore the interesting field of hydrometallurgy and ion exchange.

Dedications

Hierdie tesis word opgedra aan my ouers, Hannes en Sophia, my broer en twee susters, B.J., Nannette en Sharine, asook aan my meisie vir die afgelope drie jaar, Anja. Dankie vir al jul ondersteuning en motivering...

Contents

List of Figures

List of Tables

Nomenclature

Constants

α_B^A	separation factor; selectivity of metal A over metal B
[i]	concentration of i, g/L
E	potential, V
E^0	standard reduction potential, V
F	Faraday constant, C/mol
G	Gibbs free energy, J/mol
H	enthalpy, J/mol
K_{sp}	solubility product, L/mol
K	stability constant, L/mol
K_w	ionization constant for water, mol^2/L^2
n, y, z	stoichiometric coefficients, -
Q	resin loading, g/L
R	gas constant, $J/mol.K$
S	entropy, $J/mol.K$
T	temperature, K

Subscripts

s	solution phase
r	resin phase
e	equilibrium
i	inlet (eg. $C_{A,i}$ refers to the inlet concentration of A)

o	outlet (eg. $C_{A,o}$ refers to the outlet concentration of A)

Superscripts

n, y, z	valence
s	solution phase at the surface of the resin
r	surface of the resin

Abbreviations

A, B, Me, Ne	metal cation
Bis-PA	bis-picolylamine
BMs	base metals
BV	bed volumes
EW	electrowinning
FR	flow rate
HPAL	high pressure acid leach
HPPA	hydroxypropylpicolylamine
IDA	iminodiacetic acid
IX	ion exchange
MOI	metals of interest (copper, nickel and cobalt in this thesis)
MRT	molecular recognition technology
MTZ	mass transfer zone
PGMs	platinum group metals
SX	solvent extraction
SPE	solid phase extraction
TM	target metals (refers to nickel and cobalt in the case of recovery with Dow M4195)

Keywords

Bioleach: A process in which metals are leached from an ore using a combination of acid and micro-organisms.

Cementation: Precipitation onto a metal surface based on the difference in reduction potentials of metals.

Chelate: A metal complex with the central metal ion coordinated to the donor atoms of the ligand.

Chelating adsorbent: The functional groups are neutral ligands that form charged complexes with metal cations, and anions are co-adsorbed.

Chelating ion exchanger: The functional groups are charged and the metal cations act as the central atoms and as counter-ions.

Donor atom: Atom in the ligand molecule that shares electrons with the molecule. Either N or O for the ligands considered in this thesis.

Hydrometallurgy: The processing of raw materials such as ores and concentrates with aqueous solution to recover valuable metals.

Macrocycle: A cyclic macromolecule or a macromolecular cyclic portion of a molecule.

Molecular Recognition Technology: Employs macrocyclic ligands that can be tailor-made to be highly selective for a specific metal ion.

Precipitation: The method by which chemical reagents are added to a solution to remove impurities or valuable metals in a solid state.

Solvent Extraction: Organic extractants are dispersed in an organic phase, usually kerosene, and are used to recover metals from aqueous solutions.

Uni-, bi- or multidentate: The amount of donor atoms of a ligand.

Chapter 1

Introduction

Hydrometallurgy involves the production of metals from raw materials such as ores and concentrates using aqueous solutions. Economically these processes cannot always compete with pyrometallurgical process routes because of the much slower kinetics involved in hydrometallurgical processes, and thus the production rates of these processes are usually slower (Habashi, 1990). Hydrometallurgical processes do, however, offer the possibility of recovering metals from low grade, complex and small ore bodies, where pyrometallurgical processes are usually used to recover valuable metals from high grade ores. This, together with the strive towards cleaner technology has motivated the development of hydrometallurgical process routes for the recovery of valuable metals.

A typical hydrometallurgical flow sheet involves the following steps:

- leaching the valuable constituents from the raw material
- purification and separation processes to remove impurities and recover valuable metals from the solution using various technologies including precipitation, cementation, solvent extraction (SX), ion exchange (IX) and adsorption, and solid phase extraction (SPE)
- electrowinning (EW)/crystallization/precipitation of the target metals.

Lonmin Plc. is currently investigating the possibility of using a hydrometallurgical process route to recover the base- and precious metals from their Akanani ore body, which is situated near Mokopane in the Northern limb of

the Bushveld Complex. Ionmin is the world's third largest platinum producer. Its core operations consist of eleven shafts and inclines which are all situated in the Bushveld Complex in South Africa, which hosts nearly 80% of global PGM resources.

In the process that is currently under development, the BMs are leached from the ore with sulphuric acid and thermophilic organisms in a primary heap bioleach, followed by a second-stage heap cyanide leach for the recovery of the PGMs from the solid residue of the heap bioleach. The present work focuses on the recovery of copper, nickel and cobalt (metals of interest, or MOI) from the leach liquor of the first stage. To put the project into context, a schematic diagram is presented in figure 1.1 below.

The composition of the bioleach solution treated in this project is as follows: 2133 *ppm* Fe(II) and Fe(III), 276 *ppm* Cu, 389 *ppm* Ni, 13.41 *ppm* Co, 310 *ppm* Al(III), 6.41 *ppm* Zn, 153 *ppm* Si, 419 *ppm* Mg, 10.62 *ppm* Mn and less than 5 *ppm* other impurities (Ti, Cr, As, Se, Mo, Cd, Sb, Pb) (Mwase *et al.*, 2012; Mwase, 2009).

Several techniques could possibly be used to recover the MOI from this solution. Selective precipitation and cementation processes have traditionally been used to recover these metals from acidic leach streams and some of these processes are still in use today (Flett, 2004). Disadvantages of such processes include that careful pH control is needed to ensure that only the target species precipitate, and even if the pH is optimally controlled co-precipitation of metals still occurs (Habashi, 1990; Flett, 2004).

Over the past few decades simpler, more efficient and more robust separation techniques have been developed to recover these metals from aqueous solution and to produce products with purities much higher than are achievable with conventional techniques. These techniques include solvent extraction (SX), chelating ion exchange and adsorption (IX) and solid phase extraction (SPE).

This chapter gives an overview of the hydrometallurgical recovery of the MOI from the ore, commonly used purification and separation processes to purify and recover these metals from hydrometallurgical solutions as well as basic principles governing metal binding in chelating ion exchange and adsorption in such solutions.

1.1 Heap bioleach and composition of leach liquor

Leaching tests on flotation concentrate and coarse ore from the Platreef deposit in the Bushveld complex were done by Mwase (2009). The goal was to exploit the PGM and BM values of this undeveloped prospect. The initial BM and gangue element head grade of the flotation concentrate was as is indicated in table 1.1 (Mwase *et al.*, 2012; Mwase, 2009).

The two options investigated to exploit the BM values of the ore were:

- a heap bioleach process in which flotation concentrate coated onto granite

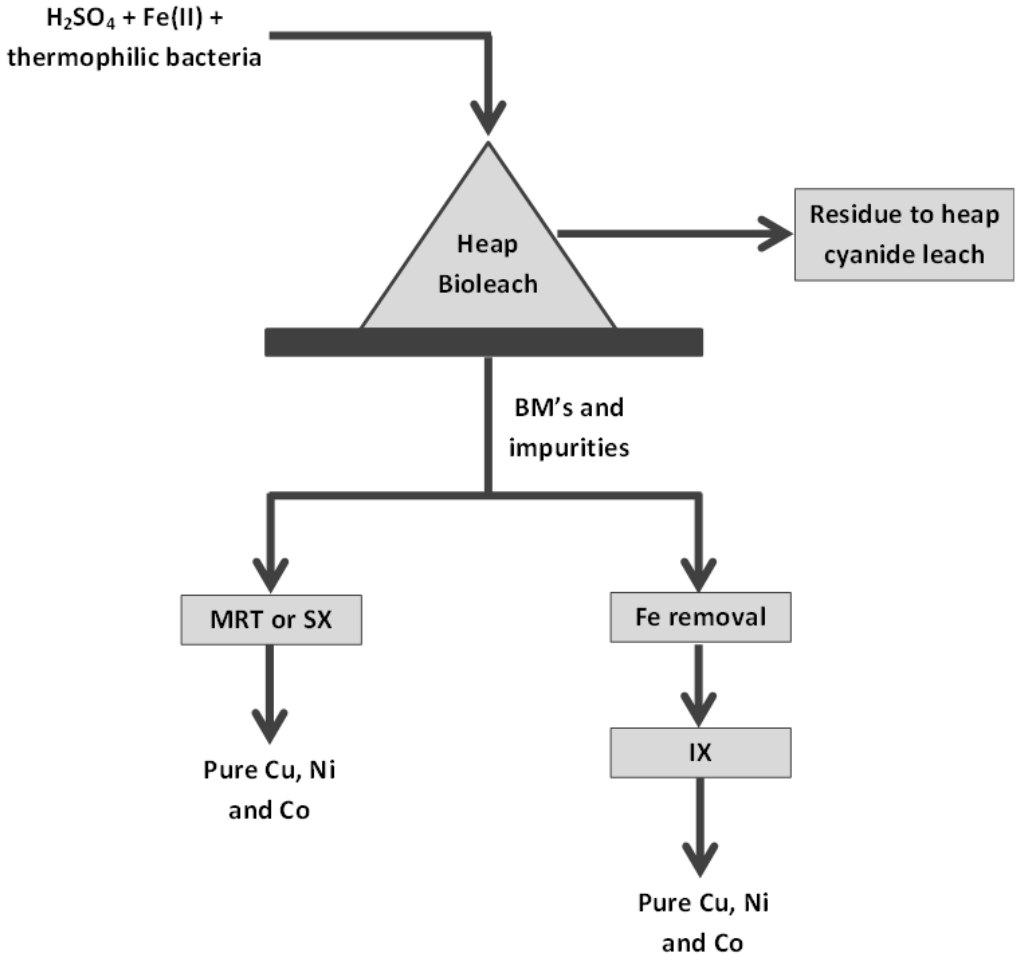

Figure 1.1: A schematic representation of the context of this thesis in the Akanani Platinum Project

Table 1.1: Flotation concentrate BM and gangue elements head grade

Metals head grade in flotation concentrate (%)								
Cu	**Ni**	**Fe**	**Co**	**Mg**	**Al**	**Si**	**Ca**	**Cr**
0.36	0.74	6.7	0.011	15	1.1	25	1.5	0.44

pebbles was leached at a rate of $1L$ per day with 30 g/L H_2SO_4 for 5 days. Thereafter the solution was replaced with the main leaching solution containing 2 g/L Fe(II) and 10 g/L H_2SO_4, as well as thermophillic bacteria amongst which *Sulfolobus Metallicus* and *Metallosphaera Sedula* were the main species. The ferrous-ferric oxidation-reduction couple provided the energy necessary for the bacteria to leach the metals from the ore, which was the motivation for adding ferrous iron to the leach solution (Mwase *et al.*, 2012; Mwase, 2009). Four columns were operated in parallel at temperatures of 65, 70, 75 and 80°C, respectively.

- an accelerated leaching process in which coarse ore was leached at an elevated temperature of 85°C with mixtures containing 40 g/L H_2SO_4 and 30 g/L HNO_3, and 40 g/L H_2SO_4 and 30 g/L Fe(III), respectively.

Of the four columns operating at temperatures ranging from 65 - 80°C, the column operating at 65°C performed the best in terms of MOI extraction. The degree of metals dissolution in this column based on ICP/AAS analysis is expressed in table 1.2 as the cumulative percent metals extraction[1] after 30 days of leaching.

Table 1.2: % Metal Dissolution in bioleach based on AAS analysis

% Metal dissolution after 30 days								
Cu	**Ni**	**Fe**	**Co**	**Mg**	**Al**	**Si**	**Ca**	**Cr**
58	96	12	85	9.2	32	0	32	6.9

The success of the process was attributed to the bulk of the BMs being contained in the sulphide minerals (Mwase *et al.*, 2012; Mwase, 2009; Schouwstra and Kinloch, 2000). Although the percentage copper dissolution was not

[1] except for iron: the values reported for iron are the maximum amount leached before precipitation occurred

at the level of the nickel and cobalt extractions, the results showed that metal extraction was still taking place and if the experiment was allowed to continue for another 60-90 days the copper extraction could have increased up to 90% as achieved by other researchers (Mwase, 2009; Petersen and Dixon, 2002). Despite the high degree of cobalt dissolution achieved in the bioleach and the high tonnage production of ore concentrate, the production potential for cobalt was low for this ore. The composition of the bioleach solution corresponding to the results in table 1.2 is shown in table 1.3.

Table 1.3: Composition of the bioleach solution

Bioleach composition (ppm)								
Cu	**Ni**	**Fe**	**Co**	**Zn**	**Al**	**Mn**	**Mg**	**Other**
276	389	2133	13.11	6.11	310	10.62	119	2

Despite the low percentage dissolution of iron in the bioleach, its concentration in the bioleach liquor was high since it was fed to the bioleach in the ferrous state at a concentration of 2 g/L. Since the bioleach is catalyzed by iron oxidizing bacteria, the effluent contains both ferrous and ferric iron. At this high concentration, iron could potentially be detrimental to the downstream MOI recovery with IX resins, therefore the solution has to be purified prior to the recovery of the MOI. Iron removal is discussed in section 1.2.

1.2 Solution purification

As mentioned in the previous section, iron constitutes the largest portion of metals in the liquor exiting the leach. Although the resins that are investigated in this study do not favour forming complexes with ferrous iron, ferric iron is at the top of the selectivity series of some of these resins (resins with iminodiactetic acid functionality) as ferric iron is considered to be a hard Lewis acid. As will be discussed in section 2.1, the selectivity of a resin towards a metal ion is dependent on many factors amongst which the concentration of the metal ion in the solution is one. For these reasons iron, whether in the ferrous or ferric oxidation state, has to be removed prior to IX.

Chemical precipitation is the oldest and simplest hydrometallurgical technique used for the removal of impurities and/or recovery of metal ions from aqueous solutions such as process leach solutions and wastewater streams. This technology involves the addition of chemical reagents that react with the ionic metal in solution to form an insoluble product (precipitate) and a simple solid-liquid separation step such as filtration or settling usually follows this process to separate the precipitate from the solution (Habashi, 1990). The three most popular chemical precipitation processes to recover metals are hydroxide precipitation, sulphide precipitation and reductive precipitation (Habashi, 1990; Falk *et al.*, 2000; Loan *et al.*, 2002).

Dissolution of sparsely soluble salts in water can be described by the chemical reaction for a divalent metal hydroxide

$$Me(OH)_2(s) + nH_2O \rightleftharpoons Me^{2+}(H_2O)_6(aq) + 2OH^-(aq) + (n-6)H_2O \quad (1)$$

and the solubility product, K_{sp}, is defined by equation 1.2.1.

$$K_{sp} = [Me^{2+}][OH^-]^2 \quad (1.2.1)$$

The solubility characteristics of metal salts can be illustrated using a precipitation diagram in which the metal ion concentration is plotted against the solution pH (Monhemius, 1981). The hydroxide precipitation diagram for various transitional metal ions are shown in figure 1.2. The data in the graph can be calculated from equation 1.2.2, where K_w is the apparent ionic power of water.

$$log[Me^{2+}] = logK_{sp} - 2(logK_w + pH) \quad (1.2.2)$$

From the diagram in figure 1.2 it can be seen that in the purification of a solution in which the MOI are copper, nickel and cobalt, it is impossible to separate ferrous iron from the MOI without co-precipitating the MOI. Ferric iron, on the other hand, precipitates out of the solution at a much lower pH than the rest of the metal ions in the diagram. Therefore, the ferrous iron

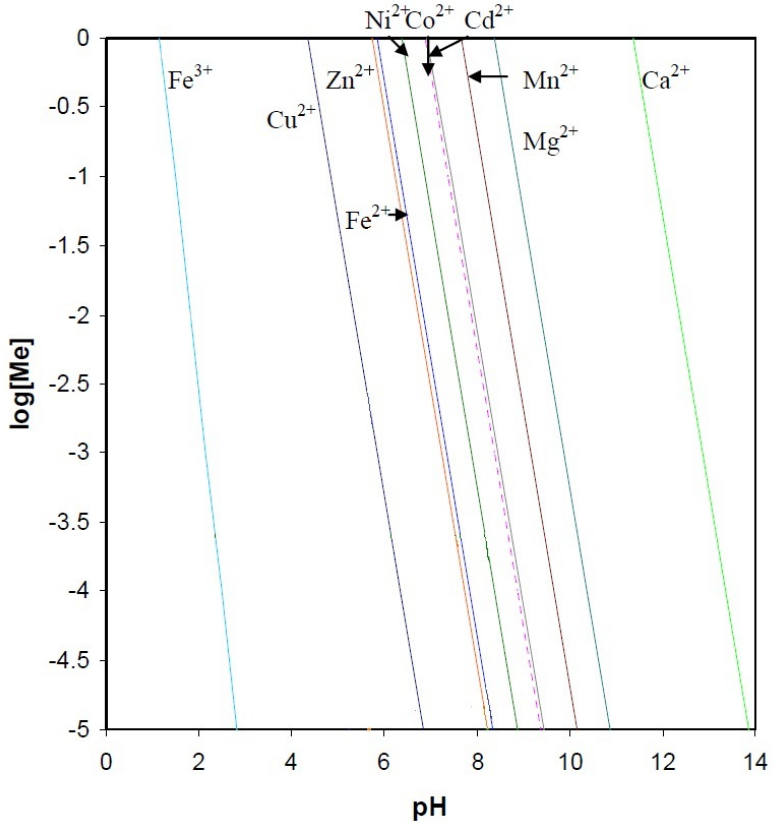

Figure 1.2: Precipitation diagram for metal hydroxides. Adapted from (Sirola, 2009)

in the solution must first be oxidized to ferric iron after which it could be precipitated from the solution without co-precipitation of the MOI.

The rate of oxidation of ferrous iron by oxygen is very slow at pH values below 2.5 and the reaction is highly dependent on Fe(II) concentration and dissolved oxygen concentration (Mouton *et al.*, 2007; Ho and Quan, 2007). By adding SO_2 to oxygen or air, peroxy-monosulphate free radicals are produced in the solution, which is a stronger oxidizing agent than oxygen alone (Zhang and Muir, 2010). As a result the oxidation rate of ferrous iron to ferric iron in the air/SO_2 system is almost independent upon the Fe(II) concentration. Therefore, this system offers a particularly attractive option for Fe(II) oxidation to Fe(III) as the oxidation rate is much faster than using O_2 alone and the oxidant is relatively cheap.

The reactions involved in Fe(II) oxidation with air/SO_2 are briefly summarized in reactions 2 to 4 (Mouton *et al.*, 2007; Zhang and Muir, 2010).

Catalyzed oxidation reaction (high O_2/Eh):

$$Fe^{2+} + SO_2 + O_2 \rightleftharpoons Fe^{3+} + 2SO_4 \tag{2}$$

Reduction reaction (low O_2/Eh):

$$2Fe^{3+} + SO_2 + 2H_2O \rightleftharpoons 2Fe^{2+} + SO_4^{2-} + 4H^+ \tag{3}$$

Side reaction:

$$2SO_2 + O_2 + 2H_2O \rightleftharpoons 4H^+ + 2SO_4^{2-} \tag{4}$$

According to the reactions the total SO_2 output includes SO_4^{2-} production as well as unreacted SO_2 that escapes to the off-gas . The extent to which the above reactions proceed is dependent on the SO_2/O_2 ratio. The SO_2/O_2 ratio can be selected such that the first reaction is dominating. Acid production in the second and third reaction becomes significant if there is excessive SO_2 in the gas phase (Zhang and Muir, 2010).

The concentrations of other metals present in the solution also influence the rate of ferrous oxidation, especially that of copper, which was found to inhibit the oxidation (Zhang *et al.*, 2000). Therefore, depending on the solution composition, an optimal rate of SO_2 exists where free acid production is minimized and maximum SO_2 utilization is achieved (Zhang and Muir, 2010).

Complete iron removal has been achieved within 2 hours from a dilute cobalt solution containing 2 g/L ferrous iron and 1.5 g/L Mn by selective oxidation with SO_2/air followed by hydroxide precipitation and removal of the precipitate by filtration (Mouton *et al.*, 2007). Copper, nickel and cobalt losses were reported to be less than 5%.

Although the iron removal step is beyond the scope of the present study, it is proposed that the SO_2/air oxidation system followed by hydroxide precipitation is used to remove this impurity. Conventional methods of MOI recovery are compared in section 1.3 to further narrow the scope of this project.

1.3 Conventional methods of metals recovery

As previously mentioned, separation methods used to recover valuable transition metal ions from hydrometallurgical solutions include precipitation and cementation processes, SX, SPE and IX. The main features of these technologies are summarized in table 1.4.

Table 1.4: Comparison of conventional separation technologies

Separation Process	**Advantages**	**Disadvantages**
Precipitative separation	•Old, well understood technology.	•Inability to produce high purity products.
SX	•Studied extensively and widely employed in the industry. •Suitable in many applications due to large variety of extractants. •Fast and selective.	•Organics entrained in the aqueous phase. •Regular replacement of volatile diluents. •Entrained organics can be detrimental in EW circuit.
SPE	•Extremely selective. •Can selectively remove trace quantities of metal. •Suitable in many applications due to large variety of products.	•Expensive.
Chelating IX and adsorption	•Highly selective and eco-friendly. •Can be used at low metal concentrations. •Range of commercial products available for many applications.	•Selective chelating separation materials are expensive. •Metal capacity relatively low (<3 $mequiv/g$). •May degrade by oxidation, attrition, temperature or osmotic shock. •Often slow uptake rates.

Chelating IX and SPE were the most attractive technologies for the recovery of the MOI from the bioleach solution given the diluteness of the solution.

Due to the expensiveness of SPE technology, which costs in the order of R5000 per liter of resin, chelating ion exchange was selected for investigation in this project as the ion exchange resins considered in this thesis cost between R150 and R550 per liter.

1.4 Objectives

The objectives of this research were:

- to select suitable chelating ion exchange resins and chelating adsorbents from literature for the recovery of the MOI from a synthetic bioleach solution
- to screen these resins based on their performance in batch experiments and to select the most appropriate resins for MOI recovery in column experiments
- to determine batch kinetic and equilibrium parameters of the resins and to elucidate the effects of process parameters on dynamic metal loading and elution
- to construct a workable flow sheet for the recovery of the MOI from the BM leach solution based on the results obtained.

Chapter 2

Literature Review

A review of published literature on copper, nickel and cobalt recovery from aqueous sulphate solutions with ion exchange was conducted in an effort to establish what resin functionalities are worth investigating for the application, what procedures other researchers followed to determine the effects of factors influencing target metal adsorption and recovery, and how well these resins performed in the applications they were used for.

2.1 Chelating ion exchange and chelating adsorption for the recovery of the MOI

2.1.1 Ion exchange and adsorption

Ion exchangers are insoluble electrolytes containing labile ions that easily exchange with other ions in the surrounding medium without any significant physical change in the structure of the electrolyte. The reaction taking place in the ion exchange process is the reversible exchange of labile ions in the ion exchanger. The IX electrolyte is usually a macromolecular structure of complex nature, but essentially all electrolytes consist of cations and anions upon dissociation; thus the ionic sites in the macromolecular structure can also be classified as anions and cations. As a result the macromolecular resin carries a surplus electrostatic charge neutralized by counter ions. Cationic exchangers have negative ionic sites with mobile cations (A^+) electrostatically bound

that can be exchanged for other cations (B^+). The opposite is true for anionic exchangers. The IX mechanism is illustrated in reactions 5 and 6:

Cation exchangers:

$$I^-A^+ + B^+ \rightleftharpoons I^-B^+ + A^+ \tag{5}$$

Anionic Exchangers:

$$I^+Y^- + Z^- \rightleftharpoons I^+Z^- + Y^- \tag{6}$$

Because standard ion exchangers prepared by the incorporation of ionogenic functional groups do not show any selectivity for specific ions in a mixture, its applications are limited (Dorfner, 1991). Therefore, these resin types will not be considered for the selective recovery of the MOI as it is essential for exchangers to be either specific or highly selective for the MOI to the exclusion of others.

Chelating ion exchangers are macromolecular polymeric materials to which chelating functional groups are covalently bonded. The chelating agent is able to incorporate metal ions to form a ring by chemical bonding. Metal ions are therefore extracted from solution not only by ion exchange but also by chemical bonding. The reaction mechanism is as follows:

$$chelating\ agent - H_2 + Me^{2+} \rightleftharpoons chelating\ agent - Me + 2H^+ \tag{7}$$

Kinetics of metal sorption with chelating ion exchangers tend to be slower than for conventional ion exchangers because there are two steps involved in chelating IX - ion exchange and ring formation. The overall rate of adsorption is usually controlled by boundary layer diffusion, intrapartical diffusion, the chemical reaction at the surface of the resin bead, or by a combination of them (Jay, 1998; Helfferrich, 1995; Hamdaoui, 2009; Dorfner, 1991). In this study the kinetics of the different resins are compared on the basis of the rate at which metal adsorption with the resins approach equilibrium (Zainol and Nicol, 2009). This approach will be further discussed in chapter 4.

Because of the higher selectivity of chelating ion exchangers or adsorbents towards certain metal ions, higher concentrations or dosages of eluting agent

are usually required to strip the metal ions from the exchanger than for non-selective ion exchangers (Dorfner, 1991).

Several chelating ion exchange resins that have a high specificity for transitional metal ions are commercially available (Grinstead, 1984; Mendez and Martins, 2004; Nicol, 2003; Rodgers *et al.*, 2010). These functionalities include iminodiacetic acid (IDA), aminophosphonic acid (AP), bispicolylamine (bis-PA), diphonix and hydroxypropylpicolylamine (HPPA). Those relevant to this study are IDA, bis-PA and HPPA type resins.

The chelating materials considered in this study consist of organic chelating ligands supported by a polymeric backbone. These materials include both chelating ion exchange resins and chelating adsorbents. Chelating ion exchangers and chelating adsorbents differ in the sense that in chelating ion exchangers the ligands are charged and the metal ions act as central atoms as well as counter-ions, while the neutral ligands form charged chelates with metals and anions are co-adsorbed in the case of chelating adsorbents (Mendez and Martins, 2004; Sirola, 2009). This principle is illustrated in figure 2.1 A, B and C.

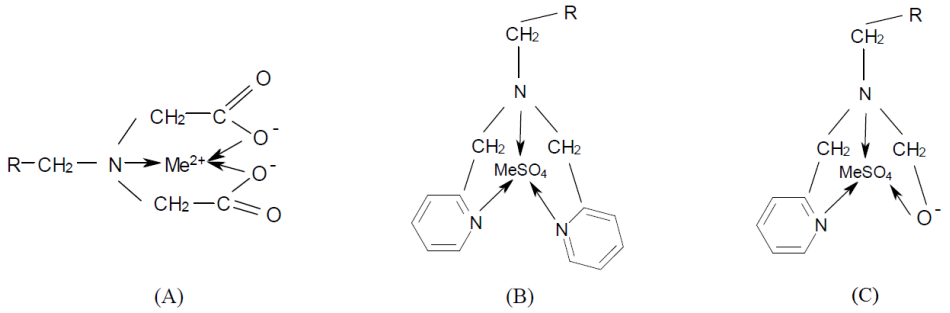

Figure 2.1: Metal complexation by (A) a chelating ion exchanger with IDA functionality, (B) a chelating adsorbent with bis-PA functionality and (C) a chelating resin with HPPA functionality

The ligands in figure 2.1 act as electron donors and form coordinative bonds to the central metal atom (Davies *et al.*, 1996). When there are two or more donor atoms in the complex molecular structure and they participate in a ring-closure reaction, it is called a chelating ligand (Davies *et al.*, 1996). The metal atom acts as a Lewis acid as it accepts electrons and the chelating ligand acts as a Lewis base as it donates the electrons (Pearson, 1963; Williams,

1952). It is known that complex formation constants increase as the number of electron donor atoms increases. Thus, complex formation constants are larger for multidentate ligands than for uni- and bidentate ligands (Davies *et al.*, 1996). All of the ligands considered in this thesis (see figure 2.1) are tridentate ligands. In the case of bis-PA all three donor atoms are nitrogen. HPPA was developed by replacing one of the aliphatic rings on bis-PA by a hydroxy group, which makes it less basic than bis-PA. Instead of having two aliphatic rings with nitrogen atoms as electron donors, IDA acid has two acetate groups attached to each branch making this ligand weakly acidic. The order of basicity of these ligand are therefore, in increasing order IDA $<$ HPPA $<$ bis-PA. Hence the ability of bis-PA to operate in more acidic solutions than HPPA and IDA.

2.1.2 Selectivity of chelating ion exchangers and adsorbents

The selectivity of a chelating ion exchanger depends on various factors including the conditions of polymerization, which in turn affects the number and distribution of functional groups on the resin structure and the moisture content, the solution composition and pH, as well as the functional groups (or ligands) attached to the resin structure itself and its affinity towards the metal ions in the solution (Sirola, 2009). Amongst these the ligand-metal affinity has the greatest influence on the resin selectivity. As mentioned previously, the ligands considered in this study are IDA, bis-PA and HPPA.

Several theories revolve around metal-ligand interaction (Davies *et al.*, 1996; Cotton and Wilkinson, 1988). A qualitative way of looking at these interactions is by considering Pearson's theory of hard and soft acids and bases. The ligand field theory provides a more quantitative approach, while the kinetic metal-ligand complexing theory gives insight into the steps involved in metal complexation with ligands. Pearson's theory and the ligand field theory are discussed below.

2.1.2.1 Hardness of metals and ligands

Pearson's theory can be used to describe the affinity of a ligand towards a given metal ion based on their respective hardness (Pearson, 1963). Table 2.1 divides metals and ligands into hard, soft and borderline acids and bases. In general, hard bases form stronger bonds with hard acids, and soft bases with soft acids. The hardness of a metal is associated with its ionic radius, oxidation state, polarizability and electronegativity. Hard acids and bases have small atomic radii, high oxidation states, low polarizability and high electronegativity, while the opposite is true for soft acids and bases. There are however borderline cases, which are difficult to categorize. These metals are generally the ions of the first row transition metal ions on the periodic table.

Table 2.1: Hardness of Lewis acids and bases

Acids			**Bases**		
Hard	**Soft**	**Borderline**	**Hard**	**Soft**	**Borderline**
H^+	Cu^+	Mn^{2+}	OH^-	H^-	C_6H_7N
Li^+	Ag^+	Fe^{2+}	RH^-	RS^-	C_5H_5N
Na^+	Au^+	Co^{2+}	F^-	I^-	N_2
K^+	Hg^+	Ni^{2+}	Cl^-	PR_3	N_3^-
Mg^{2+}	Cs^+	Cu^{2+}	NH_3	SCN^-	Br^-
Ca^{2+}	Pd^2+	Zn^{2+}	H_3COO^-	CO	NO_3^-
Sn^{2+}	Cd^2+	Pb^{2+}	CO_3^{2-}	C_6H_6	SO_4^{2-}
Al^{3+}	Pt^2+		N_2H_4		
La^{3+}	Hg^2+				
Cr^{3+}					
Fe^{3+}					
As^{3+}					

From this theory, the association of transition metals with iminodiacetic, picolylamine and acetate is not clear. Therefore, the ligand field theory is considered next.

2.1.2.2 Ligand field theory

Complex formation of the first row transition metals (also defined in the previous section as borderline Lewis acids) is affected by their partially-filled d-

orbitals, therefore these metals can form high-spin octahedral metal complexes (Vallet *et al.*, 2003). The general order of stability is $Mn^{2+}<Fe^{2+}<Co^{2+}<Ni^{2+}-<Cu^{2+}>Zn^{2+}$ and this series is termed the Irving-Williams series (Irving and Williams, 1953; Williams, 1952). The Irving-Williams series has been found to hold for a number of ligands and the stability order has been explained by the ligand field theory. The order of stabilities for bis-PA and HPPA are shown in figure 2.2 (Rodgers *et al.*, 2010) (Rosato *et al.*, 1984).

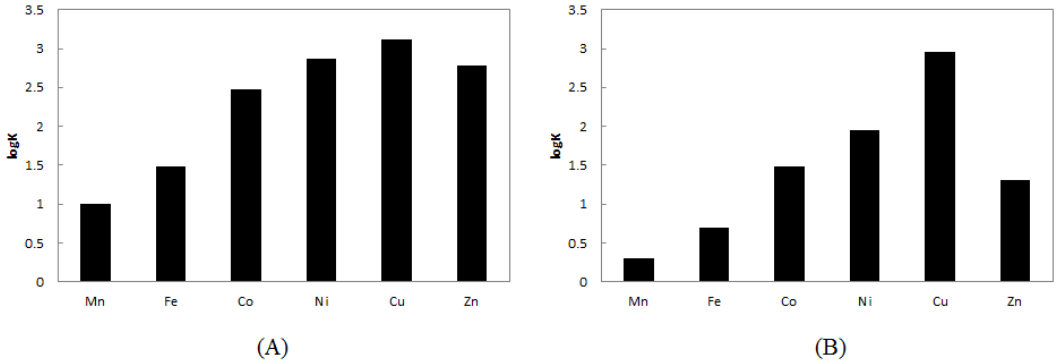

Figure 2.2: Stability constants for complexation of (A) bis-PA and (B) HPPA with the first row transition metal ions. Data obtained from (Rodgers *et al.*, 2010) and (Rosato *et al.*, 1984)

Following from figure 2.2 the selectivities of these ligands follow the Irving-Williams series, and so does IDA at high pH values, although it is not demonstrated here.

2.2 Resin functionality

As mentioned previously, there are a wide range of commercially available resin functionalities for the recovery of transition metal ions. IX for the recovery or removal of copper, nickel and cobalt from process solutions has been studied widely, which is reflected by the extensive amount of published work available on this topic. Table 2.2 highlights the literature on IX that was considered in this thesis, the resins investigated by these authors as well as the applications that the resins were used for.

Table 2.2: Applications of IX for MOI recovery

Author	Resin(s) used	Functionality	Application
Diniz et al. (2000) Diniz et al. (2002)	Dow M4195	Bis-PA	Dynamic purification of a 45 g/L $MnCl_2$ solution containing 85 ppm Cu, 100 ppm Ni, 48 ppm Co, 40 ppm Pb and 6 g/L Fe at 25°C and 1M free acid.
Grinstead (1984)	Dow M4195	Bis-PA	Characterizing adsorption of Cu, Ni, Co, Fe(II), Fe(III), Zn, Cd and UO_2 with Dow M4195.
Jeffers and Harvey (1985)	Dow M4195	Bis-PA	Dynamic recovery of cobalt from copper cementation effluent containing 30 ppm Co, 35 ppm Ni, 60 ppm Cu, 2 g/L Fe, 200 ppm Zn, 4.5 g/L Al, 7.2 g/L Mg and 400 ppm Mn at pH 3.
Mendes and Martins (2004)	Dow M4195 IRC748 SR-5 S930Plus	Bis-PA IDA IDA IDA	Selective removal of nickel and cobalt from a HPAL solution of a laterite Ni ore. Solution composition: 6.9 g/L Al, 500 ppm Co, 130 ppm Cu, 3 g/L Fe, 8.96 g/L Mg, 1.7 g/L Mn, 6.5 g/L Ni, 180 ppm Zn.
Rosato et al. (1984)	Dow M4195	Bis-PA	Dynamic separation of nickel from cobalt in a solution containing 15-30 g/L Co and 0.3-.07 g/L Ni.
Rodgers et al. (2010)	XUS43758 XUS43605	Bis-PA HPPA	Pilot plant demonstration of copper and cobalt recovery from a copper SX raffinate. Solution contained 150 ppm Cu, 600 ppm Fe, 55ppm Co, 45 ppm Ni, 250 ppm Zn, 800 ppm Mn, 7.7 g/L Mg.

Table 2.2 (continued)

Author	Resin(s) used	Functionality	Application
Sirola et al. (2009) Sirola et al. (2010a) Sirola et al. (2010b)	CuWRAM	AMP	Removal of Cu and Ni from concentrated $ZnSO_4$ solutions containing 250-fold zinc excess.
Pavlides and Wyethe (2000)	S950	Aminophosphonic	Removal of copper, zinc and lead from cobalt electrolyte.
Zainol and Nicol (2009)	IRC748 TP 207 TP 208 S930Plus	IDA IDA IDA IDA	Recovery of Ni and Co from acid leach pulp.
Zainol and Nicol (2009)	IRC748	IDA	Recovery of nickel and cobalt from sulphate solution.

It is clear from table 2.2 that the the most widely studied resin functionalities for the application of copper, nickel and cobalt refining are bis-PA and IDA.

2.3 Effects of operating conditions on metal complexation

Operating conditions such as solution pH, temperature and flow rate have a strong influence on metal complexation and the dynamic recovery of metals with resins.

2.3.1 Effect of pH

Metal ions compete with hydrogen ions for donor atoms on the resin. Displacement of protons from the ligand in the protonated form as well as the reverse reaction depends on the basicity of the ligand. It was mentioned earlier that the order of basicity of the ligand considered in this study is bis-PA>HPPA>IDA. This is reflected by the apparent pK_a values of these ligands, which are in the order of 3.5, 4 and 4.5 for bis-PA, HPPA and IDA, respectively.

As mentioned previously, the effect of pH on adsorption of copper, nickel and cobalt with ion exchange resins and adsorbents has been studied to a great extent following from the pH dependence of metal extraction with weakly basic and weakly acidic chelating agents (Rosato *et al.*, 1984; Grinstead, 1984; Mendez and Martins, 2004; Diniz *et al.*, 2002; Pavlides and Wyethe, 2000). The effect of pH on the equilibrium binding constant for typical bis-PA, HPPA and IDA type resins are shown in figures 1, 2 and 3, respectively. Weakly basic resins such as bis-PA-type resins can function in slightly more acidic conditions than weakly acidic resins such as IDA-type resins.

The effect of pH on nickel and cobalt recovery from a high pressure acid leach solution (HPAL) with metal concentrations as indicated in table 2.2 with resins Dow M4195, Amberlite IRC748, Ionac SR-5 and Purolite S930 was investigated by Mendes and Martins (2004). Purolite S930 performed poorly in the entire pH range studied (1-3), exhibiting selectivity towards copper only. The resin extracted less than 10% of all other metals present in the solution. The degree of metal uptake with the IDA-type resins increased markedly as the pH increased from 1 to 3. Copper extraction increased from 50% at pH 1 to nearly 100% at pH 4 for both of these resins, while nickel and cobalt extraction increased from less than 5% at pH 1 to more than 30% and 10%, respectively, at pH 4. Copper was extracted to completion with Dow M4195 at all pH levels, and nickel extraction increased from 25% at pH 1 to 45% at pH 4. From this study it was concluded that Dow M4195 performed the best in terms of selectively recovering nickel and cobalt in the entire pH range studied. Also, the best iron rejection was observed with Dow M4195, extracting less than 5% iron at pH 1 while other resins extracted more than 20%.

The effect of pH on the maximum equilibrium capacity of Amberlite IRC748 for nickel, cobalt, manganese and magnesium was also studied by Sirola (2009). Synthetic solutions of nickel, cobalt, magnesium and manganese were prepared containing 2.5 g/L of each metal and 250 mL of each metal solution was equilibrated with 2-80 mL of the resin. Results showed that the equilibrium capacity of the resin for nickel increased from 30 g/L at pH 3 to 35 g/L at pH 5, and for cobalt it increased from 20 g/L at pH 3 to approximately 34 g/L at pH 5. The capacity of the resin for magnesium and manganese was lower than 10 g/L in the pH range studied. Therefore, from a solution containing these metals,

nickel and cobalt could easily be separated from magnesium and manganese using Amerlite IRC748. Unfortunately leach solutions encountered in practice are much more complex and single component data is not of much worth in such cases.

2.3.2 Effect of temperature

The temperature dependence of the adsorption constant can be illustrated by the thermodynamic expression for the Gibbs free energy (equation 2.3.1). The reaction enthalpy, δH_n and reaction entropy δS_n can be calculated with the linearized form of equation 2.3.1 from adsorption constants at different temperatures. The linearized form of equation 2.3.1 is known as the van't Hoff equation (equation 2.3.2) (Koretsky, 2003).

$$\delta G_n = -RTlnK_n = \delta H_n - T\delta S_n \tag{2.3.1}$$

$$lnK_n = \frac{\delta S_n}{R} - \frac{\delta H_n}{RT} \tag{2.3.2}$$

Very little literature seemed to be available on the effect of temperature on copper, nickel and cobalt adsorption with the chelating ion exchange resins and adsorbents considered in this thesis, since many hydrometallurgical operations are carried out at room temperature. Of the studies listed in table 2.2, only Sirola (2009-2010) and Rosato *et al.* (1984) considered the effect of temperature on metal binding. Since the metal adsorption reaction with the ligands investigated in this thesis is exothermic in nature, according to equation 2.3.2 the equilibrium constants of acid and metal binding should decrease with increasing temperature, which corresponds to a decrease in equilibrium loading of acid and metals on the resin at elevated temperatures.

Literature data has shown that the acid binding constant decreases for ethylenediamine, 2-(aminomethyl)picolylamine and 1.10-phenanthroline as temperature increases and the stability constants of metal complexation with the ligands decrease in a similar way (Sirola, 2009). These ligands are bidentate ligands with nitrogen as both donor atoms. The results obtained by Sirola *etal.* (2010a) were somewhat contradictory as the stability constants of nickel and copper binding with 2-(aminomethyl)picolylamine was found to decrease with

increasing temperature, which was expected given the exothermic nature of the adsorption reaction, but at the same time higher nickel and copper loadings were reported at 90°C than at 25°C. The nickel and copper loadings reported increased from 0.5 to 0.8 $mmol/L$ and 0.6 to 0.8 $mmol/L$, respectively, when the temperature was increased from 25°C to 90°C. From these results, it is expected that temperature will have the same effect on the metal complexation constant for the ligands investigated in this thesis, but the equilibrium loading is expected to be lower.

The rate of metal binding and dynamic sorption of copper and nickel were also studied by Sirola *etal.* (2010b). The rate of acid and metal adsorption is controlled by pore diffusion and increasing temperature was found to markedly increase the adsorption rate. The pore diffusion coefficients reported increased from $9x10^{-10}$ (m^2/s) to $13x10^{-10}$ (m^2/s) for sulfuric acid and for copper and nickel it increased from $0.8x10^{-10}$ to $1.7x10^{-10}$ (m^2/s). This increase was ascribed to the decrease in viscosity of the aqueous phase.

In terms of the dynamic sorption of copper and nickel, an enhanced copper over nickel selectivity was observed at higher temperatures. The breakthrough point of copper shifted to a higher bed volume (BV) and the mass transfer zone (MTZ) became steeper as the temperature was increased from 25°C to 60°C and 90°C, indicating that more copper has loaded onto the resin up to the breakthrough point at elevated temperatures than at lower temperatures. At a flow rate of 12 bed volumes per hour, or 12 BV/h, the copper breakthrough point (where the ratio of copper in the effluent to that in the feed solution becomes greater than 0) shifted from BV 20 to BV 27. At a loading rate of 30 BV/h the copper breakthrough point at 25°C was observed at BV 5, which was much earlier than the breakthrough BV observed at 25°C and 12 BV/h, and as the temperature increased to 60 and 90°C the copper breakthrough BV shifted to 11 and 18, respectively. These results also illustrate the effect of flow rate as well as the interaction between temperature and flow rate on the dynamic recovery of metals.

To illustrate the advantage of operating at an elevated temperature (assuming that no costs are involved in heating the solution for the purpose of this study), consider the following: the copper breakthrough BV observed by Sirola *etal.* (2010b) at 25°C and a flow rate of 12 BV/h was BV 20, and at

90°C and 30 BV/h the observed copper breakthrough BV was 18. Thus, essentially the same loading was obtained after 1.67 hours at 25°C and 0.6 hours at 90°C. Therefore, the production rate is much higher at 90°C than at 25°C. It is unrealistic, though, that no costs are involved in heating the solution to 90°C, but in the case of this thesis the bioleach exits the heap at 60°C, therefore no additional costs are incurred in heating the solution.

Rosato *et al.* (1984) was the other researchers who have reported on the effect of temperature on dynamic metal recovery. An increase in nickel over cobalt selectivity for bis-PA was observed at higher temperature in the dynamic recovery of these metals (Rosato *et al.*, 1984). The ratio of nickel to cobalt loaded to the resin at equilibrium increased from 3.8 to 4.8 when the temperature was increased from 25°C to 50°C for a feed containing a cobalt to nickel ratio of 12.3 to 1, and for a feed containing a cobalt to nickel ratio increased from 1.2:1 to 1.6:1. The slight increase in selectivity was however considered to be outweighed by the costs involved in heating the solution.

Following from this discussion, the effect of temperature has not been fully elucidated, which motivates temperature, in particular, to be considered in this study.

2.3.3 Effect of flow rate

The effect of flow rate was briefly discussed in conjunction with the effect of temperature.

While the maximum theoretical capacity of an ion exchanger and the rate of metal loading onto the resin are determined by batch equilibrium tests, breakthrough and elution characteristics of metals with ion exchangers and adsorbents are evaluated in column sorption and elution studies. Since the objective of this study is not to purify the bioleach solution from impurities, but rather to recover the MOI, the MTZ should be kept as narrow (or steep) as possible to maximize the loading of the MOI on the resin and to minimize losses of the MOI to the effluent. This is accomplished by operating at a flow rate as low as possible. A schematic illustration of the effect of flow rate on the metal breakthrough profile is illustrated in figure 2.3 (Dorfner, 1991) (Nicol, 2003).

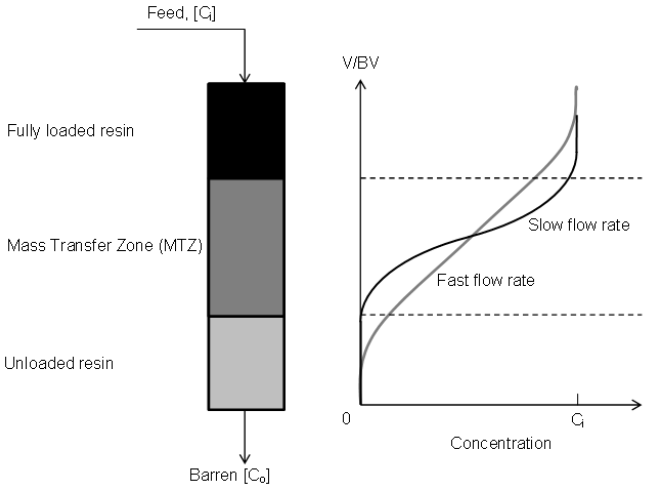

Figure 2.3: Schematic illustration of the effect of metal breakthrough in dynamic column operation (Nicol, 2003)

It is, however, not economically viable to operate at such low flow rates as the corresponding rate of metal production is low, therefore it is also important to consider the effect of flow rate on metal adsorption characteristics with the resins investigated in this study in column sorption and elution studies.

The effect of flow rate on the dynamic sorption of nickel and cobalt with resin Dow M4195 was investigated in the range of 1.2-7.1 BV/h by Rosato *et al.* (1984). The metal loading profiles obtained illustrated the significant effect of flow rate on the nickel loading behaviour of the resin. The MTZ markedly broadened as the flow rate increased, and consequently more nickel was lost to the column effluent as the flow rate increased. The resin loadings corresponding to the different flow rates were unfortunately not reported, but by inspection of the breakthrough profiles it could be seen that the nickel loading on the resin was more or less 30% and 50% lower at 3.6 and 7.1 BV/h, respectively, than at 1.2 BV/h. Higher flow rates were not investigated due to the slow kinetics of Dow M4195 at 25°C.

A pilot-scale study was conducted by Rodgers *etal.* (2010) to recover copper and cobalt from copper solvent extraction raffinate. The solution composition used in this study was shown in table 2.2. Although the effect of flow rate was not considered in this study, it was interesting to note that a flow rate of 20 BV/h was used for the recovery of copper with Dow XUS43605 and cobalt with Dow XUS43578, the smaller particle size equivalent of Dow M4195, which

is relatively high considering that resin manufacturing companies generally do not advise operating at flow rates higher than 10 BV/h. Both these resin particle sizes are small (± 300-400μm), therefore mass transfer kinetics are faster with these resins than with resins having larger PSDs (such as Dow M4195 and Amberlite IRC748 with average particle sizes of 575μm) and thus a flow rate of 20 BV/h is justified. The solution treated also contained low copper and cobalt tenors further justifying this high flow rate.

2.4 Elution of metals

Once metals have been loaded onto a resin they have to be removed in the elution process. This entails contacting the loaded resin with an eluting agent (typically a diluted acid when working with weak acid cationic exchangers) to reverse the adsorption reaction. The objectives of elution are firstly to selectively remove the target metals from the resin in as small a fraction as possible (smallest amount of bed volumes), and secondly to return the resin to the protonated form (in other words to regenerate the resin). In the realization of these objectives the concentration of the target metals in the eluate is maximized and no additional process steps are necessary to regenerate the resin prior to recycling it back to the loading cycle.

Metal elution from ion exchange resins has been studied to the same extent as metal adsorption onto the resins. In each of the studies listed in table 2.2 metals adsorbed onto the resins were also eluted.

The efficiency of elution is affected by the eluant used for metal elution, the eluant concentration, the eluant flow rate through the column as well as the temperature at which the elution is carried out.

2.4.1 Effect of eluant type

The effect of the type of eluant on the elution of metals from chelating resins is illustrated at the hand of a study conducted by Mendes and Martins (2004). In their study resins with different functionalities (bis-PA and IDA functionalities) were loaded with metals in batch mode followed by contacting the resins with a variety of eluants (H_2SO_4, NH_4OH and HCl) for 1 hour. Some metals,

including cobalt, iron, nickel and zinc, were 64.3, 88.7, 78.2 and 100% eluted from Dowex M4195 with $1M$ H_2SO_4 while copper was selectively removed to an extent of 82.1% with 1M NH_4OH. $1M$ H_2SO_4 was only able to remove 49.7% of the copper on the resin. HCl selectively eluted nickel over cobalt (96% nickel elution as opposed to 29.81% cobalt elution) while insignificant amounts of other metals were eluted. The results for Dowex M4195 suggested that selective elution is possible if eluting agent concentrations were optimized. For Amberlite IRC 748 and Ionac SR-5, on the other hand, selective elution did not seem like an option as most of the metals were eluted with 1M H_2SO_4 and 1M HCl without much selectivity. NH_4OH did not elute any metal from Amberlite IRC 748 as this resin has weakly acidic functional groups (as opposed to Dowex M4195, which has weakly basic properties) and therefore has no selectivity towards OH^- ions (Mendez and Martins, 2004).

Diniz *et al.* (2002) also investigated the elution of copper, nickel, cobalt, lead, manganese and iron from Dow M4195. The eluants used were $1M$ H_2SO_4 and $6M$ HCl and $4M$ NH_4OH. $1M$ H_2SO_4 was reported to elute more metal than $6M$ HCl, therefore HCl was not considered further. Nitric acid was not used on the alert from Dow Chemical Company that strong oxidizing agents should not be used as it could damage the resin. $1M$ H_2SO_4 eluted no copper, 71.5% nickel and 28% cobalt, while copper was fully eluted with $4M$ NH_4OH.

2.4.2 Effect of eluant concentration

Dynamic column elution of Dow M4195 loaded with 16-18 g/L nickel and 13.1-15.3 g/L cobalt was performed with 25 g/L, 50 g/L and 100 g/L H_2SO_4 by Rosato *et al.* (1984). The flow rate and temperature of these experiments were fixed at 6 BV/h and 25°C, respectively. Results indicated that virtually all of the cobalt was eluted after 4-6 BV, while nickel eluted only 64, 80 and 98% after treatment with 10 BV of H_2SO_4. As a result, a split elution was possible to first elute the majority of the cobalt (80%) together with only 15% of the nickel with 4 BV of 25 g/L H_2SO_4 at 15 BV/h, after which the remaining nickel and cobalt were eluted with 10 BV of 50 g/L H_2SO_4.

In the pilot-scale ion exchange plant operated by Dow Water and Process Solutions at ASAARCO, Dow XUS43605, loaded primarily with copper (12

g/L), was eluted with 20% H2SO4 at 8 BV/hr. The elution curve indicated that copper was stripped from XUS43605 within 2 BV of 20% H_2SO_4. It can also be seen from the curve that the eluate was relatively pure with a maximum copper concentration of 25 g/L and small amounts of other metals. Therefore, the copper in the raffinate was upgraded by a factor of more than 100. For nickel and cobalt elution from Dow XUS43578 a split elution was performed with 2% H_2SO_4 to first elute the cobalt, followed by 20% H_2SO_4 to elute the nickel. The elution was also carried out at 8 BV/h.

2.4.3 Effect of temperature

No literature was obtained for elution at elevated temperatures. The only information that was found regarding acid binding at elevated temperature was for CuWRAM Sirola2. As previously mentioned the equilibrium binding constant, $\log K$, of H_2SO_4 decreased from 1.96 at 25°C to 1.77 at 90°C, while the diffusion coefficient for sulfuric acid, D_p, increased from 9 at 25°C to 13 at 60°C. Thus, it is expected that the rate of elution would be faster at 60°C.

2.5 Purpose and scope of this thesis

As mentioned earlier, the objectives of study are to investigate the feasibility of using commercially available IX resins and adsorbents to recover the MOI from the solution that is shown in table 1.3. Because of the high concentration of iron in the solution originating from the bioleach, it has to be removed prior to the recovery of the MOI with IX resins due to high selectivities of IDA towards ferric iron, as well as the effect of metal concentration on metal binding constants of resins. This is, however, beyond the scope of this thesis, therefore an assumption based on literature has been made regarding the degree of iron removal that can be achieved (refer to sections 1.2 and 3.3).

Bis-PA and IDA as chelating ligands on solid support have been extensively studied and effects of operating conditions, with the exclusion of temperature, are well understood. Application of HPPA-type resins, on the other hand, has been researched to a lesser extent. Moreover, the interaction between operating conditions in the dynamic recovery of the MOI have not been addressed

in literature. This motivated the investigation of various operating conditions including flow rate, temperature, initial solution pH and initial metals concentration on the effect of metal breakthrough characteristics with the resins considered in this study in an attempt to determine optimal metal loading and elution conditions of these resins. Finally, a flow sheet for the recovery of the MOI was proposed based on the results obtained.

2.6 Summary

IX for the recovery of copper, nickel and cobalt from dilute sulphate solutions has been studied extensively and the most popular resin functionalities for this application were found to be bis-PA and IDA. HPPA-type resins for the selective recovery of copper was researched to a lesser extent.

Dow M4195 was found to have the best iron rejection, but because of the dependence of resin selectivity on the concentration of metal ions in the solution, iron, which constitutes the highest proportion of the bioleach solution exiting the heap, should be removed prior to the IX operation to selectively recover the MOI.

The most important operating variables in the adsorption of the MOI using chelating ion exchangers and adsorbents are the equilibrium pH, temperature and flow rate. Of these, literature on temperature was very scarce which motivated the investigation of its effect on metal adsorption.

In the elution of metals from the resins the type of eluant and its concentration determine which metals are removed from the resin in the elution process. More concentrated eluants are necessary to elute metals for which resins have stronger affinity. In the case of some resins, such as Dow M4195 (or XUS43578) which exhibit weakly basic behaviour, it is necessary to strip copper (for which the resin is extremely selective) with ammonium hydroxide. Column elution should be done at the lowest possible flow rate as to minimize the fraction in which the metal is stripped from the resin and thus to maximize the concentration of the target metal in the eluate. For Amberlite IRC 748 selective elution of nickel and cobalt is not a possibility as they are removed from the resin in the same fraction regardless of the acid type or its concentration. Therefore, metal loading should rather be optimized with this resin.

A split elution can however be performed to separate the target metal from Fe(III) as Fe(III) can only be stripped with strong acid. A split elution can be performed with Dow M4195 (or XUS43578) to separate nickel and cobalt loaded to the resin.

Chapter 3

Experimental

A series of experiments were conducted in an attempt to achieve the objectives discussed in chapter 1. This chapter discusses details of the experimental procedures followed and analytical methods used.

All experiments and analyses were completed by the author at Stellenbosch University in the Hydrometallurgy laboratory at the Department of Process Engineering.

3.1 Materials

The IX resins that were considered for the selective recovery of copper, nickel and cobalt are listed in table 3.1.

Reagents that were used to prepare synthetic bioleach solutions and eluting agents in this study, along with their respective suppliers and purities, are reported in table 3.2.

Table 3.1: Commercially available IX polymeric resins for the selective adsorption of copper, nickel and cobalt

Resin	Manufacturer	Functionality	Matrix
Dow M4195	Dow Chemical Company	Bis-PA	Macroporous St-DB
Dow XUS43605	Dow Chemical Company	HPPA	Macroporous St-DB
Amberlite IRC748	Rohm and Haas	IDA	Macroporous St-DB
Purolite S930Plus	Purolite	IDA	Macroporous St-DB
Purolite S911	Purolite	A/C	Macroporous St-DB

Table 3.2: List of chemicals

Reagent	Supplier	Purity
$CuSO_4.5H_2O$	Kimix	99-100 %
$NiSO_4.6H_2O$	Kimix	99-100 %
$CoSO_4.7H_2O$	Kimix	99-100 %
$ZnSO_4.7H_2O$	Kimix	99-100 %
$Fe_2(SO_4)_3.10H_2O$	Kimix	99-100 %
$FeSO_4.H_2O$	Kimix	99-100 %
$Al_2(SO_4)_3.18H_2O$	Kimix	99-100 %
$MnSO_4.4H_2O$	Kimix	99-100 %
NaOH	Kimix	99-100 %
H_2SO_4	Kimix	95-98 %
HNO_3	Kimix	55 %
NH_3 solution	Kimix	33 %
HCl	Kimix	37 %

3.2 Pre-treatment of resins

The resins tested in this study were conditioned by packing them in a glass column with a sintered bottom and washing them with 10 BV of distilled water at a flow rate of 10 BV/h to remove impurities. The resins were then washed with 10 BV of $1M$ H_2SO_4 at a rate of 5 BV/h to ensure that they were all in the protonated form, after which they were washed with 10 BV of distilled water at 10 BV/h to remove excess acid. After the resins have been removed from the column and excess water has been removed through filtration, they were stored at room temperature in the containers that they were supplied in.

3.3 Preparation of synthetic bioleach solution

As discussed in section 1.1, 52% copper, 95% nickel and 85% cobalt were extracted in the bioleach over a 30 day period and extraction was still increasing at that stage. The corresponding bioleach liquor composition after 30 days of leaching was reported in table 1.3. As mentioned previously, the resulting pH of the solution was in the order of 0.8-1.2. A bioleach solution that would be encountered in practice would be more concentrated than a solution obtained in a single pass, pilot-scale leaching operation where the environmental conditions are controlled, for the following reasons:

- a full-scale heap leach operation would be carried out outside, open to the atmosphere and thus subjected to variation in environmental climate. Depending on the location of the heap and the seasonal climate, the effect of the climate could either enhance the concentration of the solution (in warm, arid environments), or it could enhance the dilution of the solution (in environments with high rainfall).

- the leach liquor exiting the heap would have had a residence time inside the heap of a few months at the start, and as time progresses more layers of ore is piled on the heap which could potentially increase the residence time of the solution inside the heap to a few years. This would have a concentrating effect on the solution.

- recycling would be employed in practice. This would also enhance concentration of the solution.

The bioleach solution composition reported in table 1.3 was based on 30 days of leaching and it was observed that metal dissolution had still taken place at that stage. Mwase (2010) projected that copper could be dissolved to the same extent as nickel and cobalt if the test had been allowed to continue for another 60 days. Because of the difficulty associated with the approximation of the composition of the bioleach liquor that would be encountered in the real-life heap bioleach operation, the solution in table 1.3 was concentrated by a factor of 2.5 . It was also assumed that 95% of the iron in the solution could be removed from the solution by selectively oxidizing the ferrous iron in the solution to ferric iron and subsequently precipitating it by adjusting the pH to 2-3. The composition of the simulated leach solution after clarification was therefore as shown in table 3.3.

Table 3.3: Composition of the synthetic bioleach solution

Metal concentrations in bioleach solution in ppm						
Cu	**Ni**	**Co**	**Fe**	**Zn**	**Mn**	**Al**
690	974	34	267	16	27	776

Two types of synthetic bioleach solution were prepared: one consisting of all the metals shown in table 3.3 (solution A), and one containing all metals except for copper (solution B). Solution A was used to test the resins for their ability to recover copper while solution B was used to test the resins for their ability to extract nickel and cobalt assuming that it is possible to completely extract copper from the solution with one of the resins selected for this study.

The solutions were prepared by dissolving the correct amounts of the respective metal salts in distilled water, except for ferric iron that was dissolved in 1M sulfuric acid before it was added to the solution containing the other metals. The resulting solution pH was in the order of 0.8-1.2. The pH of the solution was then raised to the desired pH through the addition of concentrated NaOH. Precipitate that formed as a result of adjusting the solution pH was allowed to settle out overnight under gravity after which the clarified solution was separated from the precipitate for use in the experiments.

3.4 Batch loading experiments

The aims of these experiments were:

- to test the suitability of the resins listed in table 3.1 for extracting copper, nickel and cobalt from the pregnant bioleach solution based on their selectivity towards the target metals
- to investigate the effect of pH on metal extraction with different resins
- to determine kinetic and equilibrium loading parameters
- to investigate the effect of metal concentration on metal uptake
- to model metal adsorption isotherms with either the linear isotherm, Freundlich isotherm or Langmuir isotherm models.

A series of batch loading experiments was carried out by contacting the IX resins and synthetic bioleach solutions in continuously stirred beakers. Since all the resins selected for this study were either resins with weakly basic or weakly acidic functionalities, the pH of the solution had to be controlled during

these experiments. This was achieved by adding 1M NaOH drop-wise to the experiment using automatic pH controllers supplied by Eutec Instruments. A schematic diagram of the experimental setup is shown in figure 3.1.

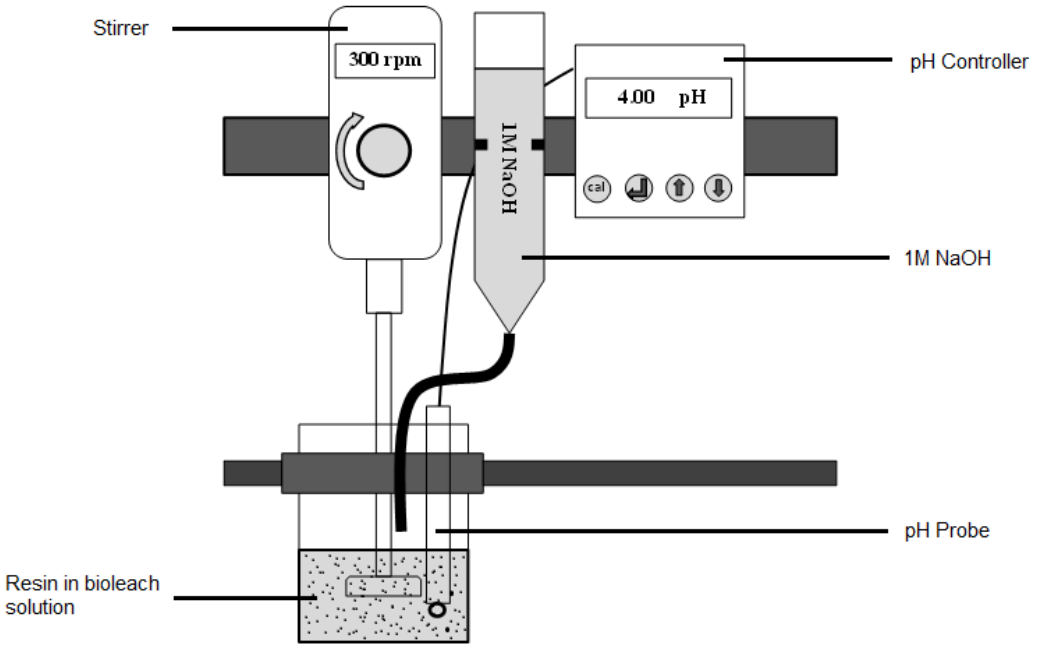

Figure 3.1: Batch experimental setup

3.4.1 Resin screening

Five commercially available resins that show high selectivity towards transitional metal ions have been selected to investigate in this study. These resins are listed in table 3.1.

Resins Amberlite IRC748 and Purolite S930Plus are typical chelating ion exchangers with IDA functional groups attached to the polymeric backbone while DOW M4195 and DOW XUS43605 are chelating adsorbents with bis-PA and HPPA functional groups, respectively, attached to the styrene divinylbenzene matrix.

Using the setup depicted in figure 3.1 the capability of the resins listed in table 3.1 to adsorb copper, nickel and cobalt was tested by equilibrating 5 mL

of each resin with 250 mL synthetic leach solution for 48 hours at different pH values in the range of 2 to 4. A 10 mL sample was withdrawn from the solution after 48 hours for each experiment.

3.4.2 Kinetics of loading

Using the same setup as shown in figure 3.1, batch kinetic experiments were performed by contacting 5 mL of tapped-settled resin with 250 mL of synthetic bioleach solution for 48 hours and withdrawing 2 mL samples from the solution at various time instances over the 48 hour period.

3.4.3 Equilibrium isotherm experiments

Batch isotherm testing was performed by equilibrating different volumes of tapped-settled resin (2.5 mL, 5 mL, 10 mL, 25 mL, 40 mL and 50 mL) with 250 mL of the synthetic bioleach solution. For each resin to solution ratio tested, a sample of the solution phase was taken after 48 hours.

3.5 Dynamic column loading experiments

The aims of these experiments were:

- to study the dynamic metal loading behaviour of the resins that were selected based on the results obtained with batch experiments
- to determine the effects of different process parameters (flow rate, temperature, pH and initial metals concentration) on column metal adsorption with the selected resins
- to develop statistical models that are able to predict column loading parameters such as the loading of target metal ions on the resins at a certain degree of breakthrough and the corresponding BV where that degree of breakthrough occurs
- to validate the statistical models with additional experimental data.

Fixed-bed columns are used in hydrometallurgical applications to remove metals by ion exchange. In this study, 10 mL of tapped settled resin was placed in a glass column, 300 mm long, 12 mm in diameter, with a sintered bottom and a water jacket. The synthetic bioleach solution was pumped from an overhead reservoir, of which the temperature was controlled at a desired value, into the column (which was kept at the same temperature as the reservoir) using a peristaltic pump. Samples of the barren solution were collected at the bottom of the column. A schematic illustration of the experimental setup is shown in figure 3.2.

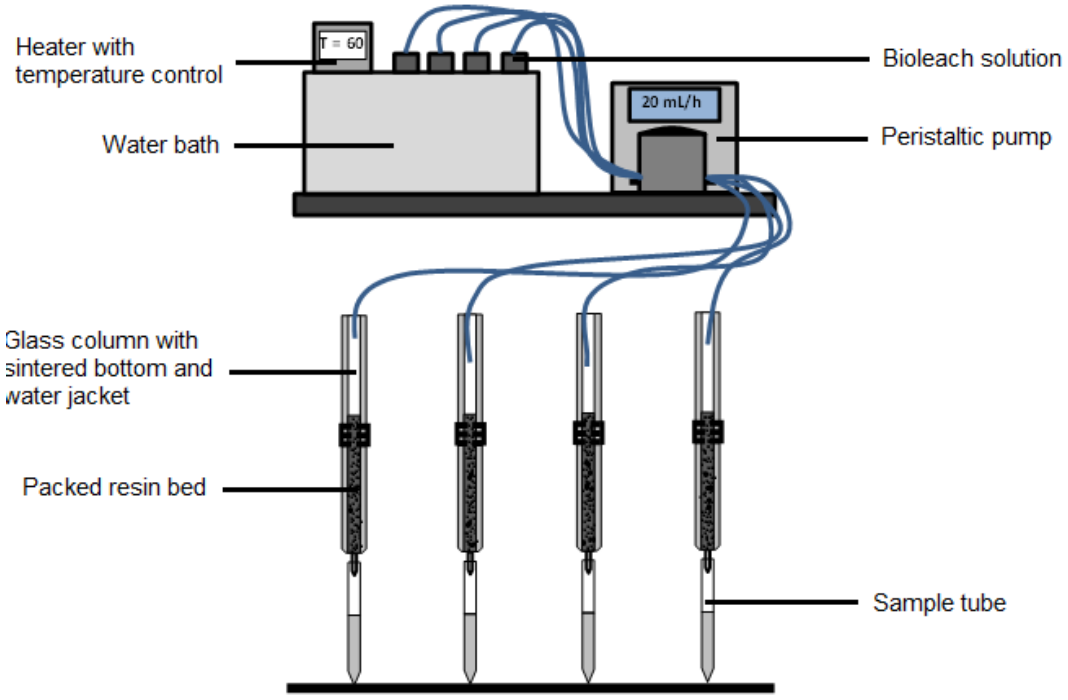

Figure 3.2: Column adsorption and elution experimental setup

3.5.1 The effects of operating conditions on column metal loading

Based on the results of the screening tests, batch kinetic tests and batch equilibrium isotherm tests, two resins were selected to study dynamic column adsorption with: one for copper recovery and the other for nickel and cobalt

recovery. In each case the effects of temperature, flow rate, initial solution pH and initial metals concentration on target metal loading onto these resins were investigated by following a half fraction factorial ($2^{(5-1)}$) experimental design. The experimental designs for copper recovery and nickel and cobalt recovery with the selected resins are shown in tables 3.4 and 3.5, respectively.

The effect of temperature was tested at two levels, 25 and 60 °C. Although it has been reported by Rosato *et al.* (1984) that the increase in nickel selectivity over cobalt with weakly basic anionic resins (eg. bis-PA type resins) is outweighed by the costs involved in heating the solution, it was decided to test the resins at 60 °C. This decision was based on the fact that the temperature in a commercial heap bioleach is controlled at 65 to 75 °C for optimal activity of thermophilic micro-organisms, and since it was demonstrated by Petersen and Dixon (2002) that a heap conserves its heat, the leach liquor would therefore exit the heap at the temperature of the heap.

The bioleach solution flow rate through the column was controlled at either 5 BV/h or 15 BV/h. In terms of utilizing the resin capacity to its fullest, it is favourable to operate at the lowest possible flow rate (lower than 2 BV/h), thereby keeping the mass transfer zone at its smallest. It is, however, not economically favourable to operate at such low flow rates since the production rate of the MOI is low, therefore higher flow rates were investigated (Rosato *et al.*, 1984; Mendez and Martins, 2004).

In the copper recovery experiments the initial bioleach solution pH was either 3 or 4. HPPA-type resins are able to extract copper at pH values well below 2, while nickel, and especially cobalt, extraction with bis-PA type resins are at its optimum at pH values between 2 and 4. As the solution passes through the copper recovery column, protons on the resin are displaced into the solution by copper (and other metals) that adsorb onto the resin, and thus the pH of the solution drops. Considering that the nickel and cobalt recovery section is downstream from the copper recovery section, the pH of the solution entering the copper recovery section should be as high as possible. There is, however, an upper solution pH constraint: as the pH of the solution is raised to 4.5 and 5, up to 30% of the copper, nickel and cobalt are lost to the precipitate that forms (see figure 3.3). For this reason, the highest solution pH investigated in this study is 4.

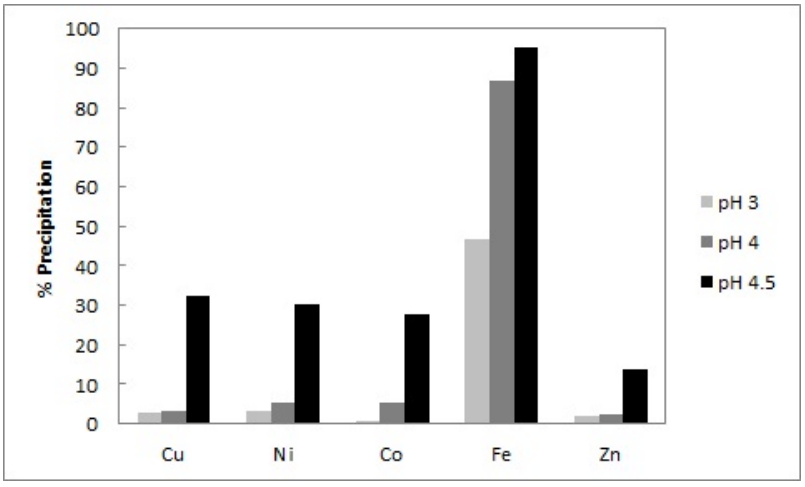

Figure 3.3: Precipitation of metals as a result of solution pH adjustment

Linear regression models were fitted to the data to obtain statistical models that are able to predict certain column loading parameters such as the copper loading on the resin when its concentration in the effluent reaches 1% of that in the inlet ($C_{Cu,0}/C_{Cu,i} = 0.01$), the nickel and cobalt concentration on the resin when $C_{Ni,0}/C_{Ni,i} = 0.1$, as well as the corresponding BVs where 1% copper breakthrough and 1% nickel breakthrough occur.

Table 3.4: Experimental design for copper recovery

Run	Temperature (°C)	Flow rate (BV/h)	pH	Initial metals concentration (ppm)							
				[Cu]	[Ni]	[Co]	[Zn]	[Fe^{2+}]	[Fe^{3+}]	[Mn]	[Al]
1	25	5	3	518	1217	42	20	67	267	33	970
2	25	5	4	518	730	25	12	40	160	20	582
3	60	5	3	518	730	25	12	40	160	20	582
4	60	5	4	518	1217	42	20	67	267	33	970
5	25	15	3	518	730	25	12	40	160	20	582
6	25	15	4	518	1217	42	20	67	267	33	970
7	60	15	3	518	1217	42	20	67	267	33	970
8	60	15	4	518	730	25	12	40	160	20	582
9	25	5	3	863	730	25	12	40	160	20	582
10	25	5	4	863	1217	42	20	67	267	33	970
11	60	5	3	863	1217	42	20	67	267	33	970
12	60	5	4	863	730	25	12	40	160	20	582
13	25	15	3	863	1217	42	20	67	267	33	970
14	25	15	4	863	730	25	12	40	160	20	582
15	60	15	3	863	730	25	12	40	160	20	582
16	60	15	4	863	1217	42	20	67	267	33	970

Table 3.5: Experimental design for nickel and cobalt recovery

Run	Temperature (°C)	Flow rate (BV/h)	pH	Initial metals concentration (ppm)						
				[Ni]	[Co]	[Zn]	[Fe^{2+}]	[Fe^{3+}]	[Mn]	[Al]
1	25	5	3	730	42	20	67	267	33	970
2	25	5	4	730	25	12	40	160	20	582
3	60	5	3	730	25	12	40	160	20	582
4	60	5	4	730	42	20	67	267	33	970
5	25	15	3	730	25	12	40	160	20	582
6	25	15	4	730	42	20	67	267	33	970
7	60	15	3	730	42	20	67	267	33	970
8	60	15	4	730	25	12	40	160	20	582
9	25	5	3	1217	25	12	40	160	20	582
10	25	5	4	1217	42	20	67	267	33	970
11	60	5	3	1217	42	20	67	267	33	970
12	60	5	4	1217	25	12	40	160	20	582
13	25	15	3	1217	42	20	67	267	33	970
14	25	15	4	1217	25	12	40	160	20	582
15	60	15	3	1217	25	12	40	160	20	582
16	60	15	4	1217	42	20	67	267	33	970

3.5.2 Validation of statistical models

The statistical models that were developed as discussed in section 3.5.1 were validated by fitting them to an additional set of experimental data. The conditions at which these experiments were conducted are shown in tables 3.6 and 3.7. The temperature was controlled at either 25 or 60 °C, the flow rate at 2.5, 5 or 7.5 BV/h, and the pH at either 2 or 4. Solution A (table 3.3) was used in the experiments for the copper recovery section, and for the nickel and cobalt recovery section the same solution composition was used except that the solution did not contain copper (solution B).

Table 3.6: Experimental conditions for validation of statistical models: copper recovery section

Run	Temperature (°C)	Flow rate (BV/h)	pH
1	25	2.5	4
2	25	5	4
3	25	7.5	4
4	60	2.5	4
5	60	5	4
6	60	7.5	4

3.6 Column elution experiments

The same experimental setup that was used for the column adsorption experiments (see figure 3.2) was used for the elution experiments. Dow XUS43605 and Dow M4195 were loaded with a solution having a composition that is shown in table 3.3 (note that in the case of Dow M4195 copper was omitted from the solution) at a flow rate of 5 BV/h, a temperature of 60°C and an initial solution pH of 4. To achieve homogeneously loaded resins, the resins were mixed after having been loaded in separate batches.

10 mL of tapped settled loaded resin was then packed in a column and the eluting agent was pumped from the overhead reservoir through the resin bed. Samples of the column effluent were collected at the bottom of the column.

Table 3.7: Experimental conditions for validation of statistical models: nickel and cobalt recovery section

Run	Temperature (°C)	Flow rate (BV/h)	pH
1	25	2.5	2
2	25	5	2
3	25	7.5	2
4	60	2.5	2
5	60	5	2
6	60	7.5	2
7	25	2.5	4
8	25	5	4
9	25	7.5	4
10	60	2.5	4
11	60	5	4
12	60	7.5	4

The conditions at which Dow XUS43605 and Dow M4195 were eluted are shown in tables 3.8.

Table 3.8: Conditions for metals elution from Dow XUS43605 and Dow M4195

Run	Temperature (°C)	Flow rate (BV/h)	Acid concentration (g/L)
1	25	2	20
2	25	2	100
3	25	2	200
4	25	10	20
5	25	10	100
6	25	10	200
7	60	2	20
8	60	2	100
9	60	2	200
10	60	10	20
11	60	10	100
12	60	10	200

3.7 Analysis

Flame Atomic Absortion was used to analyze all samples for the metals in the solution. To determine the error involved in analyses, two sets of measurements of the same sample, which contained nickel and cobalt only, with the AA. The AA was first calibrated for these elements and measurements (in triplicate) were taken after which the AA was switched off and turned on again to take a second set of measurements. The analytical results and the repeatability of analyses are shown in table 3.9.

Table 3.9: Repeatability of analysis

Replicate	**Set 1**		**Set 2**		**%Error Set 1**		**%Error Set 2**	
	Ni	**Co**	**Ni**	**Co**	**Ni**	**Co**	**Ni**	**Co**
1	117.4	7.841	121.4	8.211	2.68	3.18	0.64	1.39
2	125.3	8.323	127.5	8.177	3.87	2.78	5.69	0.97
3	115.2	8.098	117	7.939	4.50	0.00	3.01	1.97

Chapter 4

Batch loading results

4.1 Resin screening

The different resin functionalities listed in table 3.1 were screened for their suitability to recover copper, nickel and cobalt from the bioleach solution. The procedure followed in the screening tests was outlined in chapter 3.4.1. Metal extractions obtained with the different resin functionalities tested are reported in figures 4.1 and 4.2 for solution pH values controlled at 3 and 4, respectively. It should be noted that only the total iron content was measured as the analytical instrument used to quantify metals concentration in solution (AA) could not distinguish between ferrous and ferric iron. Therefore, the absolute position of the two oxidation states of iron in the selectivity series of the resins could not be established. In general, ferric iron is higher up the selectivity series of chelating resins and adsorbents than ferrous iron (Rosato *et al.*, 1984; Grinstead, 1984; Mendez and Martins, 2004; Sirola *et al.*, 2010*a*; Deepatana *et al.*, 2006; Lin and Juang, 2007).

All the resins had shown a high affinity for copper, although the iminodiacetic acid-type and amine/carboxylic-type resins also showed high selectivity towards iron at a controlled solution pH of 3. Even when the pH was increased and controlled at a value of 4 did these resins exhibit high selectivity towards iron. Regardless of the high nickel and cobalt extractions achieved with Amberlite IRC748, Purolite S930Plus and Purolite S991, these resins failed to selectively extract nickel and cobalt over iron.

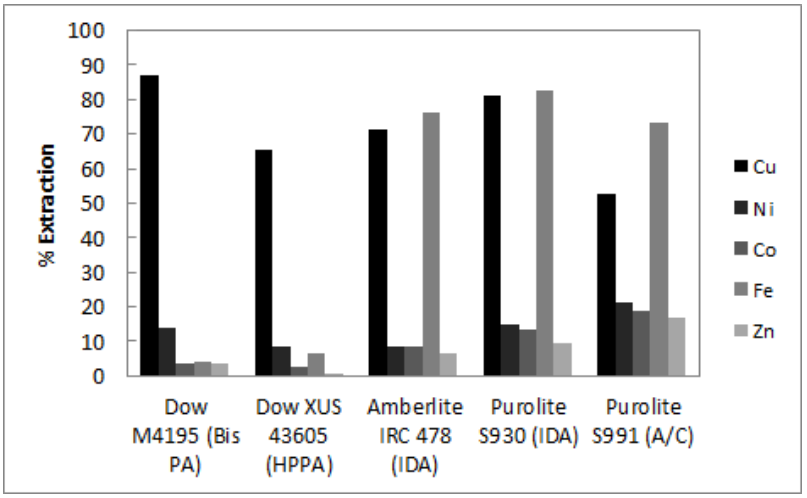

Figure 4.1: Resin screening results at a controlled solution pH of 3

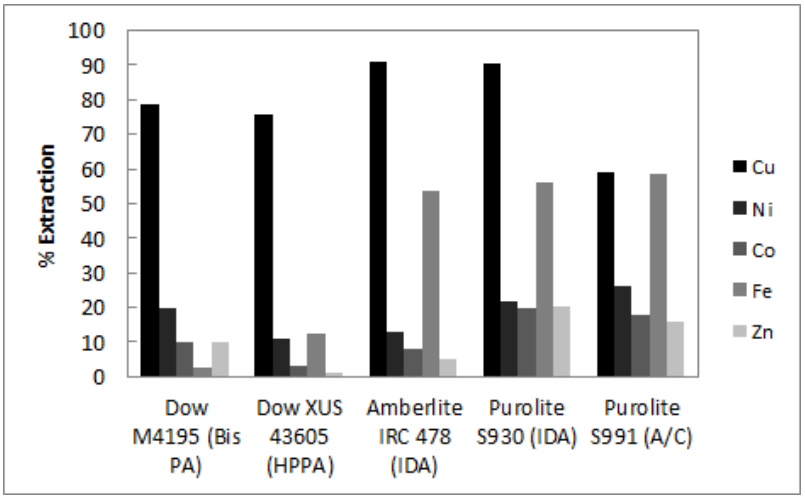

Figure 4.2: Resin screening results at a controlled solution pH of 4

The selectivity series obtained for the different resins in this study correlate well with those obtained in literature. For Dow M4195 the observed sequence of selectivity was Cu $\gg$ Ni $>$ Fe $>$ Co $\simeq$ Zn, which is similar to those reported by Grinstead (1984), Rosato *et al.* (1984), Diniz *et al.* (2005) and Mendes and Martins (2004). For the IDA-type resins the selectivity sequences also correlated well with those obtained in literature, which are Fe $>$ Cu $>$ Ni $>$ Co $>$ Zn $>$ Mn (Zainol and Nicol, 2009; Mendez and Martins, 2004; Deepatana *et al.*, 2006; Lin and Juang, 2007).

It is known that difficulties are encountered in the elution of copper from

Dow M4195 as the stability constant of the copper-bis-PA complex is very high, and thus conventional acids are not able to elute copper (Rosato *et al.*, 1984; Grinstead, 1984; Deepatana *et al.*, 2006). Instead ammoniacal solution is used. The stability constants of all metals for Dow XUS43605 are lower than for Dow M4195 (refer to figures 1 and 2 in the Appendix), thus copper can be eluted from this resin using sulfuric acid (Rodgers *et al.*, 2010). IDA resins, on the other hand, are extremely selective towards ferric iron and also highly selective towards copper, thus strong acids have to be used for the elution of these metals from the resin (Mendez and Martins, 2004; Lin and Juang, 2007; Deepatana *et al.*, 2006).

Although Amberlite IRC748 and Purolite S930 are both IDA-type resins, differences in their selectivity sequences and percentage metal extraction were observed, which were probably caused by variations in the synthesis procedure, which results in variations in the structure of the matrix, degree of cross-linking, particle size, density of the functional groups as well as proportion of iminodiacetic groups (Nicol, 2003; Zainol and Nicol, 2009). Nicol (2003) explained that the degree of cross-linking has an impact on the moisture content of the resin, and in turn the moisture content has an effect on the selectivity of a resin. A resin bead with a high moisture content has a high porosity, therefore the functional groups are spaced further apart. Zainol and Nicol (2009) compared different commercially available IDA-type resins for the recovery of nickel and cobalt from laterite leach tailings and found that Amberlite IRC748 is superior to Purolite S930Plus in both kinetics of loading and kinetics of metal elution.

Selectivities of copper, nickel and cobalt over iron are reported in table 4.1 for the various resins screened.

From the values reported in table 4.1 the following can be concluded regarding the suitability of using these resins for this application:

- All resins can selectively adsorb copper over iron at pH 4, while Amberlite IRC748, Purolite S930 and Purolite S991 failed at this purpose at pH 3.
- All resins (except for Dow XUS43605) exhibited higher iron selectivity at pH 3 than at pH 4. This is because more ferric iron is present in the solution at pH 3 than at pH 4, and as mentioned previously, all resins

Table 4.1: Separation factors of copper, nickel, cobalt and iron

	pH 3			pH 4		
Resin	α_{Fe}^{Cu}	α_{Fe}^{Ni}	α_{Fe}^{Co}	α_{Fe}^{Cu}	α_{Fe}^{Ni}	α_{Fe}^{Co}
Dow M4195 (Bis-PA)	153	0.362	0.167	1492	9.73	3.86
Dow XUS 43605 (HPPA)	26.6	0.130	0.079	226	0.878	0.429
Amberlite IRC 748 (ID)	0.767	2.9E-03	5.7E-03	87.1	0.130	0.147
Purolite S930 (ID)	0.918	3.7E-03	6.5E-03	73.0	0.217	0.381
Purolite S991 (A/C)	0.406	9.8E-03	0.017	10.1	0.250	0.309

are more selective towards ferric iron than ferrous iron. In the case of Dow XUS43605, the selectivity of copper over ferrous iron decreases from $\alpha_{Fe(II)}^{Cu}$=900 at pH 3 to $\alpha_{Fe(II)}^{Cu}$=225 at pH 4 (as determined from 2), which explains the higher extraction of iron at pH 4.

- Only Dow M4195 proved able to selectively recover nickel and cobalt over iron (at pH 4).

Based on the results of the screening tests and the discussion above, Dow M4195 and Dow XUS43605 were selected for subsequent test work. Amberlite IRC748 was also selected as it was found that it is superior to Purolite S930Plus in both kinetics of loading and kinetics of metal elution (Zainol and Nicol, 2009), and it is a less expensive resin than Dow M4195 and Dow XUS43605.

4.2 Kinetics of loading

The rates of copper and nickel adsorption onto the selected resins (Dow M4195, Dow XUS43605 and Amberlite IRC748) were determined by performing batch experiments as explained in section 3.4.2. The metal adsorption process can be considered as initially involving mass transport from the bulk of the solution to the surface of the IX bead, followed by diffusion of the metal ions into the bulk of the resin bead (Fleming and Nicol, 1980). The following reaction illustrates the mechanism:

$$[Me]_s \xrightarrow{k_s} [Me]_s^s \xleftrightarrow{k_a} [Me]_r^s \xrightarrow{k_r} [Me]_r \tag{8}$$

The subscripts s and r refer to the solution and resin phase respectively and the superscript s refers to the concentration of the metal ion at the surface of the resin particle. k_s and k_r are the mass transfer coefficients of the metal between the respective phases and k_a is the rate constant of the metal adsorption reaction.

The rate of copper loading onto the resin in a batch adsorption setup was assumed to follow a second-order approach-to-equilibrium. The second order rate expression is shown in equation 4.2.1.

$$\frac{1}{[Me]_{s,t}} - \frac{1}{[Me]_{s,0}} = k \cdot t \tag{4.2.1}$$

Zero and first-order models were also fitted, but the second-order approach-to-equilibrium model fitted the data for the first five hours of metal adsorption with all three resins the best, therefore only the data for the second order model is reported in this thesis. The goal of using the same model for modelling the equilibrium approach rate of copper and nickel adsorption for all three resins was to compare the resins based on the rate constants, k, calculated from the model.

The equilibrium loading of either copper (in the case of Dow XUS43605) or nickel (in the case of Dow M4195) on the resins at equilibrium was taken as the reference point. Following from this, the rate expression in equation 4.2.1 can therefore be expressed in terms of the rate at which metal extraction equilibrium is attained:

$$\frac{1}{[Me]_{r,e} - [Me]_r} - \frac{1}{[Me]_{r,e}} = k \cdot t \tag{4.2.2}$$

As will be discussed in chapter 5, it is more desirable in the dynamic recovery of metals for a resin to have a lower capacity and attain equilibrium fast than for the resin to have a high capacity and attain equilibrium slowly. In the former case the resin capacity is utilized to a greater extent and such a resin can operate well at a higher flow rate, whereas in the latter case resin

capacity is utilized to a lesser degree and the resin functions poorly at a high flow rate. This principle will be demonstrated and discussed in chapter 9.

By plotting the term on the left of equation 4.2.2 versus time and fitting a straight line to the data, the rate constant of copper adsorption approach to equilibrium can be determined from the slope of the line.

4.2.1 Rate of copper loading onto IX resins

Plots of the kinetic data of copper adsorption onto Dow M4195, Dow XUS43605 and Amberlite IRC748 at controlled solution pH values of 2, 3 and 4 are shown in figures 4.3, 4.4 and 4.5, respectively.

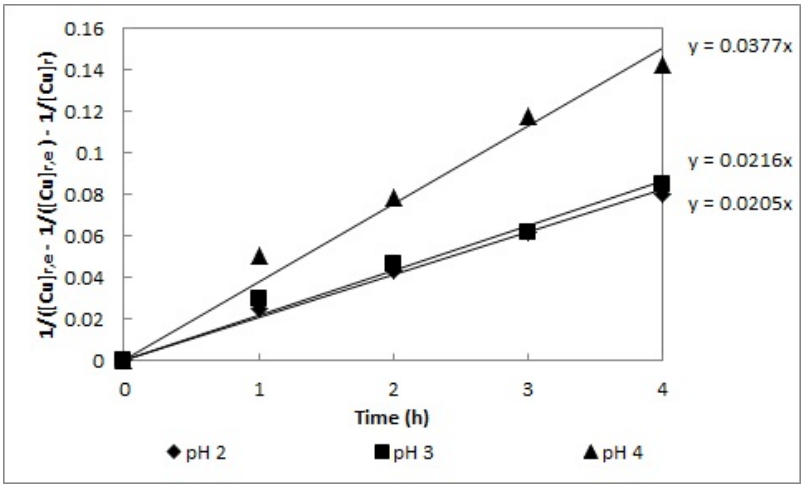

Figure 4.3: Kinetics of copper loading onto Dow M4195

The rate of approach to equilibrium of copper adsorption with Dow M4195 increased as the solution pH was increased from 2 to 4. With reference to figures 4-6 in Appendix B, the degree of copper adsorption decreased from 80% to 65% as the pH increased from 2 to 4, while nickel adsorption increased from 1% to 20%. This can be explained by the pH distribution profiles of copper and nickel for Dow M4195 (see figure 1 in Appendix A as determined by Grinstead (1984)). The resin is extremely selective towards copper, even at pH values below zero. The copper adsorption constant (K) reaches a maximum at pH 1.5 and remains constant as the pH increases beyond this point. The resin is, however, much less selective towards other metals such as nickel and cobalt

at low solution pH values and its selectivity towards these metals increases rapidly as the pH increases to values higher than 2, especially for cobalt and zinc. Therefore, as the pH was increased the competition between copper and other metals in the solution for active sites became more significant and because nickel occupied larger fractions of the available sites at pH values of 3 and 4, the resin reached its maximum capacity for copper at a faster rate at these pH values.

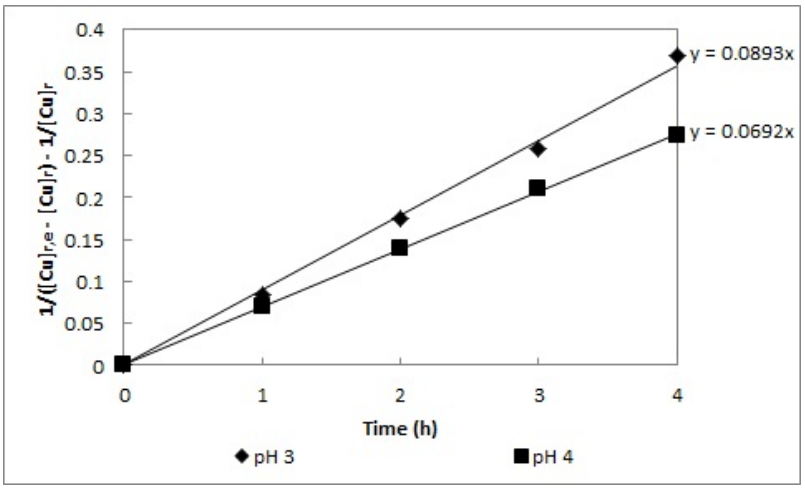

Figure 4.4: Kinetics of copper loading onto Amberlite IRC748

Amberlite IRC748's selectivity towards ferric iron was greater than it was towards copper at a solution pH of 2, therefore the copper that was initially adsorbed onto the resin was later displaced by ferric iron (see figures 7 in Appendix B). Hence, a second-order rate constant for copper adsorption onto Amberlite IRC748 at a pH of 2 could not be determined. As the solution was neutralized to pH values of 3 and 4, the majority of the ferric iron precipitated out of the solution and therefore copper was at the top of the selectivity series of the resin at these pH values (figures 8 and 9 in Appendix B). In terms of the copper adsorption rate constants determined at pH 3 and 4, the opposite trend was observed for Amberlite IRC748 than for Dow M4195. As opposed to Dow M4195 which reaches its maximum copper capacity at a pH of 1, the capacity of Amberlite IRC748 for copper is only achieved at a pH value of 3.5-4, and that for nickel is achieved at a pH of 4. Thus, because of the resin's

higher capacity for copper at pH 4, it took more time to utilize this capacity than it did at pH 3.

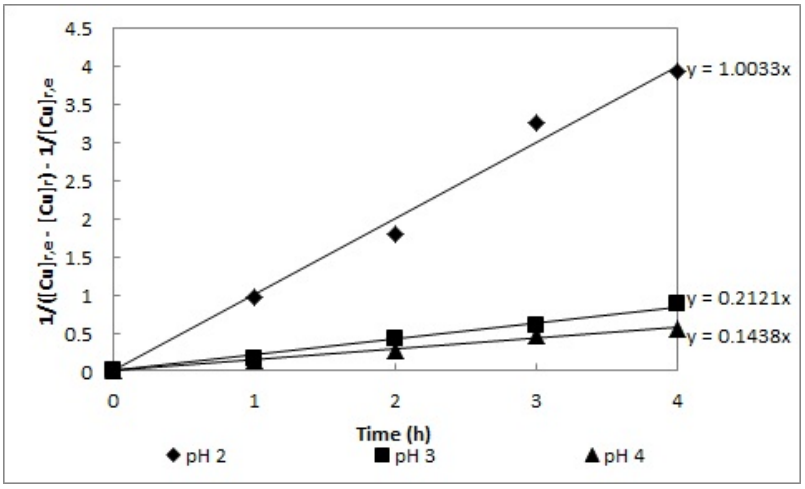

Figure 4.5: Kinetics of copper loading onto Dow XUS43605

Similar to Amberlite IRC748, the copper capacity of Dow XUS43605 increased as the pH of the bioleach solution increased, which is evident from figures 10-12 in Appendix B, and therefore the rate of approach to equilibrium for copper adsorption decreased with increasing pH.

Shown in table 4.2 are the equilibrium loadings of metals on Dow M4195, Amberlite IRC748 and DowXUS43605 and the rate constants of copper loading onto the resins as determined from figures 4.3 to 4.5 at a solution pH of 4. It should be noted that the trends observed at pH 2 and 3 were the same as in the discussion that follows.

Table 4.2: Pseudo-equilibrium and kinetic parameters for Cu loading

Resin	**Metal loading after 4h** $(\frac{g}{L})$					**Rate constant**	$\mathbf{R^2}$
	Cu	*Ni*	*Co*	*Fe*	*Zn*	$\mathbf{k}_{Cu}$ $(\frac{L}{g.h})$	
M4195	16.38	14.74	0.30	0.16	0.17	0.038	0.98
IRC 748	29.25	9.95	0.27	0.81	0.29	0.069	0.99
XUS43605	22.88	6.49	0.10	0.10	0.08	0.144	0.986

In general the rate of copper loading decreased in the order Dow XUS-43605>Amberlite IRC748>Dow M4195. Equilibrium with Dow XUS43605

was attained twice as fast as with Amberlite IRC748, and almost 4 times as fast as with Dow M4195. From a kinetic point of view Dow XUS43605 poses a significant advantage over Dow M4195 and Amberlite IRC748. In terms of equilibrium loading, the highest copper loading was observed for Amberlite IRC748, followed by Dow XUS43605 and Dow M4195. Despite its high selectivity for copper, Dow M4195 co-extracted a significant amount of nickel, which reflects this resin's high affinity for nickel at this pH. Although Dow XUS43605 has a lower total capacity (25-30 g/L Cu) compared with Dow M4195 (35-40 g/L Cu) and Amberlite IRC748 (37-42 g/L Cu), it extracted copper efficiently with the least amount of co-extraction of other metals.

Based on these results Dow XUS43605 was selected to recover copper from the pregnant bioleach solution. Subsequent test work was performed on this resin in dynamic column adsorption studies, which will be discussed in chapter 5.

4.2.2 Rate of nickel loading onto IX resins

The same approach that was followed to determine the rate of copper loading onto Dow M4195, Amberlite IRC748 and Dow XUS43605 was followed to determine the loading rates of nickel onto these resins.

To determine the rate of approach to equilibrium for nickel adsorption in each case,

$$\frac{1}{[Ni]_{r,e} - [Ni]_r} - \frac{1}{[Ni]_{r,e}} \tag{4.2.3}$$

was plotted versus time and the slope of the linear line fitted to the data was taken to be the rate constant. The kinetic data of nickel adsorption onto Dow M4195, Amberlite IRC748 and Dow XUS43605 are plotted in figures 4.6 to 4.8.

As the pH increased from 2 to 4, the selectivity of Dow M4195 towards nickel increased, therefore the nickel equilibrium loading on this resin increased and hence the rate of loading decreased.

For Amberlite IRC748 it was not possible to calculate rate constant at solution pH's of 2 and 3 because of the resin's high affinity towards iron. As for copper, nickel that was initially loaded onto the resin was displaced by iron at a later stage. At a pH of 4 the resin exhibited the highest nominal nickel

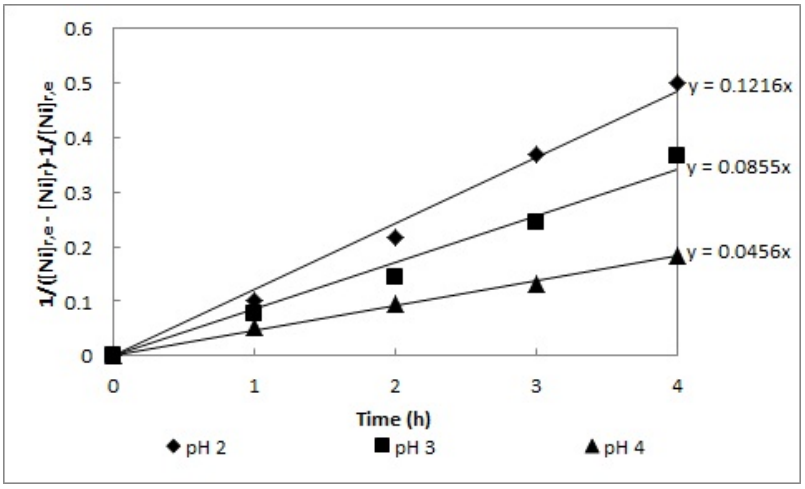

Figure 4.6: Kinetics of nickel loading onto Dow M4195

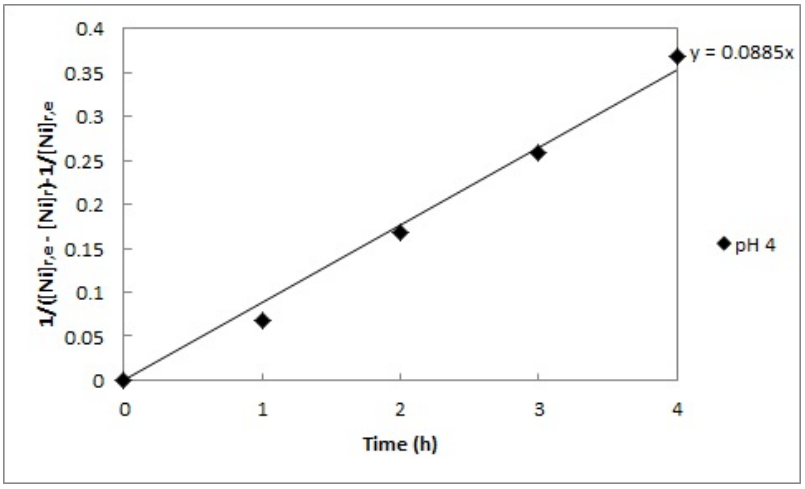

Figure 4.7: Kinetics of nickel loading onto Amberlite IRC748

loading, extracting almost 70% of the nickel in the solution, but in terms of selectively extracting nickel and cobalt the resin did not perform well, co-extracting between 60 and 70% of the other impurities present in the solution.

Finally, the results obtained for Dow XUS43605 are shown in figure 4.8. The pH did not influence the kinetics of nickel loading onto this resin significantly, but as can be seen from figures 19 to 21 in Appendix B, the resin's selectivity towards nickel was poor and extraction of this metal increased by a mere 10%, from 23% to 33%, by increasing the pH from 2-4.

The rate constants for nickel adsorption onto Dow M4195, Amberlite IRC748 and Dow XUS43605 are shown in table 4.3, as well as the equilibrium loadings

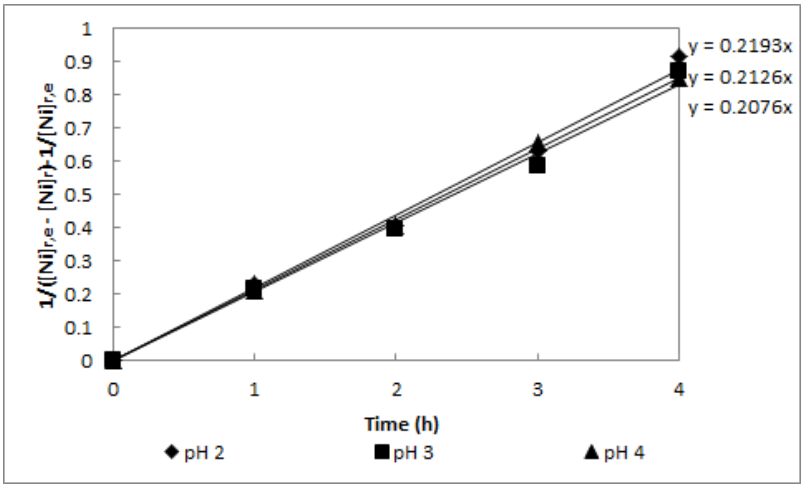

Figure 4.8: Kinetics of nickel loading onto Dow XUS43605

achieved with these resins.

Table 4.3: Pseudo-equilibrium and kinetic parameters for Ni loading (pH 4)

Resin	**Metal loading after 4h** $(\frac{g}{L})$				**Rate constant**	$\mathbf{R^2}$
	Ni	*Co*	*Fe*	*Zn*	$\mathbf{K}_{Ni}$ $(\frac{\mathbf{L}}{\mathbf{g.h}})$	
M4195	22.6	0.198	0.215	0.094	0.045	0.99
IRC 748	29.95	0.489	0.895	0.446	0.074	0.99
XUS43605	15.5	0.152	0.735	0.071	0.182	0.99

Despite the slower kinetics of Dow M4195, a loading of 22.6 g/L nickel was achieved after 4 hours, which is considerably higher than the 16 g/L nickel loading obtained with Dow XUS43605 that is a resin that attains equilibrium at a relatively fast rate. Once again, the highest nominal loading was observed at pH 4 for Amberlite IRC748, but the selectivity of this resin towards nickel was lower than for Dow M4195 as a result of its higher selectivity towards the other metals in the solution. Amberlite IRC748 extracted on average 4 times as much impurities at pH 4 as Dow M4195. Based on the kinetic results in conjunction with the equilibrium loadings achieved with the three resins, Dow M4195 was selected to recover nickel and cobalt from the bioleach solution. The dynamic metal loading and elution behaviour of this resin was further investigated in column loading and elution experiments as discussed in chapters 5 and 6.

4.2.3 Effect of temperature on metal loading rate

It was necessary to establish the effect of temperature on the kinetics of metal loading onto the selected resins as the bioleach solution exits the heap bioleach at 60-65°C. It has been reported previously that the kinetics of adsorption increase with increasing temperature (Sirola *et al.*, 2010*b*), but as the adsorption reaction is exothermic in nature, the equilibrium constant is expected to be lower at higher temperatures (Sirola *et al.*, 2010*a*). The effect of temperature on the rate of copper adsorption onto Dow XUS43605 and nickel loading onto Dow M4195 was investigated and the results are reported in figures 4.9 and 4.10.

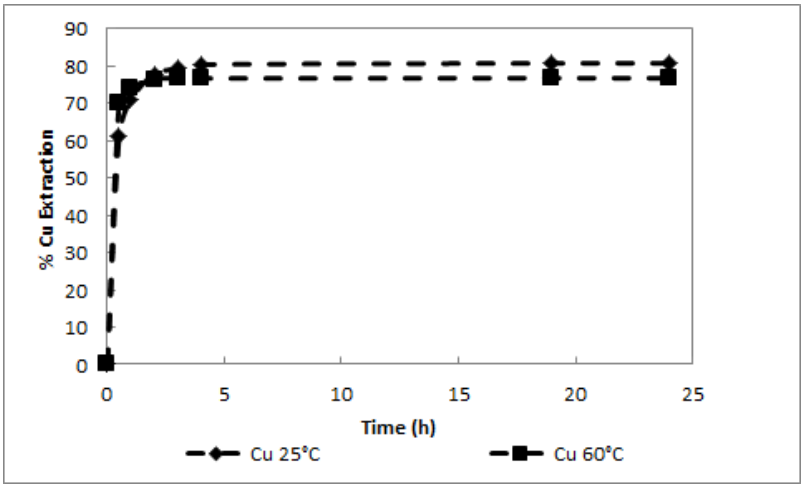

Figure 4.9: The effect of temperature on the kinetics of copper loading onto Dow XUS43605

Although the copper extraction at equilibrium was lower at 60°C than at 25°C (see figure 4.9), equilibrium was attained at a faster rate at the elevated temperature, which is consistent with literature (Sirola, 2009; Sirola *et al.*, 2010*a*,*b*). It is clear that the rate of metal loading increased considerably when the temperature was increased to 60°C. The distribution of copper at equilibrium decreased from 210 to 165 when the temperature was increased from 25°C to 60°C.

Equilibrium for nickel loading onto Dow M4195 was also attained at a much faster pace when the temperature increased from 25°C to 60°C, while

the equilibrium loading itself decreased from 27 g/L to 24.7 g/L for the increase in temperature (see figure 4.10).

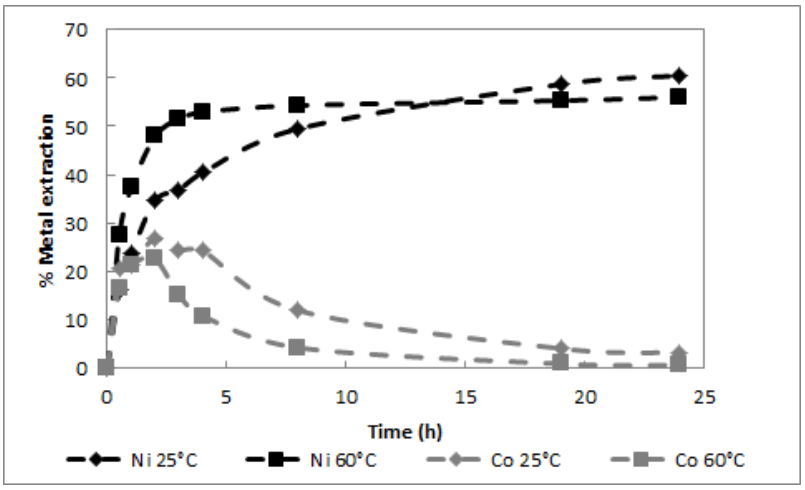

Figure 4.10: The effect of temperature on the rate of nickel and cobalt loading onto Dow XUS43605

4.3 Equilibrium isotherms and isotherm modelling

The effect of the metals concentration in the bioleach solution on the equilibrium concentrations of metals on Dow XUS43605 and Dow M4195 was investigated by contacting these resins with solution A and solution B, respectively, at resin to solution ratios of 1:5, 1:15, 1:30, 1:50, 1:75, 1:100 and 1:120. These experiments were all carried out at room temperature. Single component Langmuir and Freundlich isotherm models were fitted to the data for copper loading on Dow XUS43605 and that for nickel loading on Dow M4195.

4.3.1 Metal equilibrium isotherms for Dow XUS43605

The metal binding isotherms for Dow XUS43605 are shown for individual metals in figure 4.11[1]. From the graphs in figure 4.11 it is clear that the selectivity of Dow XUS43605 was the highest towards copper, nickel and iron. The resin

[1]Units of axes in figure 4.11: horizontal axes in ppm and vertical axes in g/L

was not selective towards Co, Zn, Mn and Al (although not illustrated in the figure) and less than 25 ppm copper was able to displace these metals from the resin.

The maximum observed copper capacity was 24 g/L. It can be seen that the maximum nickel adsorption achievable with this resin (11 g/L) occurred when the copper concentration in the solution was less than 50 ppm. Nickel was displaced by copper when its concentration in the solution increased beyond 50 ppm. Thus, these results indicate that the equilibrium concentration of nickel on Dow XUS43605 would be zero if the solution contains more than $\pm$250 ppm copper.

The selectivity of Dow XUS43605 towards iron was sufficiently high, which illustrates the importance of removing this impurity metal completely prior to the IX process. The results indicate that the iron concentration on the resin increased with increasing iron concentration in the solution, even though the copper concentration increased as well. Because of the low concentration of iron in the solution treated in this project at a pH of 4, it does not pose a significant threat to the achievable copper loading on the resin since the maximum iron concentration on the resin observed was $\pm$500 ppm.

4.3.2 Metal equilibrium isotherms for Dow M4195

The metal binding isotherms for Dow M4195 at solution pH values of 2 and 4 are shown in figures 4.12[2] and 4.13[3], respectively.

The selectivity of Dow M4195 towards nickel over other metals was high at pH 2 (see figure 4.12). At this solution pH the maximum observed nickel capacity was 23.9 g/L. The selectivity of the resin towards iron was lower than that of Dow XUS43605, but iron adsorption still occurred to a significant extent and nickel was not able to completely displace iron in the concentration range studied.

Cobalt and zinc selectivities were much the same at pH 2. Both metals loaded to some extent when the nickel concentration in the solution was sufficiently low (lower than 300 ppm). Manganese and aluminium selectivities

[2]Units of axes in figure 4.12: horizontal axes in ppm and vertical axes in g/L
[3]Units of axes in figure 4.13: horizontal axes in ppm and vertical axes in g/L

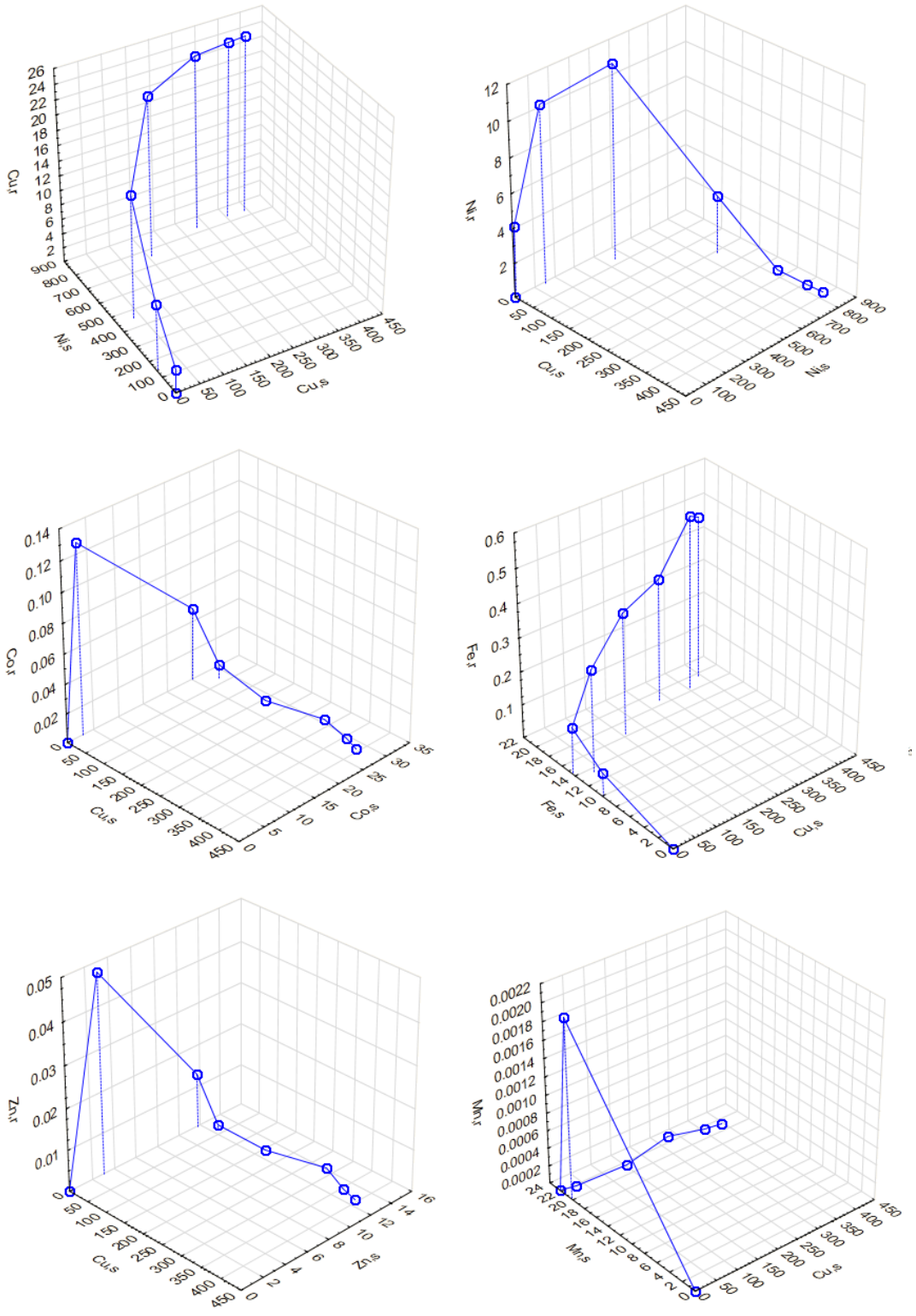

Figure 4.11: Multi-component metal isotherms for Dow XUS43605. Solution pH = 4; temperature = 25°C

were low and the highest loadings achieved on Dow M4195 at very low nickel concentrations (less than 50 ppm) for these metals were 8 and 12 ppm, respectively.

From figure 4.13 the nickel selectivity for Dow M4195 was still the highest at a controlled solution pH of 4, but selectivities of all other metals increased relative to the resin's selectivities towards these metals at pH 2. The resin's capacity for nickel increased from 23.9 g/L at pH 2 to 29.88 g/L at pH 4. The maximum achievable capacity of the resin for cobalt was observed to be 409 ppm at nickel concentrations below 10 ppm. When the nickel concentration increased to higher values cobalt was gradually displaced from the resin until its displacement reached completion at ± 500 ppm nickel in the solution.

Once again, zinc selectivity was observed to be similar to that of cobalt. Approximately 170 ppm zinc was adsorbed at low nickel concentration and as nickel concentration increased zinc was gradually displaced into the solution. Dow M4195 did not exhibit much selectivity towards manganese and aluminium as the maximum observed loading of these metals were 14 and 35 ppm, slightly higher than observed at pH 2.

4.3.3 Isotherm modelling

The most widely used models to describe equilibrium loading of metals onto IX resins are the Linear, Freundlich and Langmuir isotherms (equations 4.3.1, 4.3.2 and 4.3.3 respectively).

$$Q_r = KC_s \tag{4.3.1}$$

$$Q_r = A(C_s)^{1/n} \tag{4.3.2}$$

$$Q_r = \frac{(Q_{r,max}C_s b)}{(Q_{r,max} + bC_s)} \tag{4.3.3}$$

The Freundlich model (equation 4.3.2) is empirically based and describes adsorption based on heterogeneous surface energy. The constant 1/n is a measure of the adsorption intensity or surface heterogeneity and for favourable

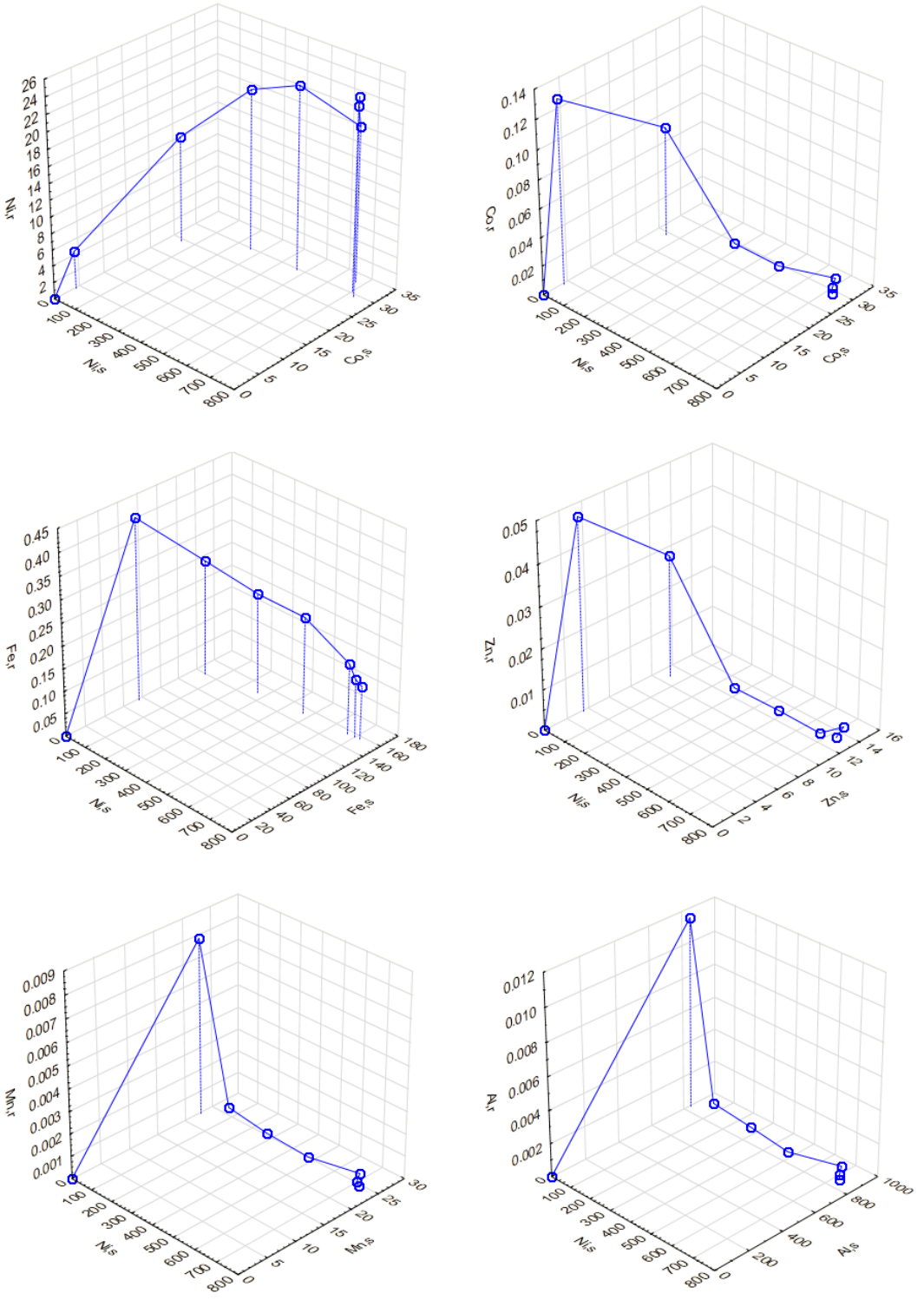

Figure 4.12: Multi-component metal isotherms for Dow M4195. Solution pH = 2; temperature = 25°C

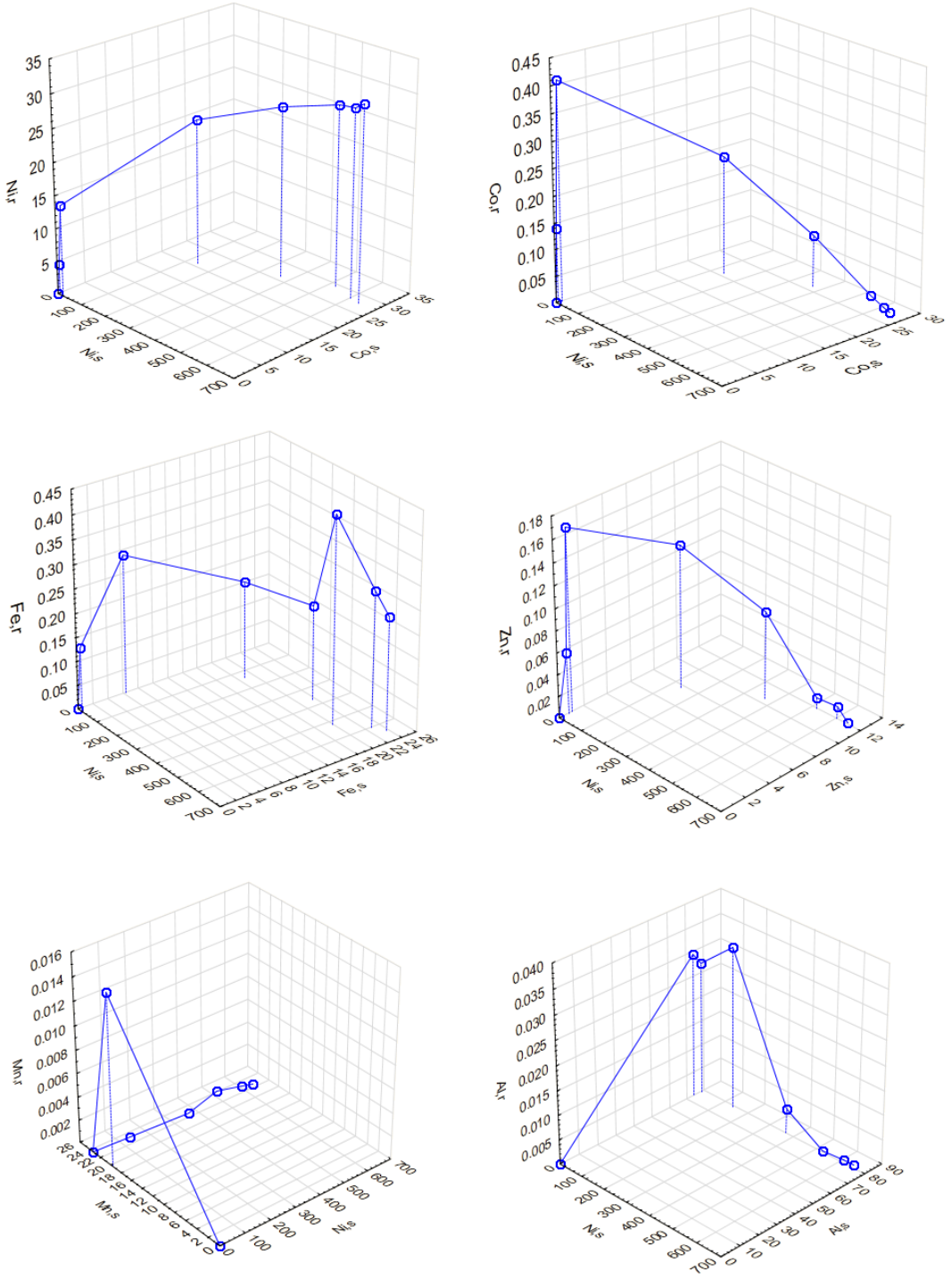

Figure 4.13: Multi-component metal isotherms for Dow M4195. Solution pH = 4; temperature = 25°C

adsorption it should vary between 0 and 1. Values of 1/n close to zero indicate heterogeneous adsorption while values above 1 mean that adsorption is unfavourable (Zainol and Nicol, 2009).

The Langmuir model (equation 4.3.3) assumes a finite amount of equivalent adsorption sites and maximum coverage is attained when all these sites are filled. The constant $Q_{r,max}$ is related to the area covered by a monolayer of metal ion and is a reflection of the maximum adsorption capacity while the constant b is a direct measure of adsorption intensity. The values of $Q_{r,max}$ and b can be obtained by linearizing the equation, plotting C_s/Q_r against C_s, fitting a straight line to the data and evaluating the slope and intercept of the line (Zainol and Nicol, 2009).

The Freundlich isotherm (equation 4.3.2) usually fits the adsorption data better when metal sorption is low while the Langmuir isotherm (equation 4.3.3) provides a better fit when loading is high. The linear isotherm (equation 4.3.1) is not used very often but can be used to model metal adsorption from very dilute solutions (Riveros and Cooper, 1988).

Single component Langmuir and Freundlich isotherms (equations 4.3.3 and 4.3.2) were fitted to the equilibrium data of copper binding with Dow XUS43605 and the data of nickel binding with Dow M4195. The results are shown in figures 4.14 and 4.15.

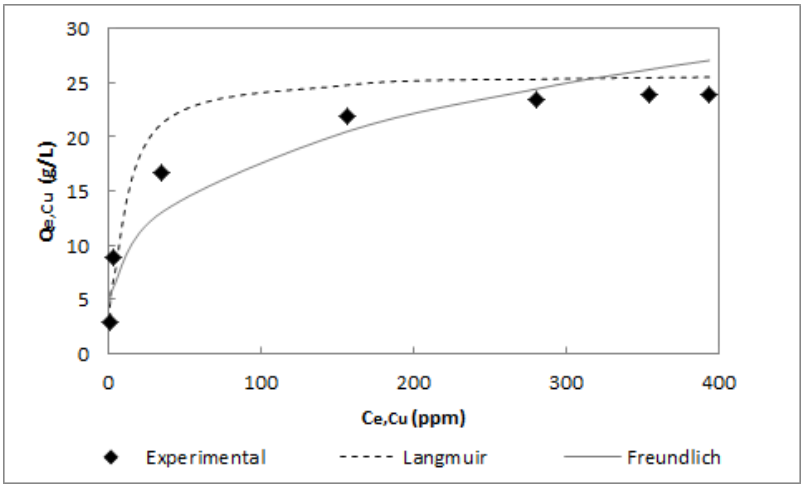

Figure 4.14: Modelling of copper adsorption isotherm for Dow XUS43605. Solution pH = 4; temperature = 25°C

Table 4.4: Parameters of Langmuir and Freundlich models for copper binding with Dow XUS43605

Parameter	Langmuir	Freundlich
Q_m	26.04	-
b	128	-
A	-	35.83
n	-	0.3
R^2	0.964	0.88

The parameters of the Langmuir and Freundlich models for copper adsorption with Dow XUS43605 are reported in table 4.4. The data in the table indicates that the Langmuir model provided a better fit for the equilibrium data than the Freundlich model. Because these models are generally used to model single component isotherms, they did not provide fits comparable to single component systems in this thesis since the system is more complex in nature. Both models accurately predicted the copper concentration on the resin at low copper concentrations, but deviation was larger at intermediate and high copper concentrations. For the Langmuir isotherm, which provided a satisfactory fit for the data, a constant over-prediction of copper loading on the resin was observed, which is believed to be the influence of other metals adsorbing to the resin, especially nickel and iron (as was shown in figure 4.11).

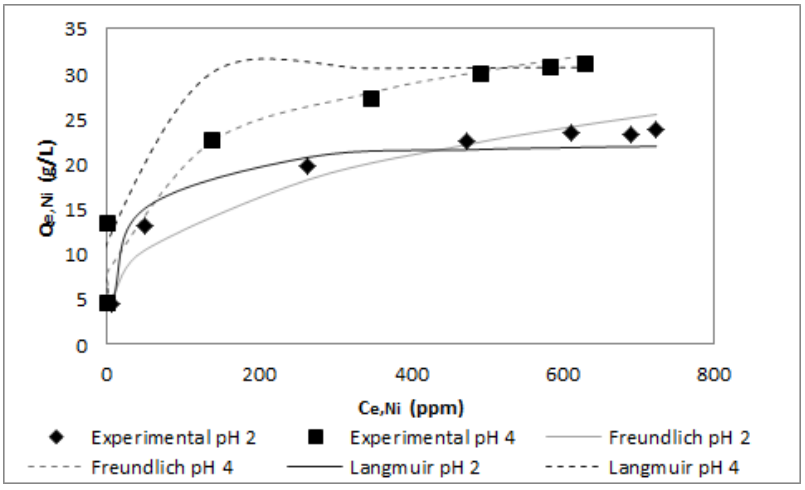

Figure 4.15: Modelling of nickel adsorption isotherms for Dow M4195. Solution pH = 2 and 4; temperature = 25°C

Table 4.5: Parameters of Langmuir and Freundlich models for nickel binding with Dow M4195

	pH 2		**pH 4**	
Parameter	**Langmuir**	**Freundlich**	**Langmuir**	**Freundlich**
Q_m	22.72	-	30.86	-
b	40	-	324	-
A	-	28.38	-	35.66
$\frac{1}{n}$	-	0.3316	-	0.232
R^2	0.995	0.96	0.97	0.86

For nickel binding with Dow M4195 the Langmuir model once again represented the actual data better than the Freundlich model at both solution pH values of 2 and 4 (figure 4.15). The parameters of these models are indicated in table 4.5. Although the nickel capacity of the resin was lower at pH 2 than at pH 4, its selectivity towards other metals present in the solution was sufficiently low so that it did not influence the nickel binding to such an extent as at a solution pH of 4, therefore both models performed better at pH 2. The Freundlich model described the data in the mid and high nickel concentration range better than in the low range, whereas the Langmuir model failed to predict the nickel loading on the resin only in the mid-range.

Chapter 5

Column Loading Results

Dynamic column sorption studies were performed to recover the MOI from the bioleach solution with Dow M4195, Amberlite IRC748 and Dow XUS43605 and to determine the effects of different process parameters on copper, nickel and cobalt recovery with these resins. A detailed discussion of the experimental procedures followed in these experiments was given in chapter 3.5.

5.1 Metal breakthrough profiles for Dow M4195, Dow XUS43605 and Amberlite IRC748

The dynamic metal loading characteristics of Dow M4195, Dow XUS43605 and Amberlite IRC748 were studied in column adsorption experiments. Although Dow XUS43605 was selected for copper recovery and Dow M4195 for nickel and cobalt recovery based on the batch kinetic and equilibrium studies, Amberlite IRC748 was also tested for the recovery of the MOI in dynamic column adsorption experiments.

5.1.1 Recovery of copper

The breakthrough profiles for Dow M4195, Dow XUS43605 and Amberlite IRC748 are illustrated in figures 5.1 to 5.6. In these graphs the ratio of each metal's concentration in the effluent (C_o) to its concentration in the inlet (C_i)

is plotted versus the volume of effluent collected. All experiments were carried out at room temperature and the loading rate used was 10 BV/h. The solution type used was solution A (containing copper) at an initial pH of 3 (figures 5.1 to 5.3) and 4 (figures 5.4 to 5.6).

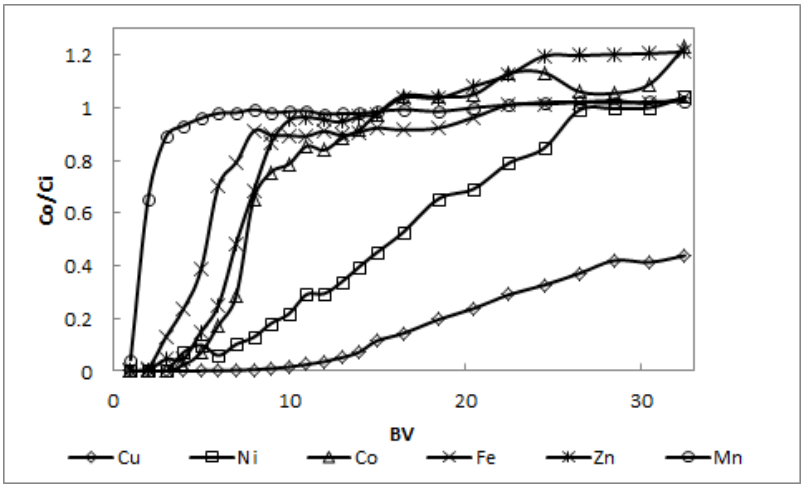

Figure 5.1: Metal breakthrough profiles for Dow M4195. Loading conditions: solution A; initial solution pH = 3; flow rate = 10 BV/h; temperature = 25°C

The selectivity sequence of Dow M4195 in figure 5.1 was more or less the same as that obtained in the batch experiments, which was Cu>Ni>Co≈Zn>Fe at an initial solution pH of 3. Because manganese was not included in the solution in the screening tests, it is apparent from figure 5.1 that the resin is the least selective towards manganese. The slower rate at which metal adsorption with Dow M4195 attained equilibrium was demonstrated by the early breakthrough of copper, which occurred at BV 10, and the wide MTZ (the slope of the copper breakthrough profile after copper breakthrough occurred) in comparison with Dow XUS43605 (see figure 5.2). Also apparent from this graph is the resin's high selectivity towards nickel (in comparison with Dow XUS43605 and Amberlite IRC748 in figures 5.2 and 5.3). The overshoot observed for metals such as cobalt and zinc resulted from other metals (mainly copper and nickel) adsorbing onto the resin and displacing the initially adsorbed cobalt and zinc from the resin.

From figure 5.2 it is clear that the relative selectivity of Dow XUS43605 towards copper was higher than for Dow M4195. Nickel was the only metal that

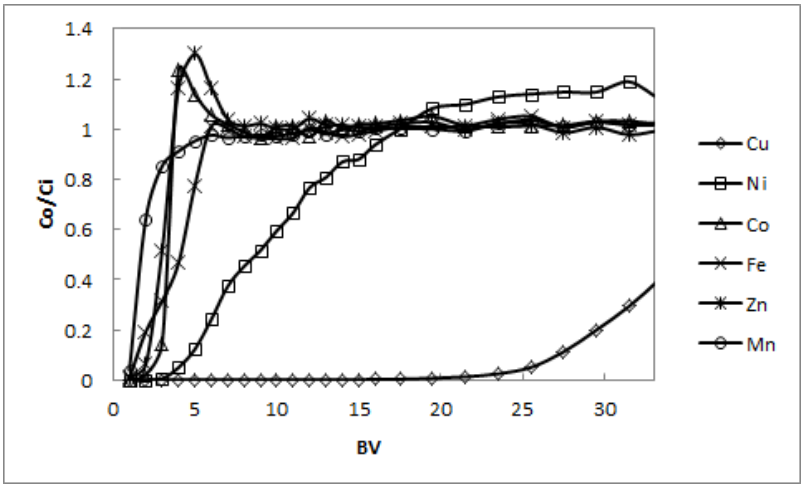

Figure 5.2: Metal breakthrough profiles for Dow XUS43605. Loading conditions: solution A; initial solution pH = 3; flow rate = 10 BV/h; temperature = 25°C

co-loaded onto the resin to a significant extent. Early breakthrough of cobalt, zinc, iron and manganese was observed, and the adsorbed metals were almost immediately displaced from the resin by copper and nickel, hence the overshoot observed for these metals. The faster rate at which metal adsorption with this resin attained equilibrium was also demonstrated by the later breakthrough of copper, which occurred at BV 22, and the steeper slope of the breakthrough profile after copper had broken through the resin bed.

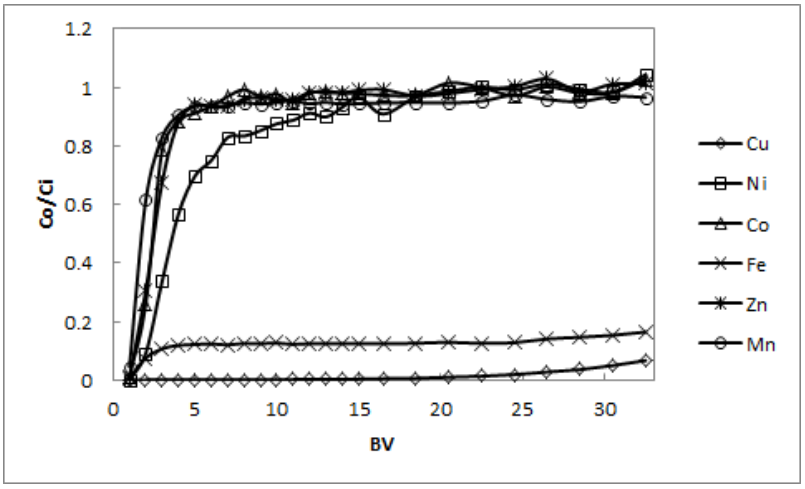

Figure 5.3: Metal breakthrough profiles for Amberlite IRC748. Loading conditions: solution A; initial solution pH = 3; flow rate = 10 BV/h; temperature = 25°C

Amberlite IRC748 in the protonated form also performed well in terms of copper loading. Less co-loading of nickel was observed at the conditions tested than for Dow M4195 and Dow XUS43605, and cobalt, zinc and manganese breakthrough occurred at an early stage. As would be expected, iron loaded onto the resin to a significant extent. Although only the total iron concentration was determined for all feed solutions and column effluents, the shape of the iron breakthrough curve can be explained with much certainty: Fe(II) breakthrough occurred after 5 BVs and Fe(III) breakthrough started occurring at the same time as copper breakthrough. Copper and Fe(III) breakthrough occurred at approximately 25 BVs, illustrating the resin's high affinity for these metals. The slower rate at which metal adsorption with this resin attained equilibrium was also demonstrated by the slower rate of copper and Fe(III) breakthrough, indicating that the resin was not nearly saturated with these metals when breakthrough started occurring.

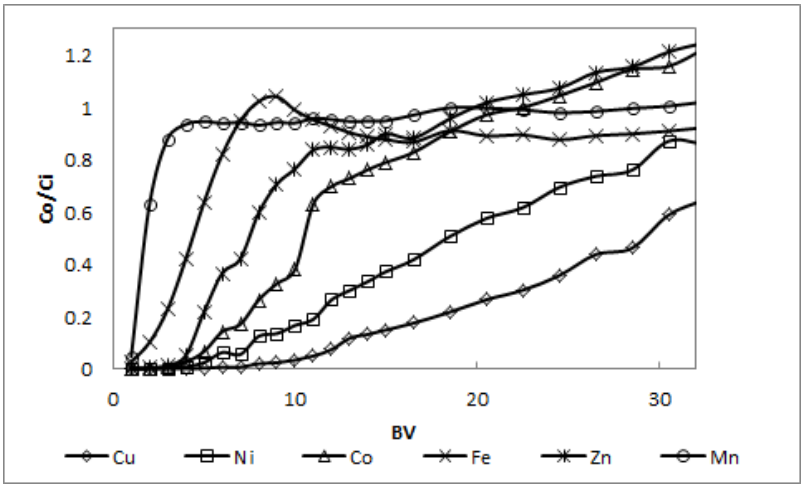

Figure 5.4: Metal breakthrough profiles for Dow M4195. Loading conditions: initial solution pH = 4; flow rate = 10 BV/h; temperature = 25°C

When the pH of the solution was raised to 4, the selectivity series of Dow M4195 towards the metals present in the solution became much more pronounced (see figure 5.4). Less copper loaded onto the resin at an initial solution pH of 4 as a result of the resin's increased affinity towards other metals, especially nickel. It is clear from the results in figures 5.1 and 5.4 that Dow M4195 is not suitable for the dynamic (or continuous) recovery of copper.

Besides, the difficulty encountered in the elution of copper from Dow M4195 due to the high stability constant of copper complexation with bis-PA, further motivates this statement.

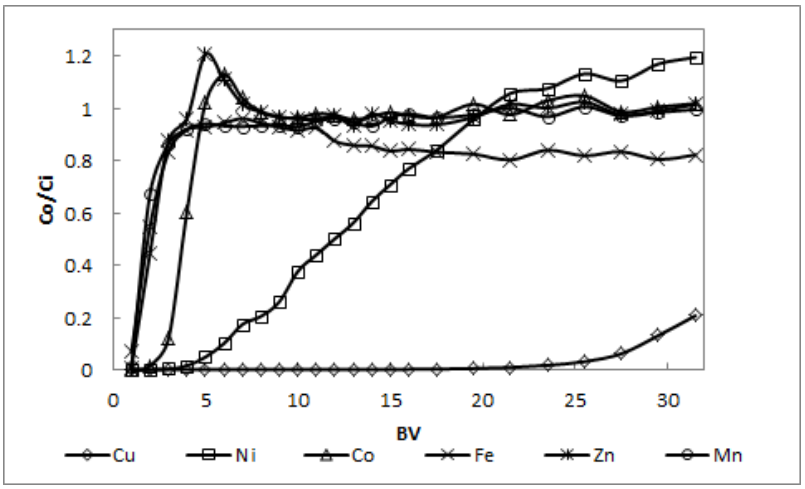

Figure 5.5: Metal breakthrough profiles for Dow XUS43605. Loading conditions: solution A; initial solution pH = 4; flow rate = 10 BV/h; temperature = 25°C

Breakthrough of copper for Dow XUS43605 when the initial solution pH was raised to 4 occurred at the same stage as when the solution pH was 3, indicating that the copper loading on Dow XUS43605 was not significantly influenced in the pH range of 3-4. More nickel was loaded, however, at the higher pH. The selectivity of the resin towards cobalt, zinc, iron and manganese remained low as demonstrated by the early breakthrough of these metals. The results for this resin (figures 5.2 and 5.5) showed that it is suitable for the dynamic recovery of copper. Also, the stability constant of copper complexation with HPPA is lower than for copper complexation with bis-PA and IDA, therefore it is expected that this metal can be removed from Dow XUS43605 with more ease than from Dow M4195 and Amberlite IRC748.

For Amberlite IRC748 the copper loading increased significantly when the initial solution pH was raised to 4. The resin's affinity towards all the other metals also increased, except towards iron. The decrease in iron selectivity could be attributed to the higher ferrous to ferric iron ratio at pH 4 and the resin's lower selectivity towards ferrous iron. Despite its high capacity and good copper selectivity, its selectivity towards other metals is also higher

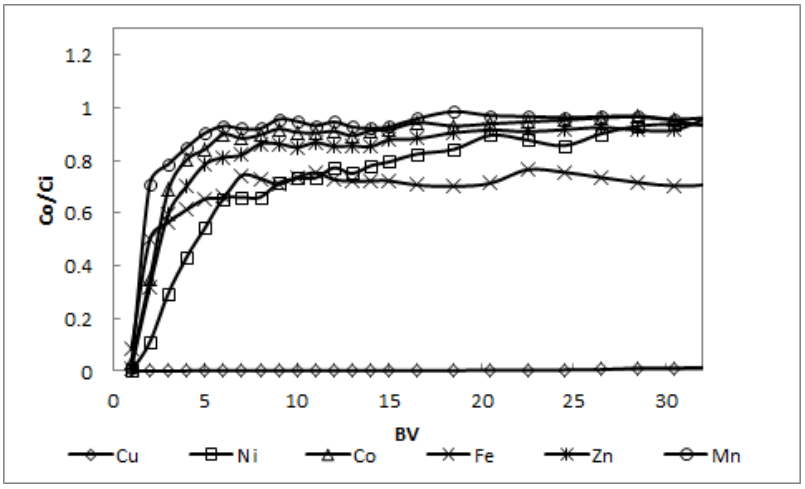

Figure 5.6: Metal breakthrough profiles for Amberlite IRC748. Loading conditions: solution A; initial solution pH = 4; flow rate = 10 BV/h; temperature = 25°C

than for Dow XUS43605. Furthermore, the ferric iron present in the solution chemically fouls Amberlite IRC748 as it cannot be effectively eluted from the resin and the sites that it occupy are not available for other metals to attach to. Also, stronger acid has to be used to elute copper from the resin, therefore it was decided that this resin is also not suitable for copper recovery in this application.

5.1.2 Recovery of nickel and cobalt

The dynamic recovery of nickel and cobalt with Dow M4195, Dow XUS43605 and Amberlite IRC748 was also tested in column adsorption experiments. The conditions at which the experiments were carried out were the same as those used in the dynamic copper recovery experiments. Solution B (the same as solution A, except that it did not contain copper) was used at an initial solution pH of 3 (figures 5.7 to 5.9) and 4 (figures 5.10 to 5.12) in these experiments.

As for copper, early nickel breakthrough occurred with Dow M4195, and once again the slower rate at which this resin attained equilibrium was demonstrated by the wide MTZ. Nickel and cobalt recovery with this resin was better than with Dow XUS 43605 and Amberlite IRC748 in the protonated form (see figures 5.8 and 5.9) at the conditions tested. The resin did however co-adsorb zinc and iron to a greater extent than Dow XUS43605, but the better nickel

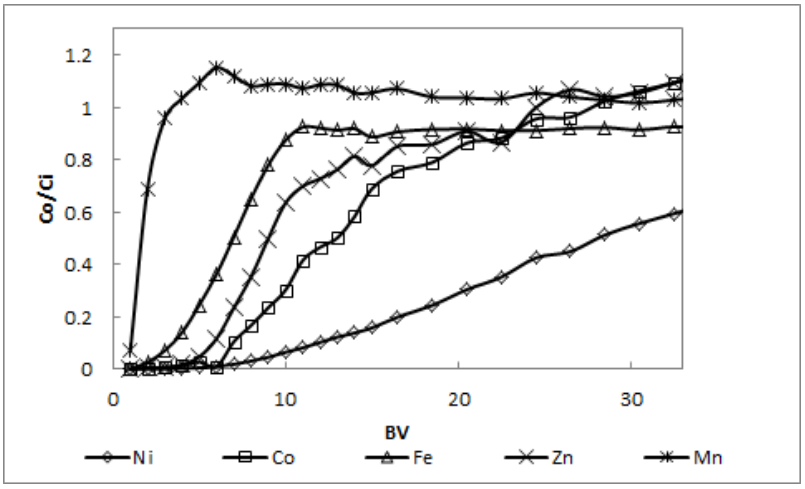

Figure 5.7: Metal breakthrough profiles for Dow M4195. Loading conditions: solution B; initial solution pH = 3; flow rate = 10 BV/h; temperature = 25°C

and cobalt recovery achieved with Dow M4195 was considered to outweigh the higher degree of impurity metals loaded onto the resin.

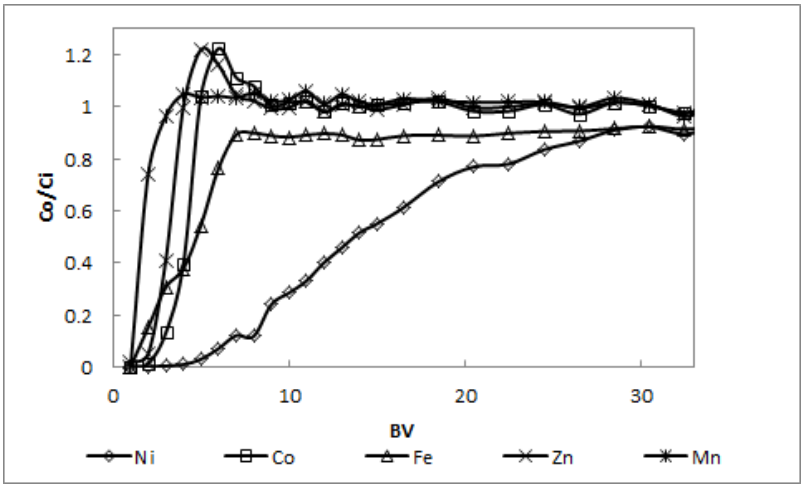

Figure 5.8: Metal breakthrough profiles for Dow XUS43605. Loading conditions: solution B; initial solution pH = 3; flow rate = 10 BV/h; temperature = 25°C

Nickel breakthrough occurred at an earlier stage and at a faster pace for Dow XUS43605 than for Dow M4195, illustrating the lower selectivity of this resin towards nickel. Also, cobalt selectivity was low as it almost instantly broke through the resin bed. Selectivity towards other metals was also low.

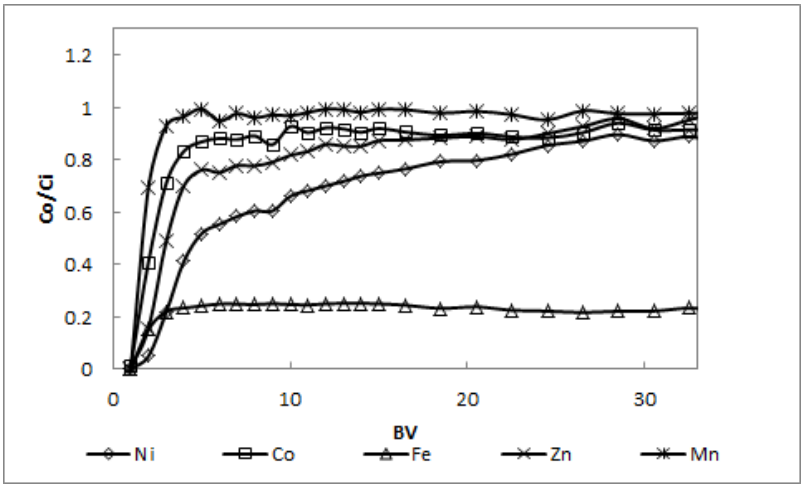

Figure 5.9: Metal breakthrough profiles for Amberlite IRC748. Loading conditions: solution B; initial solution pH = 3; flow rate = 10 BV/h; temperature = 25°C

In the protonated form Amberlite IRC748 did not seem to be selective towards any of the metals except towards Fe(III). Since hydrogen ions are displaced into the solution by metals loading onto the resin the immediate solution pH in a differential element of the packed resin bed drops. It can be seen in figure 3 that the selectivity of Amberlite IRC748 decreases dramatically as the pH is lowered from 3 to 1.5. Therefore, as the feed solution initially entered the column, the metals that loaded onto the resin at the top of the column displaced hydrogen ions into the solution, thus lowering the immediate solution pH and the fraction of the metals that did not adsorb in the top part of the bed did also not adsorb in the lower part of the bed. Hence the shape of the metal breakthrough curves. The pH of the effluent was established to be between 1.5 and 2. This motivated testing Amberlite IRC748 in the Na^{+}-form as well. These results are shown in figures 5.13 and 5.14 later in this section.

As expected metal selectivity of Dow M4195 increased as the initial solution pH increased from 3 to 4, especially towards nickel, cobalt and zinc. The selectivity of Dow M4195 towards manganese remained low. From the results in figures 5.7 and 5.10 it is clear that Dow M4195 is suitable for the dynamic recovery of nickel and cobalt. The results do, however, suggest that dynamic sorption should be carried out at a lower flow rate in order to shorten the MTZ and achieve better nickel and cobalt recoveries.

Even at an initial solution pH of 4 did Dow XUS43605 not show high

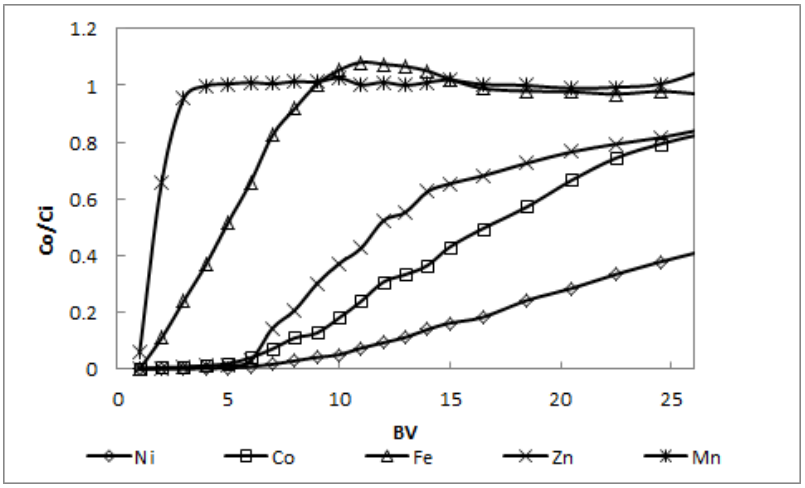

Figure 5.10: Metal breakthrough profiles for Dow M4195. Loading conditions: solution B; initial solution pH = 4; flow rate = 10 BV/h; temperature = 25°C

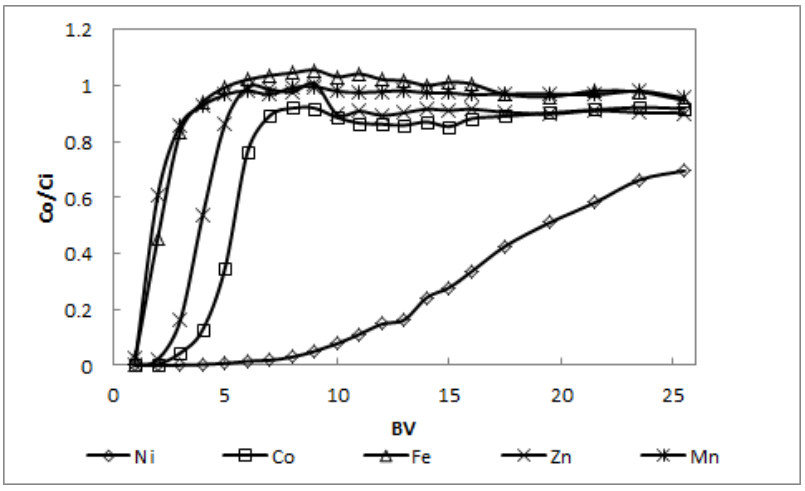

Figure 5.11: Metal breakthrough profiles for Dow XUS43605. Loading conditions: solution B; initial solution pH = 4; flow rate = 10 BV/h; temperature = 25°C

selectivity towards cobalt. Nickel breakthrough occurred at an early stage and the recovery thereof was less than for Dow M4195. From the results in figures 5.8 and 5.11 one can see that this resin is not suitable for the recovery of nickel and cobalt. The resin could, however, be used if the objective is to recover nickel only, as its selectivity towards the other metals is sufficiently low. In this case, the loading rate should also be lower in order to shorten the MTZ.

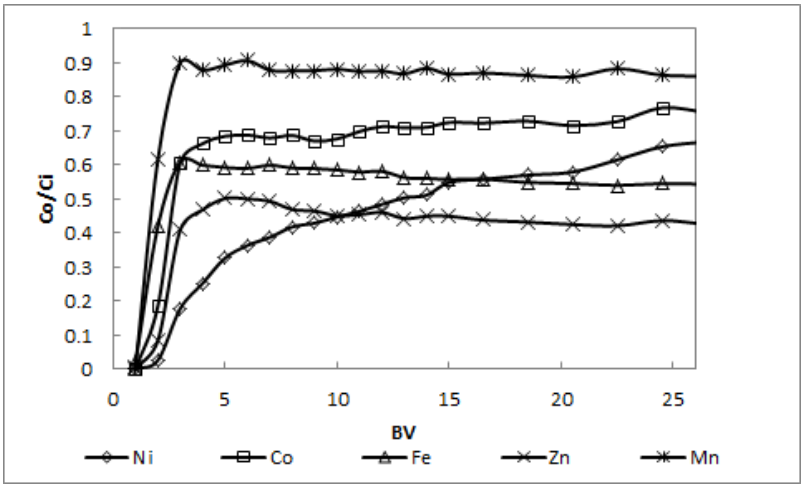

Figure 5.12: Metal breakthrough profiles for Amberlite IRC748. Loading conditions: solution B; initial solution pH = 4; flow rate = 10 BV/h; temperature = 25°C

The same explanation provided for the shapes of the breakthrough profiles in figure 5.9 can be applied to explain the shape of the metal breakthrough profiles shown in figure 5.12. From the results in figures 5.9 and 5.12 it is clear that Amberlite IRC748 in the protonated form is unsuitable for nickel and cobalt recovery. As mentioned earlier, these results motivated testing the resin in the Na^+-form. The breakthrough profiles for Amberlite IRC748 in the Na^+-form is reported in figures 5.13 and 5.14 for initial solution pHs of 3 and 4, respectively.

Amberlite IRC748 was also not suited for the application in the Na^+-form, regardless of the initial solution pH as its selectivity towards all metals was high (see figures 5.13 and 5.14). Therefore, this resin was finally eliminated as an option for the recovery of nickel and cobalt.

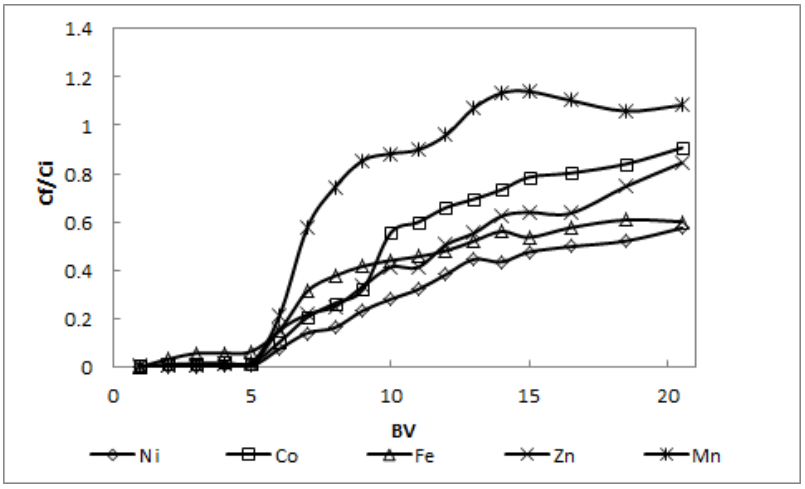

Figure 5.13: Metal breakthrough profiles for Amberlite IRC748 (Na^+-form). Loading conditions: solution B; initial solution pH = 3; flow rate = 10 BV/h; temperature = 25°C

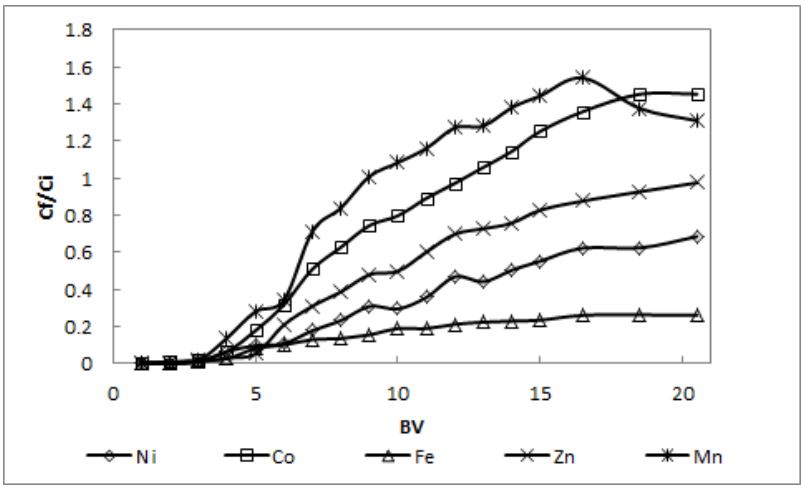

Figure 5.14: Metal breakthrough profiles for Amberlite IRC748 (Na^+-form). Loading conditions: solution B; initial solution pH = 4; flow rate = 10 BV/h; temperature = 25°C

Following from the above discussion, Dow M4195 was selected for the dynamic recovery of nickel and cobalt.

5.2 Effect of operating parameters on metal breakthrough profiles

The effects of flow rate (FR), temperature (T) and initial solution pH (in the case of nickel and cobalt recovery with Dow M4195) on dynamic copper adsorption with Dow XUS43605 and nickel and cobalt adsorption with Dow M4195 were investigated in column experiments. The loading rate was tested in the range of 2.5 to 7.5 BV/h and the temperature was tested at 25°C and 60°C. In the case of copper adsorption with Dow XUS43605 the only solution pH tested was 4, while for nickel and cobalt recovery with Dow M4195 the solution pH was tested at 2 and 4.

5.2.1 Metal breakthrough profiles for Dow XUS43605

5.2.1.1 Effect of flow rate

The effect of flow rate on the dynamic adsorption of copper and nickel at 25°C (as nickel was the only metal that co-loaded onto Dow XUS43605 to a significant extent) with Dow XUS43605 is illustrated in figure 5.15. Because of the fast rate at which copper adsorption with Dow XUS43605 attains equilibrium, the effect of increasing the flow rate from 2.5 BV/h to 7.5 BV/h was not extremely significant considering that breakthrough occurred at 27, 29 and 31 BVs when the flow rates were 2.5, 5 and 7.5 BV/h, respectively. The copper loading on Dow XUS43605 decreased by a mere 6.8% when the flow rate was increased from 2.5 BV/h to 5 BV/h and another 8% when the flow rate was further increased to 7.5 BV/h. The co-loaded nickel on the resin at 1% copper breakthrough increased with increasing flow rate as a result of the earlier breakthrough of copper at higher flow rates. In other words, less of the adsorbed nickel was displaced by copper at 1% copper breakthrough.

The effect of flow rate on copper breakthrough at 60°C was also not very significant, as illustrated in figure 5.16.

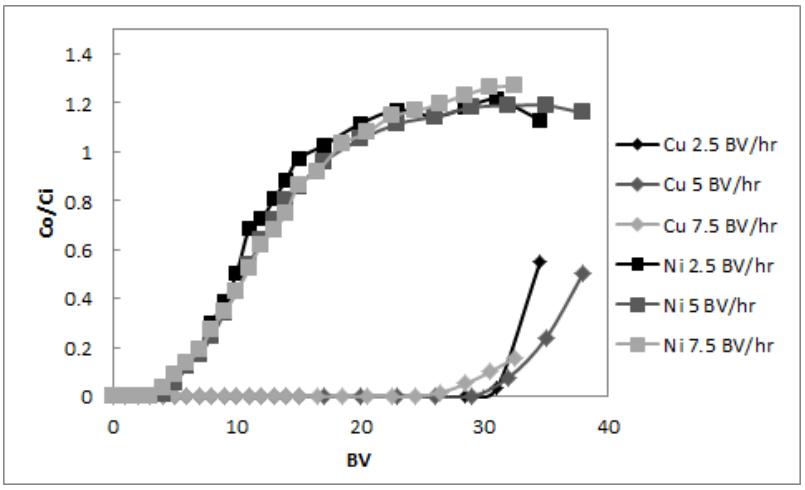

Figure 5.15: Effect of flow rate on copper and nickel breakthrough profiles for Dow XUS43605. Results at 25°C at an initial solution pH of 4

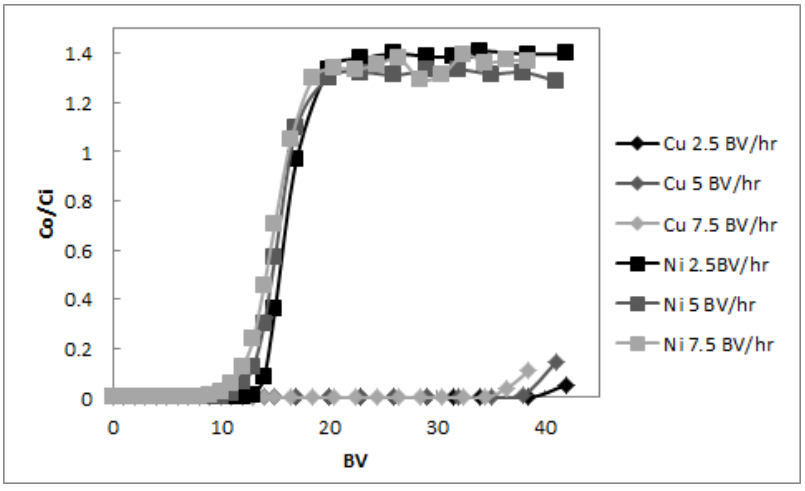

Figure 5.16: Effect of flow rate on copper and nickel breakthrough profiles for Dow XUS43605. Results at 60°C at an initial solution pH of 4

5.2.1.2 Effect of temperature

The effect of temperature on the dynamic adsorption of copper and nickel with Dow XUS43605 was already clear from figures 5.15 and 5.16. The effect of temperature on metal recovery is demonstrated at a loading rate of 5 BV/h in figure 5.17, although the effect of temperature was found to be similar at loading rates of 2.5 and 7.5 BV/h. By increasing the temperature from 25°C to 60°C, the 1% copper breakthrough point shifted from BV 29 to BV 38, which corresponds to a 36% increase in copper loading on the resin. Although nickel initially co-loaded to a greater extent at 60°C than at 25°C, the overshoot observed at 60°C ($\frac{C_{Ni,o}}{C_{Ni,i}}$=1.33) was higher than that observed at 25°C ($\frac{C_{Ni,o}}{C_{Ni,i}}$=1.19).

It was shown in figure 4.9 that an increase in temperature lowers the equilibrium capacity of Dow XUS43605. Nevertheless, the rate of metal adsorption was higher at 60°C than at 25°C, which explains the higher operating capacity of the resin at 60°C. The increased rate of metal adsorption also explains the greater extent of initial nickel adsorption at 60°C, but as a result of the lower equilibrium capacity at the higher temperature, nickel was displaced by copper to a greater extent, hence the lower nickel loading on the resin at 1% copper breakthrough at 60°C. As mentioned earlier, in terms of the degree of

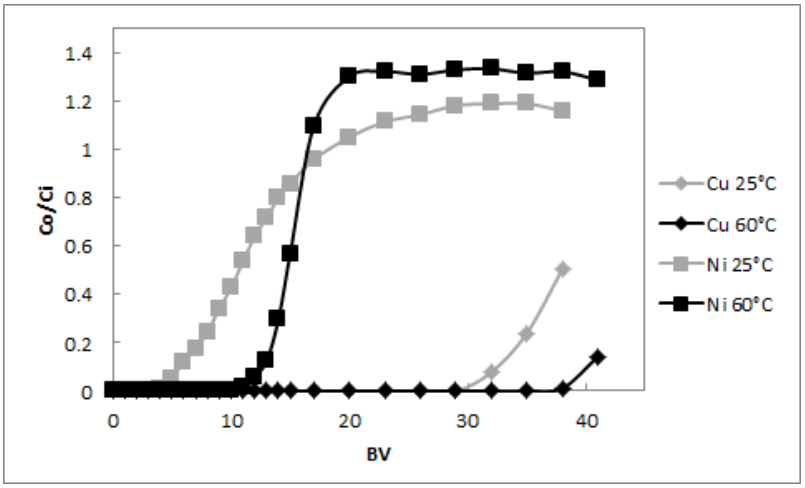

Figure 5.17: Effect of temperature on copper and nickel breakthrough profiles for Dow XUS43605. Results at 2 BV/h at an initial solution pH of 4

metal recovery and maximizing the resin capacity utilization it is desirable to

operate at the lowest possible flow rate. Economically it is not favourable to operate at such low flow rates as the rate of production is low at such low flow rates.

This principle is illustrated in figure 5.18 where the rate of copper loading onto Dow XUS43605 (up to the point where 1% copper breakthrough occurred) is plotted versus the flow rate at 25°C and 60°C. It is apparent from the figure that the rate of copper loading increased almost linearly with flow rate at 25°C. The graph demonstrates that there was no real difference in the loading rate of copper at lower flow rates (2.5, 5 and 7.5 BV/h) for an increase in temperature, whereas a slight economic advantage can be seen at 60°C and 10 BV/h.

It was, however, noticed that trace amounts of copper broke through the column when operating at flow rates higher than 10 BV/h. This occurrence is undesirable as the downstream operation utilizes Dow M4195 for the recovery of nickel and cobalt, and since the stability constant of copper complexation with Dow M4195 is extremely high, it is difficult to elute from the resin. Conventional sulfuric acid cannot be used for copper elution from Dow M4195; instead, ammoniacal solution is used. Therefore, despite the economic advantage of operating at flow rates higher than 10 BV/h, it is not advised following from the discussion above.

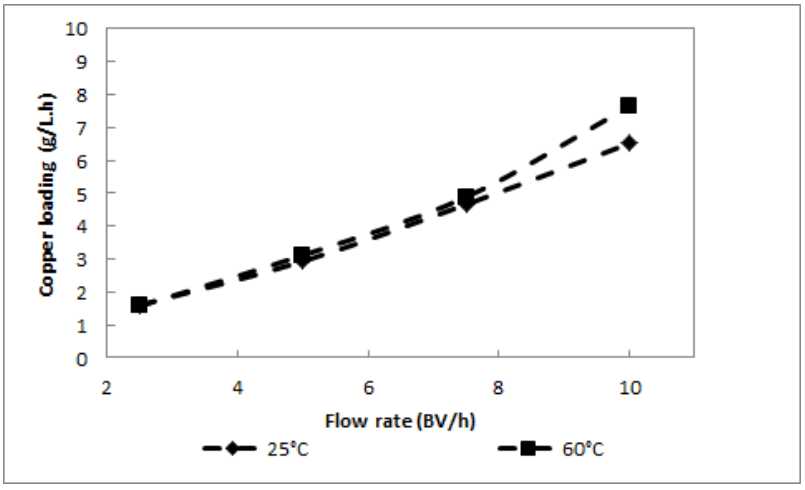

Figure 5.18: Effect of flow rate and temperature on the rate of copper adsorption onto Dow XUS43605

5.2.2 Metal breakthrough profiles for Dow M4195

5.2.2.1 Effect of flow rate

The effect of flow rate on the dynamic recovery of nickel and cobalt with Dow M4195 is shown in figures 5.19 and 5.20 at 25 and 60°C, respectively.

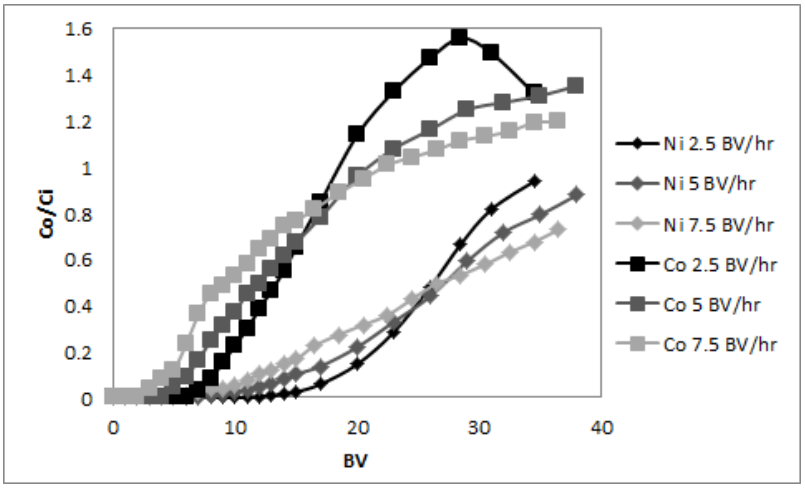

Figure 5.19: Effect of flow rate on nickel and cobalt breakthrough profiles with Dow M4195. Results shown at 25°C at an initial solution pH of 4

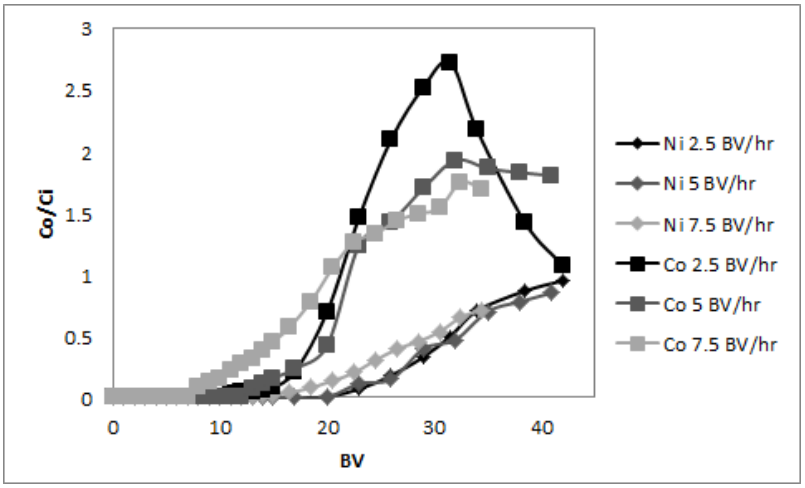

Figure 5.20: Effect of flow rate on nickel and cobalt breakthrough profiles with Dow M4195. Results shown at 60°C at an initial solution pH of 4

The effect of flow rate on nickel and cobalt breakthrough profiles was found to be the similar at 25°C and 60°C. Both nickel and cobalt breakthrough

occurred at an earlier stage as the flow rate was increased from 2.5 BV/h to 7.5 BV/h. The effect of flow rate appeared to be more pronounced at 25°C than at 60°C, which could be explained by the faster metal loading kinetics of the resin at 60°C, as was demonstrated in figure 4.10.

5.2.2.2 Effect of initial solution pH

The effect of initial solution pH on nickel and cobalt adsorption in dynamic column experiments is shown in figures 5.21 and 5.22. It is clear that the selectivity of the resin towards both metals increased when the initial solution pH was increased from 2 to 4, regardless of the temperature. The effect of pH was, however, more pronounced at 60°C; both nickel and cobalt loaded to a greater extent when the initial solution pH was increased from 2 to 4, especially cobalt.

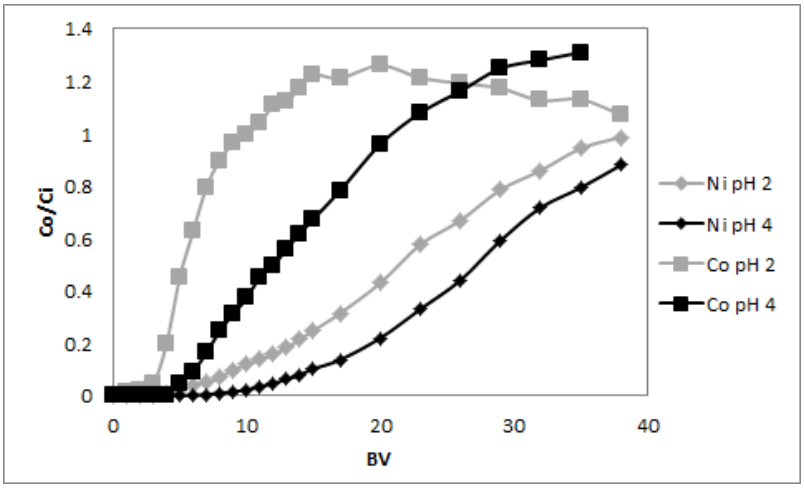

Figure 5.21: Effect of initial solution pH on nickel and cobalt breakthrough profiles with Dow M4195. Results shown at 25°C at a solution flow rate of 2.5 BV/h

5.2.2.3 Effect of temperature

The effect of temperature on nickel and cobalt breakthrough profiles for the adsorption of these metals with Dow M4195 is shown figure 5.23. The results are shown for Dow M4195 that was loaded at 2.5 BV/h with synthetic bioleach solution with an initial solution pH of 4. The effect of temperature observed at an initial solution pH of 2 and flow rates of 5 and 7.5 BV/h was similar

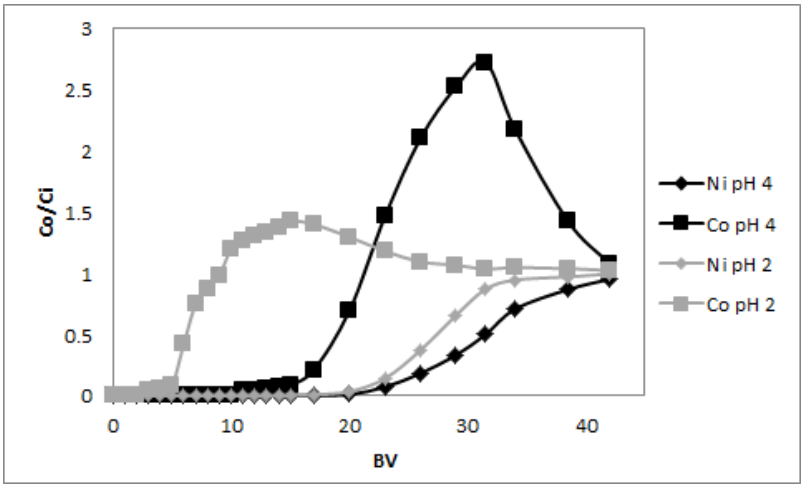

Figure 5.22: Effect of initial solution pH on nickel and cobalt breakthrough profiles with Dow M4195. Results shown at 60°C at a solution flow rate of 2.5 BV/h

to those displayed in figure 5.23. It is clear that an increase in temperature was advantageous for both nickel and cobalt adsorption with Dow M4195. As discussed earlier, this observation could be explained by the increased metal loading rate at 60°C.

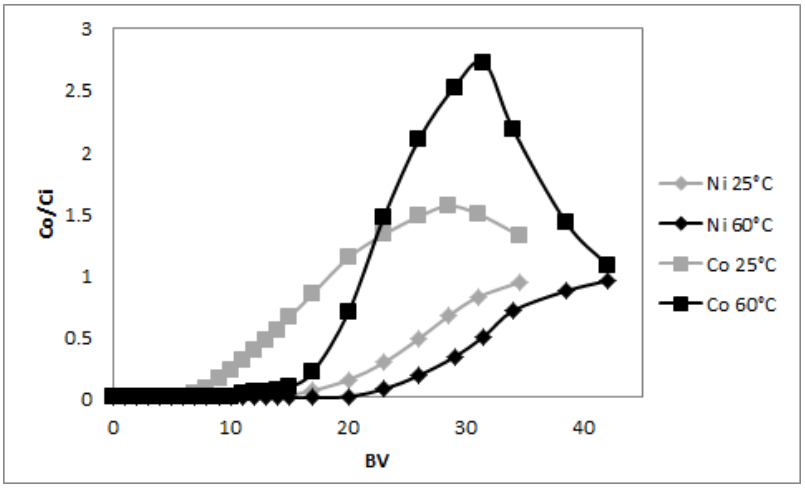

Figure 5.23: Effect of temperature on nickel and cobalt breakthrough profiles with Dow M4195. Results shown at 2.5 BV/h and an initial solution pH of 4

The same approach that was followed to illustrate the economic advantage of operating at higher flow rates in the dynamic recovery of copper was followed to illustrate the advantage of operating at higher flow rates in the recovery of

nickel and cobalt with Dow M4195. The values plotted in figure 5.24 were calculated from the nickel loadings on Dow M4195 when nickel breakthrough reached 1% ($\frac{C_{o,Ni}}{C_{i,Ni}} = 0.01$) and the corresponding bed BVs where these loadings occurred. In other words, this analysis assumed that a column is operated until 1% nickel breakthrough occurs, which might not necessarily be the case. In practice, a lead column would be operated nearly to its equilibrium capacity and a lag column (to scavenge any of the metals of interest that breaks through the first column) would be operated until the metals of interest start breaking through.

Because of the higher nickel concentration in the feed solution (in relation to the copper concentration in the feed) and the earlier breakthrough of nickel, the rate of nickel loading up to 1% breakthrough was generally higher than that of copper loading. The graph illustrates the economic advantage of operating at higher flow rates.

These results are not absolute and an in-depth investigation is necessary to determine the best operating conditions (especially flow rate) for nickel and cobalt recovery. Preferably, a lead-lag column configuration packed with Dow M4195 must be used for this analysis, but it is beyond the scope of this project.

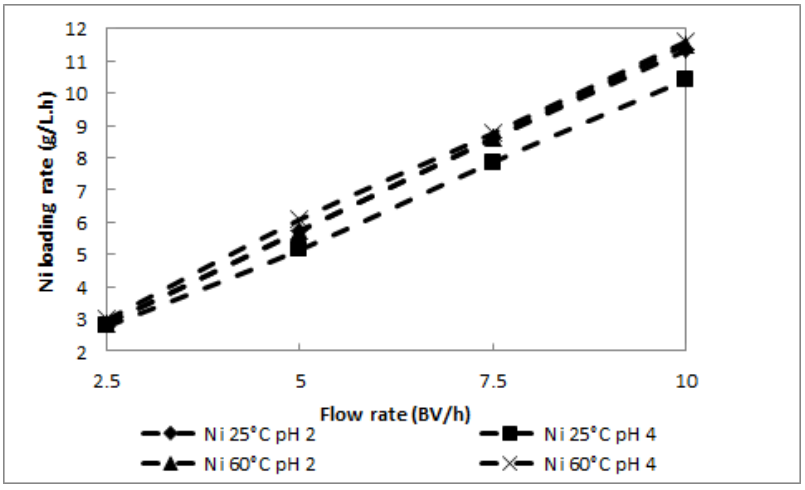

Figure 5.24: Effect of flow rate and temperature on the nickel production rate

5.3 Statistical analysis of metal adsorption with Dow XUS43605

The breakthrough profiles from which the data in this section were calculated are shown in figures 22-41 in Appendix C.

5.3.1 Adsorption of copper with Dow XUS43605

The effects of temperature, flow rate, initial solution pH, initial copper concentration and initial gangue metals concentration on the copper loading on Dow XUS43605 when $\frac{C_{Cu,o}}{C_{Cu,i}} = 0.01$ were investigated in column sorption experiments. Linear regression was performed on the data and a model was developed to predict the copper loading on Dow XUS43605. The normalized model obtained for copper loading at 1% copper breakthrough is shown in equation 5.3.1. Except for copper, nickel was the only other metal that co-loaded onto Dow XUS43605 to a significant extent, therefore the effects of other metals on the copper loading were ignored.

$$\begin{aligned}[Cu]_r &= 0.002 - 0.59FR + 0.76T + 0.07pH - 0.19[Ni]_s + \\ &\quad 0.06FR.pH + 0.04T.[Ni]_s + 0.11pH.[Ni]_s \end{aligned} \tag{5.3.1}$$

P-values, reflecting the significance of each parameter[1], are reported in table 5.1. According to this information the effects of flow rate and temperature were the most significant, followed by the nickel concentration in the feed solution. By considering the model in equation 5.3.1, an increase in the flow rate resulted in a decrease in the copper loading on the resin at copper breakthrough, and an increase in the nickel concentration in the feed had a similar decreasing effect on copper loading since nickel ions compete with copper ions for active sites on the resin. The opposite was witnessed for an increase in temperature – the copper loading on the resin increased as this parameter increased, which is consistent with the results reported in section 5.2.1 and that reported by Sirola (2010). According to the p-values listed in table 5.1 none

[1] p-values less than 0.05 indicate statistical significance of a factor

Table 5.1: Analysis of variance of the copper concentration on Dow XUS43605 at 1% copper breakthrough

ANOVA of [Cu]r at copper breakthrough					
Source	**Sum of Squares**	**df**	**Mean Square**	**F Value**	**p-value Prob > F**
Model	14.6	7	2.09	45.4	< 1E-4
FR	5.23	1	5.23	113	< 1E-4
T	8.59	1	8.59	186	< 1E-4
pH	0.07	1	0.067	1.46	0.26
[Ni]s	0.54	1	0.54	11.6	0.009
FR-pH	0.05	1	0.053	1.15	0.31
T-[Ni]s	0.02	1	0.022	0.47	0.51
pH-[Ni]s	0.18	1	0.18	3.94	0.08
Residual	0.37	8	0.046		
Cor Total	15	15			

of the interaction parameters affected the copper loading on Dow XUS43605 significantly.

The pH also did not seem to have a major influence on the copper loading achieved on the resin in the range studied (3–4). This could be explained by the pH dependence of the copper adsorption constant (see figure 2); as the pH increases from 0 the adsorption constant increases up to a pH of 3 after which it remains more or less constant. The same conclusion could be drawn from the batch loading results (consider figures 10 to 12 in Appendix B) where the copper adsorption with Dow XUS43605 increased from 50% at pH 2 to 65% at pH 3, while it increased only another 5% when the pH was increased further to a value of 4.

Shown in figures 5.25 and 5.26 are the half-normal probability plot and Pareto chart for the copper loading on Dow XUS43605 at copper breakthrough, respectively, confirming that temperature and flow rate were the main parameters influencing the copper loading on this resin at breakthrough. These figures also illustrate that the effects of pH and the initial copper concentration, as well as interaction between the main parameters, were negligible.

Finally, the normalized observed copper loadings on Dow XUS43605 were plotted versus the normalized loadings predicted by the model in equation 5.3.1. The results are shown in figure 5.27. The adjusted R^2-value, or R^2_{adj}, for

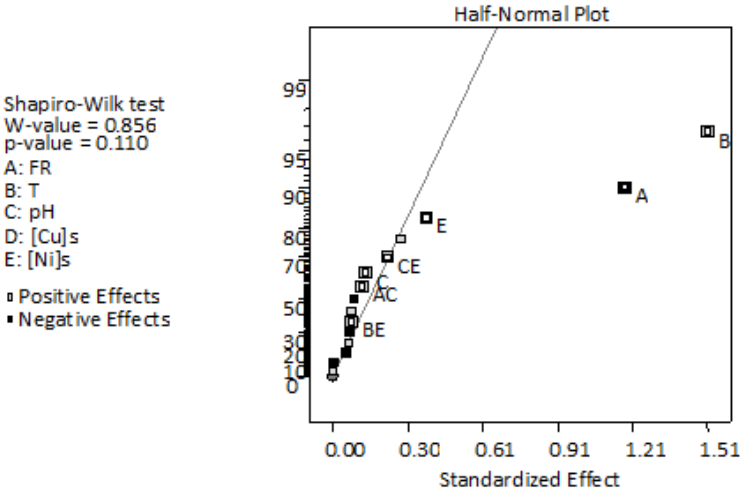

Figure 5.25: Half-normal probability plot: effects of operating conditions on the copper loading on Dow XUS43605 at copper breakthrough

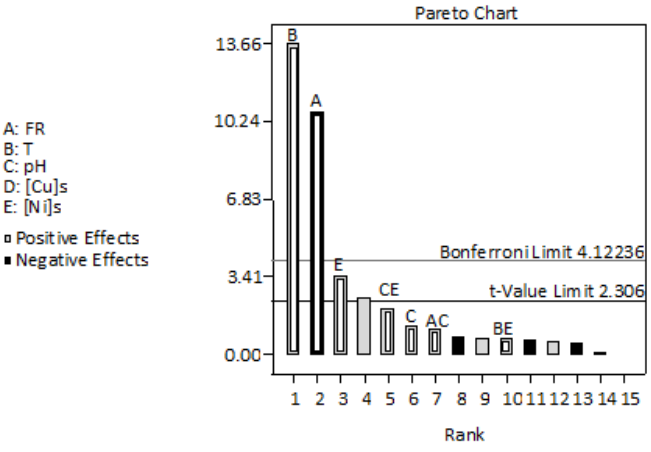

Figure 5.26: Pareto chart: effects of operating conditions on the copper loading on Dow XUS43605 at copper breakthrough

this model was 0.97 indicating that the copper loadings calculated with the model correlated well with the actual copper loadings observed.

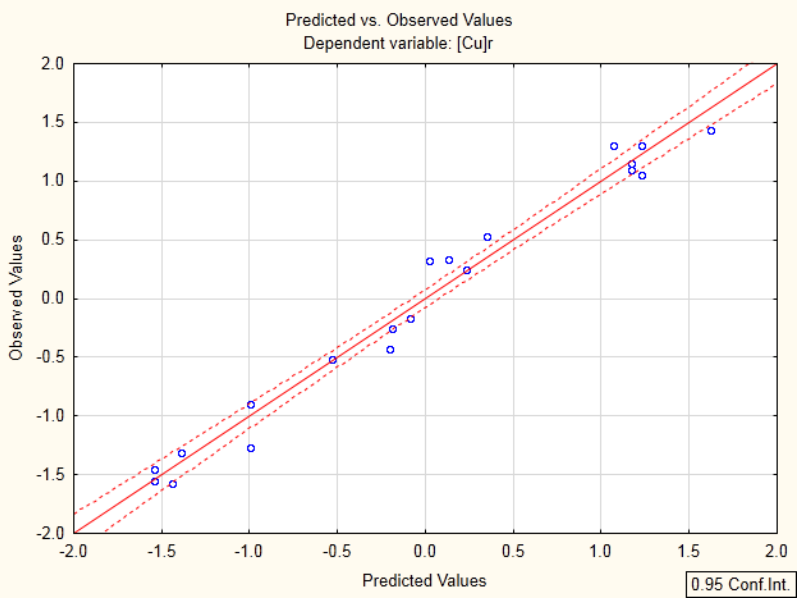

Figure 5.27: Plot of the observed copper loadings on Dow XUS43605 versus those predicted by the linear regression model in equation 5.3.1

5.3.2 Adsorption of nickel with Dow XUS43605

As mentioned in section 5.3.1, nickel was the only metal that co-loaded to a significant extent with copper onto Dow XUS43605. Nickel that initially adsorbed onto the resin was gradually displaced by copper at a later stage as a result of the resin's higher selectivity towards the latter metal ion. This was evident from the overshoot that occurred in the normalized breakthrough profiles for nickel in figures 22 to 41 in Appendix C.

A similar approach was followed in the determination of the effects of temperature, flow rate, initial solution pH, initial copper concentration and initial gangue metals concentration on the nickel loading on Dow XUS43605 when $\frac{[Cu]_o}{[Cu]_i} = 0.01$, than was followed in section 5.3.1 to determine the effects of these parameters on the copper loading on Dow XUS43605 when $\frac{C_{Cu,o}}{C_{Cu,i}} = 0.01$. A model was developed to predict the nickel loading on the resin at 1% copper

breakthrough by performing linear regression on the experimental data. This model is shown in equation 5.3.2.

$$\begin{aligned}[Ni]_r &= 4.8E - 0.01FR - 0.3T + 0.6pH - 0.3[Cu]_s + .4[Ni]_s + \\ &\quad 0.2F.T + 0.12F.[Cu]_s - 0.14T.[Ni]_s + 0.38pH.[Ni]s \end{aligned} \quad (5.3.2)$$

The p-values of the main parameters and interaction terms in equation 5.3.2 are listed in table 5.2. From these values it can be seen that the effects of pH, temperature and nickel concentration in the feed were significant, as well as the interaction between pH and the nickel concentration in the feed solution. Of all these listed, the effect of pH was the most important. The half-normal probability plot and Pareto chart are shown in figures 5.28 and 5.29, respectively. As expected, the solution pH had a positive effect on the amount of co-adsorbed nickel, which is clear from these figures and equation 5.3.2.

Table 5.2: Analysis of variance of the nickel concentration on Dow XUS43605 at 1% copper breakthrough

ANOVA for [Ni]r at copper breakthrough					
Source	**Sum of Squares**	**df**	**Mean Square**	**F Value**	**p-value Prob > F**
Model	13.62	9	1.51	6.6	0.02
FR	2.3E-03	1	2.3E-03	0.01	0.92
T	1.28	1	1.28	5.59	0.06
pH	5.75	1	5.75	25.06	2.4E-3
$[Cu]_s$	1.03	1	1.03	4.49	0.08
$[Ni]_s$	2.07	1	2.07	9.03	0.02
FR-T	0.65	1	0.65	2.81	0.14
FR-$[Cu]_s$	0.22	1	0.22	0.97	0.36
T-$[Ni]_s$	0.28	1	0.28	1.23	0.31
pH-$[Ni]_s$	1.99	1	1.99	8.68	0.03
Residual	1.38	6	0.23		
Cor Total	15	15			

A plot of the experimentally observed nickel loadings on Dow XUS43605 versus the nickel loadings calculated with the model in equation 5.3.2 is shown in figure 5.30. The R^2_{adj} for this model was 0.66, therefore it failed to predict the

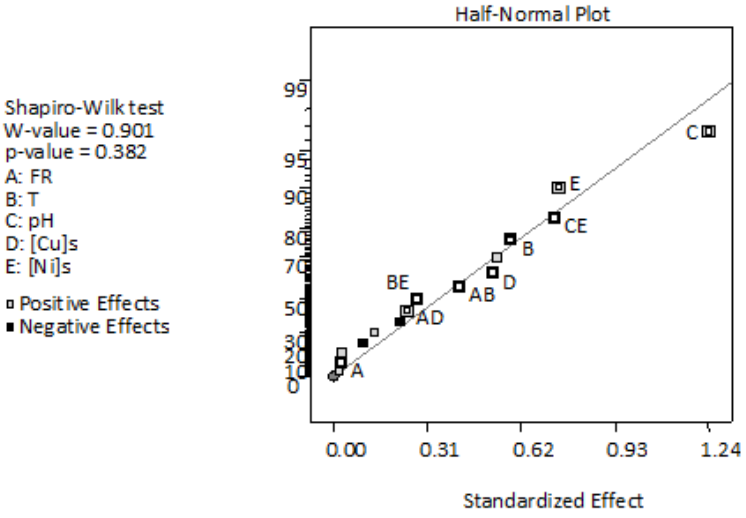

Figure 5.28: Half-normal probability plot: effects of operating conditions on the nickel loading on Dow XUS43605 at copper breakthrough

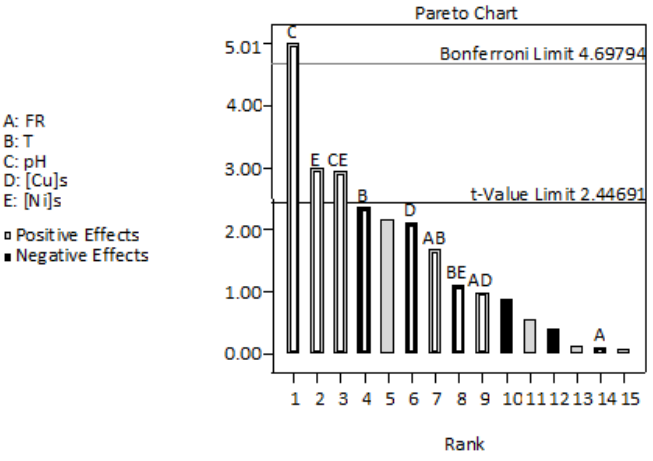

Figure 5.29: Pareto chart: effects of operating conditions on the copper loading on Dow XUS43605 at copper breakthrough

actual data with much accuracy. The analysis did, however, provide valuable qualitative information regarding the effects of operating parameters and their interactions on the nickel loading on Dow XUS43605.

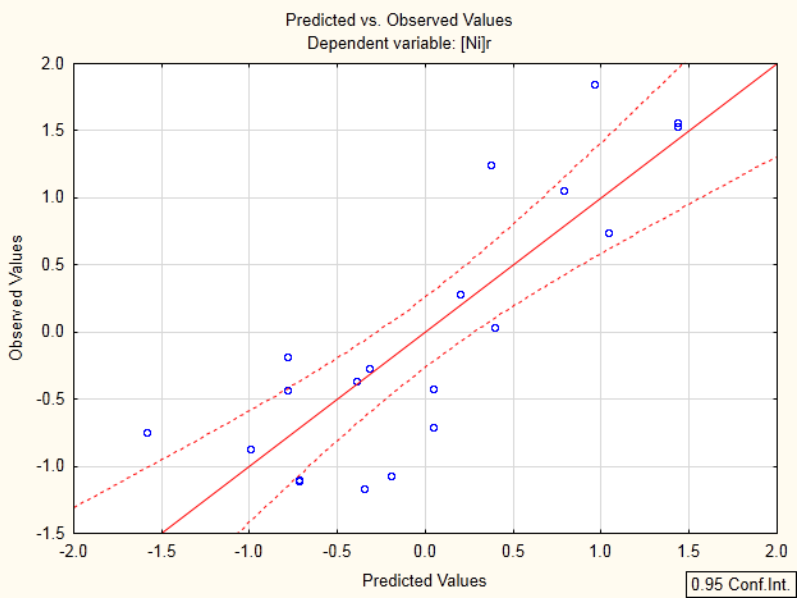

Figure 5.30: Plot of the observed nickel loadings on Dow XUS43605 versus those predicted by the linear regression model in equation 5.3.2

5.3.3 Copper breakthrough BV

The BV corresponding to the point where 1% copper breakthrough occurred was the final dependent variable to be modeled by performing linear regression on the experimental data. The model that was obtained is shown in equation 5.3.3.

$$\begin{aligned} BV_{1\%\ Cu\ breakthrough} &= -0.5F + 0.58T - 0.61[Cu]_s - 0.13[Ni]s \\ &\quad +0.14FR.[Cu]s - 0.16T.[Cu]s \end{aligned} \tag{5.3.3}$$

From the p-values listed in table 5.3 it is clear that the BV at which copper breakthrough occurred was mainly influenced to the greatest extent by the flow rate and temperature. From equation 5.3.3 and figures 5.31 and 5.32 it can be seen that an increase in flow rate resulted in earlier breakthrough

of copper (as expected), while an increase in temperature resulted in copper breaking through the column at a later stage, reflecting the higher copper loading on Dow XUS43605 at copper breakthrough at elevated temperatures. These results were in accordance with the results reported in section 5.3.1.

Table 5.3: Analysis of variance of the BV at which 1% copper breakthrough occurred with Dow XUS43605

ANOVA for copper breakthrough BV					
Source	**Sum of Squares**	**df**	**Mean Square**	**F Value**	**p-value Prob > F**
Model	14.7	6	2.45	73.8	< 1E-4
FR	3.13	1	3.13	94.1	< 1E-4
T	5.09	1	5.09	153	< 1E-4
$[Cu]_s$	5.5	1	5.5	165	< 1E-4
$[Ni]_s$	0.26	1	0.26	7.73	0.02
FR-$[Cu]_s$	0.29	1	0.29	8.75	0.02
T-$[Cu]_s$	0.35	1	0.35	10.41	0.01
Residual	0.3	9	0.033		
Cor Total	15	15			

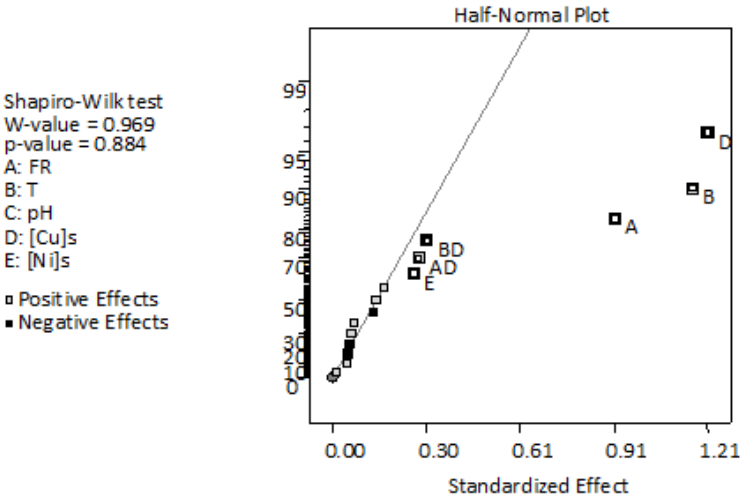

Figure 5.31: Half-normal probability plot: effects of operating conditions on the BV at which copper breakthrough occurs with Dow XUS43605

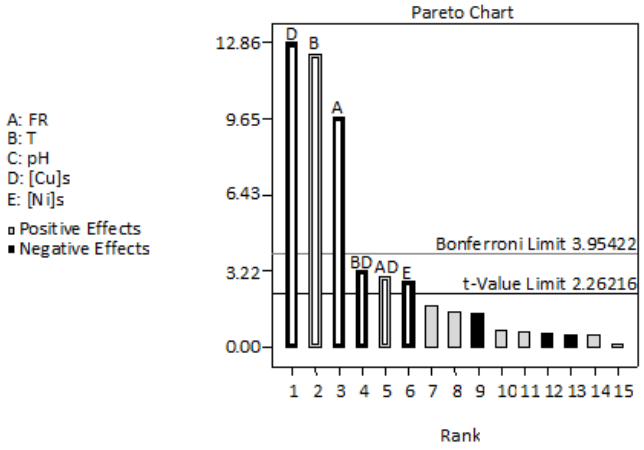

Figure 5.32: Pareto chart: effects of operating conditions on the BV at which copper breakthrough occurs with Dow XUS43605

An R^2_{adj} value of 0.97 was obtained by plotting the experimentally observed 1% copper breakthrough BV against the values predicted by the model in equation 5.3.3. This plot is shown in figure 5.33.

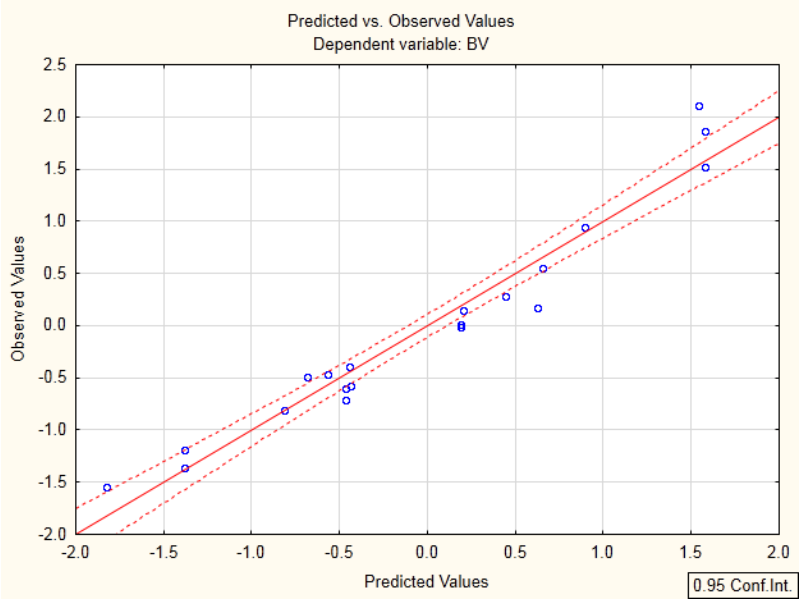

Figure 5.33: Plot of the observed BV where 1% copper breakthrough occurs versus those predicted by the linear regression model in equation 5.3.3

5.4 Statistical analysis of metal adsorption with Dow M4195

The effects of flow rate, temperature, initial solution pH, initial target metal, or TM, concentration (nickel and cobalt) and initial gangue metals, or GM, concentration (iron, zinc, manganese and aluminium) on target metal adsorption with Dow M4195 were studied in column sorption experiments. The procedures that were followed during these experiments were discussed in chapter 3.5.1. Breakthrough profiles were plotted and used to obtain the concentration of target metals on the resin when $\frac{C_{Ni,0}}{C_{Ni,i}} = 0.01$ as well as the BVs that corresponded to this point in each case. The breakthrough profiles from which these data were calculated are shown in figures 42-61 in Appendix C. Linear regression was then performed on the data to elucidate the effects that the different parameters and their interactions had on the target metal loading on Dow M4195, and to determine the significance of the effects on the target metal loading. Statistical models were developed that are able to predict the resin loading and the BV where this loading occurs when $\frac{C_{Ni,0}}{C_{Ni,i}} = 0.01$ at a specific combination of the above-mentioned independent variables.

5.4.1 TM concentration on Dow M4195

The regression model obtained from the experimental data for the TM concentration on Dow M4195 when $\frac{C_{Ni,0}}{C_{Ni,i}} = 0.01$ is shown in equation 5.4.1, and the p-values of the parameters in this model are reported in table 5.4.

$$[TM]_{r,\ 1\%\ Ni\ breakthrough} = 9.44E - 16 - 0.62FR + 0.69T + 0.22[TM]_s - 0.1[GM]_s - 0.22FR.T - 0.08T.[GM]_s \quad (5.4.1)$$

These p-values indicate that the flow rate, temperature, initial TM concentration and the interaction between the flow rate and temperature had the most significant impacts on the target metal loading achieved on Dow M4195. The model in equation 5.4.1 proposes that the TM concentration on the resin at 1% nickel breakthrough decreased as the flow rate increased, while an increase in the temperature and initial TM concentration increased the TM

Table 5.4: Analysis of variance of the TM concentration on Dow M4195 at 1% nickel breakthrough

ANOVA for [TM]r at nickel breakthrough					
Source	**Sum of Squares**	**df**	**Mean Square**	**F Value**	**p-value Prob > F**
Model	14.41	6	2.4	36.9	< 1E-4
FR	5.79	1	5.79	88.9	< 1E-4
T	7.18	1	7.18	110	< 1E-4
[TMs]	0.59	1	0.59	9.02	0.02
[OM]s	0.11	1	0.11	1.76	0.22
FR-T	0.67	1	0.67	10.2	0.01
T-[OM]s	0.09	1	0.09	1.32	0.28
Residual	0.59	9	0.07		
Cor Total	15	15			

loading on Dow M4195. These results are consistent with the results discussed in section 5.2.2. This is also apparent from figures 5.34 and 5.35, and so is the insignificance of the interaction effects of all parameters except that between flow rate and temperature.

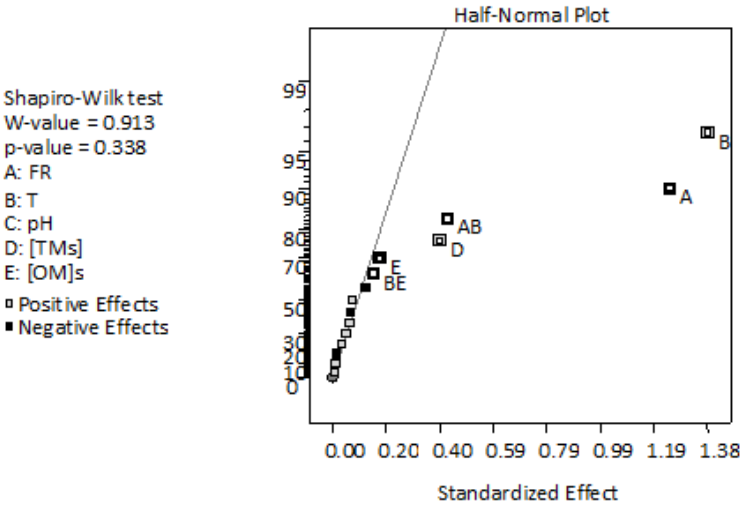

Figure 5.34: Half-normal probability plot: effects of operating conditions on the TM loading on Dow M4195 at nickel breakthrough

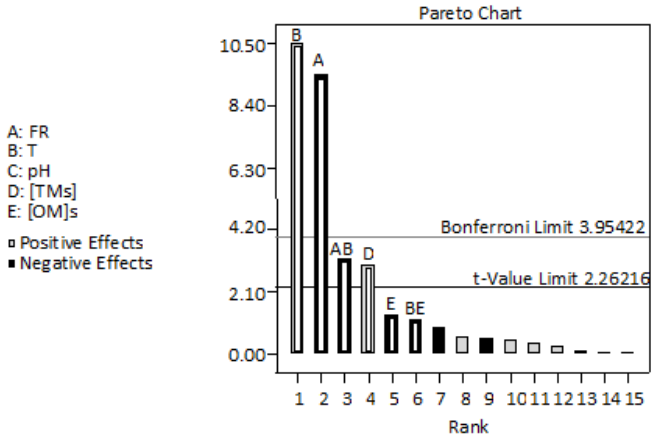

Figure 5.35: Pareto chart: effects of operating conditions on the TM loading on Dow M4195 at nickel breakthrough

The normalized observed TM loadings on Dow M4195 is plotted versus the normalized TM loadings predicted by equation 5.4.1 in figure 5.36. A R^2_{adj}-value of 0.93 was obtained for the model.

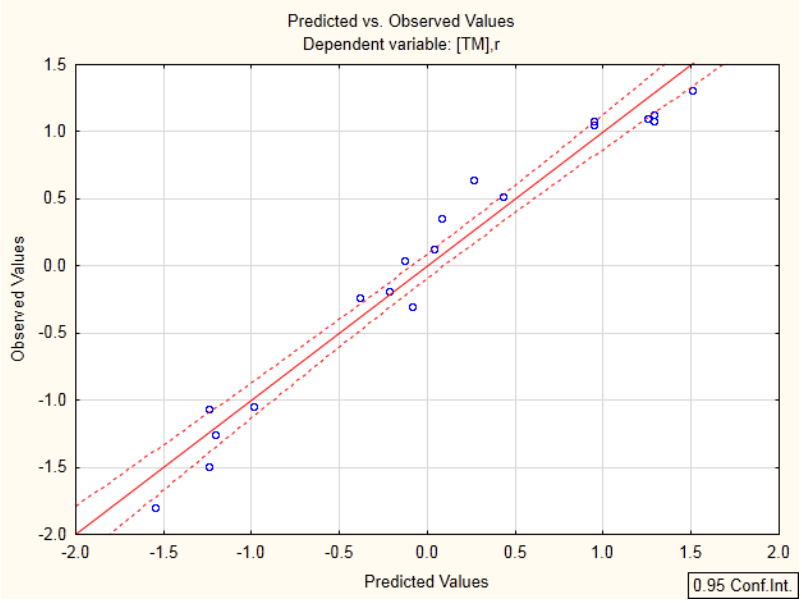

Figure 5.36: Plot of the observed TM loading, [TM]r, on Dow M4195 where 1% nickel breakthrough occurred versus those predicted by the linear regression model in equation 5.4.1

5.4.2 Breakthrough BV determination

The BV corresponding to 1% nickel breakthrough was modelled by performing linear regression on the experimental data. The model is shown in equation 5.4.2, and the observed data is plotted versus the data calculated with the model in figure 5.37. A R^2_{adj} value of 0.94 was obtained with the model.

$$\begin{aligned} BV_{1\%\ Ni\ breakthrough} = {} & 0.04 - 0.59F + 0.69T + 0.03pH - 0.09[TM]_s - \\ & 0.24[GM]_s - 0.27FR.T + 0.04FR.pH + 0.09FR.[TM]_s - \\ & 0.08FR.[GM]_s - 0.14T.[TM]_s - 0.17T.[OM]_s + \\ & 0.14pH.[TM]_s + 0.13pH.[OM]_s + \\ & 0.28[TM]_s.[OM]_s \end{aligned} \quad (5.4.2)$$

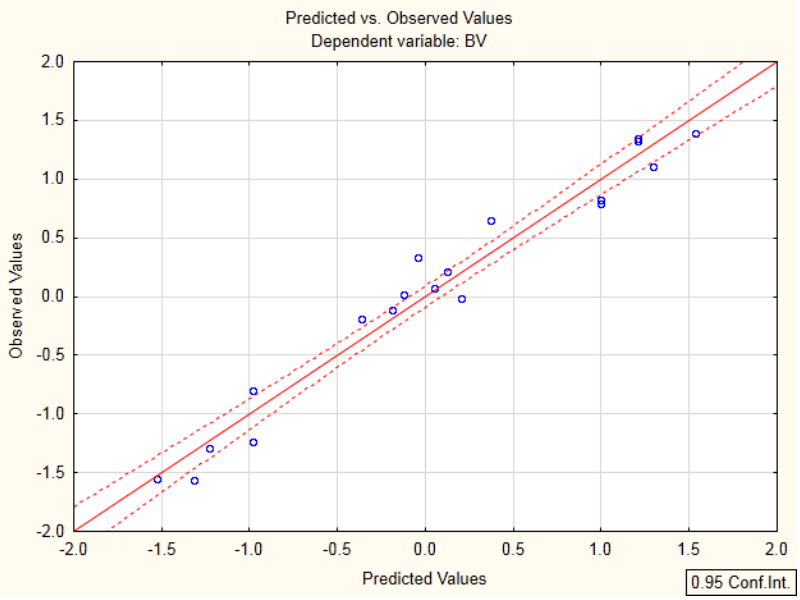

Figure 5.37: Plot of the observed BVs where 1% nickel breakthrough occurred versus those predicted by the linear regression model in equation 5.4.2

The effects of flow rate and temperature were found to be the most significant on the BV at which nickel breakthrough occurred as indicated by the p-values of these parameters in table 5.5. Furthermore, the interactions between flow rate and temperature, flow rate and initial TM concentration,

Table 5.5: Analysis of variance of the BV at which 1% nickel breakthrough occurred with Dow M4195

ANOVA for nickel breakthrough BV					
Source	**Sum of Squares**	**df**	**Mean Square**	**F Value**	**p-value Prob > F**
Model	15	14	1.07	5065	0.01
FR	5.25	1	5.25	24831	4E-3
T	7.2	1	7.2	34057	3E-3
pH	3E-04	1	3E-04	1.56	0.43
$[TM]_s$	0.01	1	0.01	63.27	0.08
$[OM]_s$	6E-03	1	7E-03	32.59	0.11
FR-T	0.11	1	0.11	520	0.03
FR-pH	0.01	1	0.01	63.37	0.08
FR-$[TM]_s$	0.08	1	0.08	352	0.03
FR-$[OM]_s$	0.03	1	0.03	131	0.06
T-$[TM]_s$	0.22	1	0.22	1029	0.02
T-$[OM]_s$	0.14	1	0.14	676	0.02
pH-$[TM]_s$	7E-03	1	7E-03	33.27	0.11
pH-$[OM]_s$	0.02	1	0.02	92.79	0.07
$[TM]_s$-$[OM]_s$	0.01	1	0.01	49.26	0.09
Residual	2E-04	1	2E-04		
Cor Total	15	15			

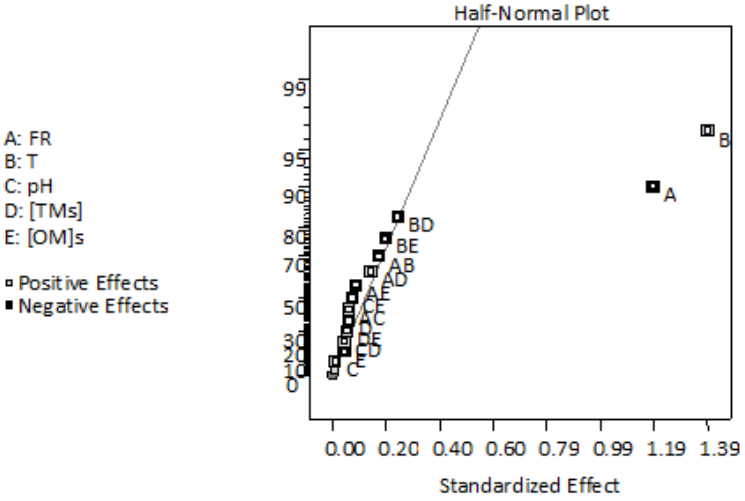

Figure 5.38: Half-normal probability plot: effects of operating conditions on the BV at which nickel breakthrough occurs with Dow M4195

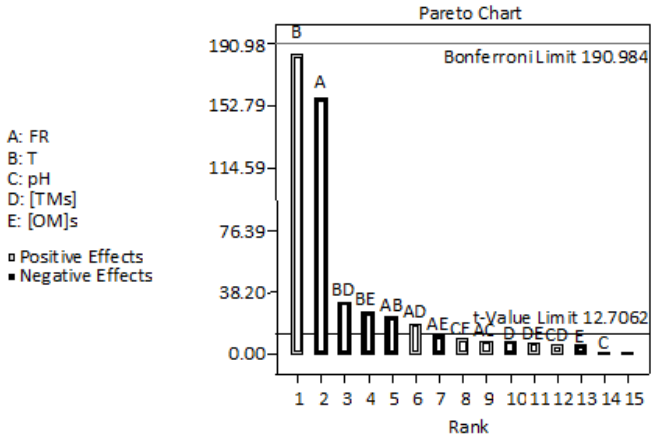

Figure 5.39: Pareto chart: effects of operating conditions on the BV at which nickel breakthrough occurs with Dow M4195

temperature and initial TM concentration, and temperature and GM concentration were also significant. The model proposed in equation 5.4.2 predicts that an increase in temperature would result in 1% nickel breakthrough occurring at a higher BV. For an increase in flow rate the model predicts a decrease in target metal loading at 1% nickel breakthrough. Qualitatively these results were consistent with the results obtained in section 5.4.1. As expected, an increase in the TM ion concentration and initial GM concentration in the solution resulted in 1% nickel breakthrough occurring at an earlier stage.

The half-normal probability plot and Pareto chart illustrating the effects of the operating conditions on the 1% nickel breakthrough BV graphically are shown in figures 5.38 and 5.39.

Chapter 6

Column Elution Results

Elution studies were performed with 20, 100 and 200 g/L H_2SO_4. Dow XUS43605 was loaded until copper started breaking through the resin bed and Dow M4195 was loaded until the concentration of cobalt in the effluent exceeded its concentration in the feed solution (i.e when nickel started displacing cobalt from the resin). The conditions under which these resins were loaded with copper, nickel and cobalt were discussed in chapter 3.6. The metal loadings on the resins used in the elution studies are reported in tables 6.1 and 6.2.

Table 6.1: Metals loading on Dow XUS43605

Metals concentration (ppm)						
Cu	**Ni**	**Co**	**Fe**	**Zn**	**Mn**	**Al**
21856	2634	7	42	<5	<5	<5

Table 6.2: Metals loading on Dow M4195

Metals concentration (ppm)					
Ni	**Co**	**Fe**	**Zn**	**Mn**	**Al**
18079	355	114	52	<5	<5

It is apparent that copper and nickel occupied the majority of the sites on Dow XUS43605, and on Dow M4195 nickel was the predominant species present.

6.1 Elution of metals from Dow XUS43605

6.1.1 Effect of eluant concentration on metal elution

Elution profiles for copper and nickel with 20 g/L, 100 g/L and 200 g/L H_2SO_4 are shown in figures 6.1 and 6.2, respectively. Both copper and nickel were fully eluted from Dow XUS43605 with 2-3 BV of 100 g/L and 200 g/L H_2SO_4, while complete copper elution with 20 g/L H_2SO_4 was achieved only after 10 BV. Nickel was completely eluted with 4 BV of 20 g/L H_2SO_4. 90% of the nickel on the resin was, however, stripped from the resin with 2 BV of 20 g/L H_2SO_4 while only 35% copper was stripped, suggesting that a split elution could be carried out to remove the majority of the nickel from the resin before the copper is removed. By selecting the appropriate conditions, a split elution could be carried out in order to obtain a purer copper-rich eluate.

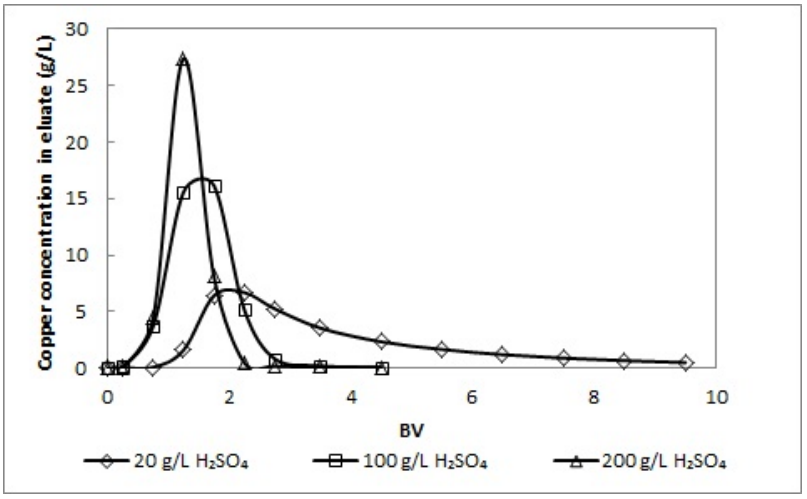

Figure 6.1: Effect of H_2SO_4 concentration on copper elution from Dow XUS43605

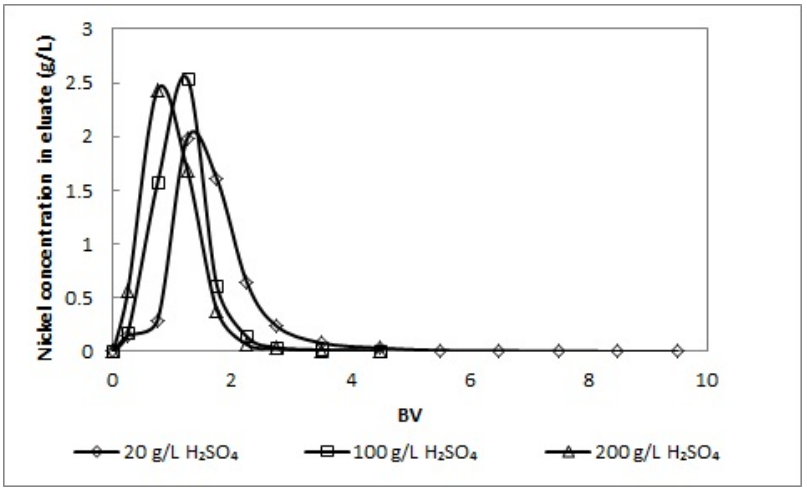

Figure 6.2: Effect of H_2SO_4 concentration on nickel elution from Dow XUS43605

6.1.2 Effect of flow rate on metal elution

The effect of eluant flow rate on metal elution was studied at 2 BV/h and 10 BV/h. The profiles for copper and nickel elution with 200 g/L H_2SO_4 at 60°C are shown in figures 6.3 and 6.3, respectively.

Increasing the flow rate from 2 BV/h to 10 BV/h did not affect the elution profiles of either one of the metals significantly. The rate of copper elution was slightly faster and showed a higher peak for the lower flow rate, and the same trend was witnessed for nickel elution under the conditions tested. Complete copper and nickel elution, however, was achieved after passing 2.5-3 BV of 200 g/L H_2SO_4 through the loaded resin bed, regardless of the flow rate.

6.1.3 Effect of temperature on metal elution

The trend observed in copper elution for an increase in temperature from 25 to 60°C was similar to the one observed for a decrease in flow rate (figure 6.5). Complete copper elution was achieved slightly earlier at 60°C than at 25°C with 200 g/L H_2SO_4. The elution of nickel, on the other hand, was affected to a greater extent by an increase in temperature - at 25°C nickel was 98% stripped with 4.5 BV of 200 g/L H_2SO_4 whereas it was completely stripped after passing 2.5 BV H_2SO_4 through the loaded resin bed at 60°C (figure 6.6).

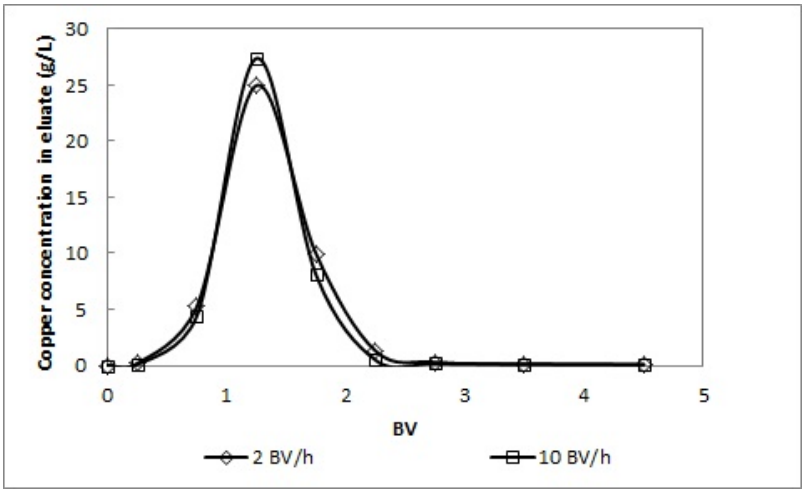

Figure 6.3: Effect of flow rate on copper elution from Dow XUS43605

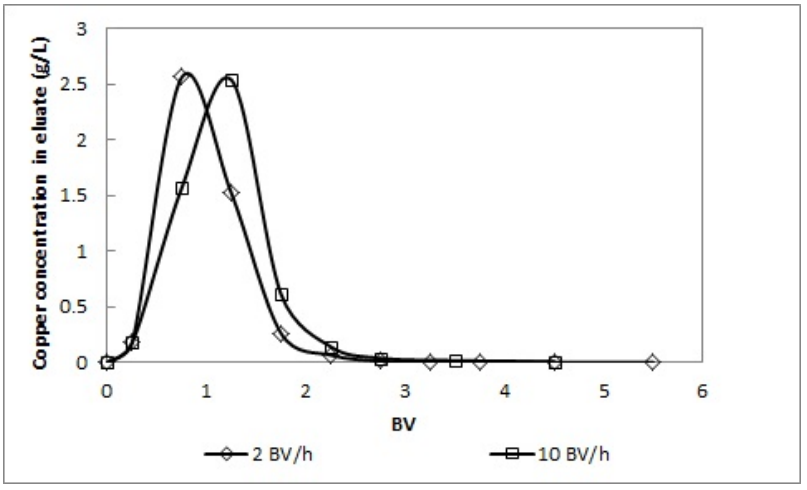

Figure 6.4: Effect of flow rate on nickel elution from Dow XUS43605

6.2 Elution of metals from DOW M4195

6.2.1 Effect of eluant concentration

The elution profiles in figures 6.7 and 6.8 demonstrate the effect of acid concentration on the elution of nickel and cobalt from Dow M4195. Virtually all of the nickel on the resin was stripped with 3-4 BV of 100 and 200 g/L H_2SO_4 while approximately only 27% of the nickel was stripped with 20 g/L H_2SO_4 (figure 6.7). It can be seen in figure 6.8 that all of the cobalt was stripped from the resin with 3-4 BV of H_2SO_4, irrespective of the eluant concentration. The

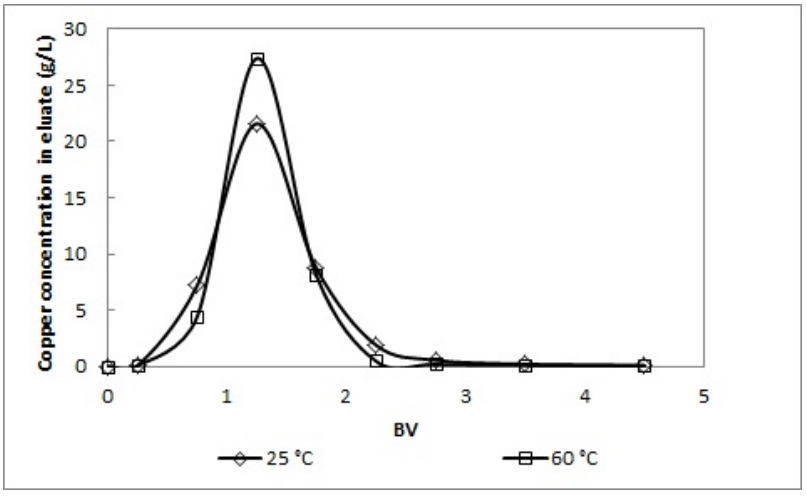

Figure 6.5: Effect of temperature on copper elution from Dow XUS43605

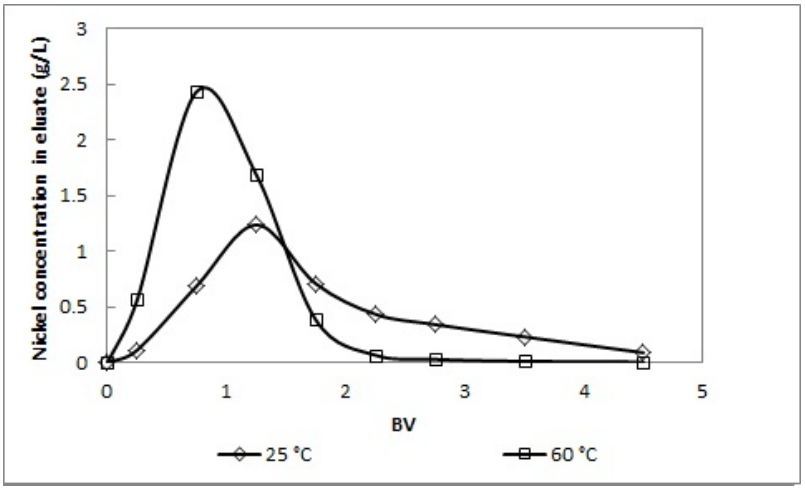

Figure 6.6: Effect of temperature on nickel elution from Dow XUS43605

maximum eluate nickel concentration occurred approximately 1.5 BV after that of cobalt when the resin was eluted with 20 g/L H_2SO_4. These results suggested that, with suitable control, a split elution could be performed to selectively strip the majority of the cobalt from the resin with 20 g/L H_2SO_4 after which nickel could be stripped with 200 g/L H_2SO_4.

These results are consistent with the results obtained by Rosato *et al.* (1984). In their study, Dow M4195, loaded with 13.1-15.3 g/L cobalt and 16.1-18.2 g/L nickel, was eluted with 2.5, 5 and 10% H_2SO_4. 64, 80 and 98% of the nickel was stripped with 6-8 BV of 2.5, 5 and 10% H_2SO_4, respectively, while nearly all of the cobalt was stripped with 4-6 BV of eluant, regardless of

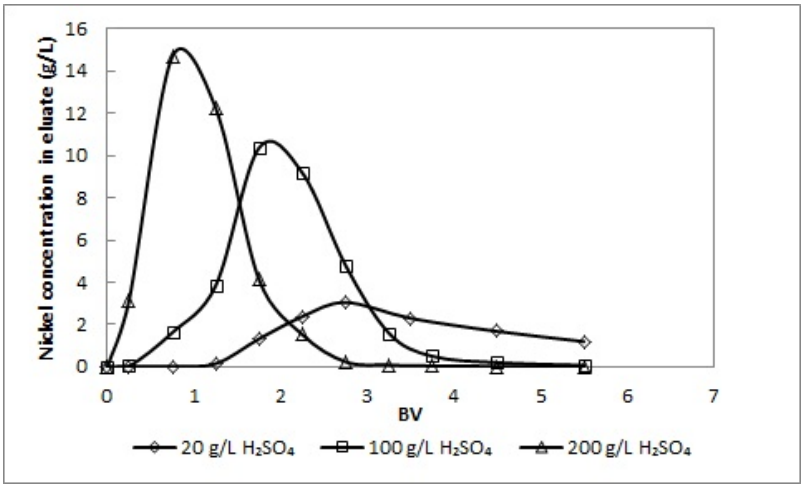

Figure 6.7: Effect of H_2SO_4 concentration on nickel elution from Dow M4195

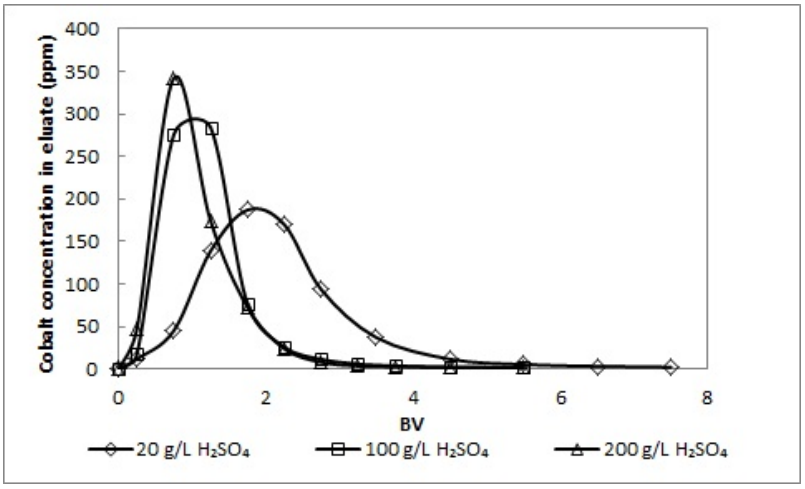

Figure 6.8: Effect of H_2SO_4 concentration on cobalt elution from Dow M4195

the eluant concentration. Both nickel and cobalt eluted faster from the resin in this study than in the work by Rosato *et al.* (1984). The discrepancies between the present study and the one by Rosato *et al.* (1984) can be explained by the differences in experimental conditions tested. The elution profiles in figures 6.7 and 6.8 are at 60 °C while those reported by Rosato *et al.* (1984) were at 25 °C. Other factors contributing to the differences between the two studies include that the columns used in this study were small in comparison with those used by Rosato *et al.* (1984), therefore the effects of channeling, dead volume and back-mixing are smaller in the present work, and also, the resin used in this study was only partially loaded with nickel whereas the resin used

by Rosato *et al.* (1984) was fully loaded with nickel and cobalt.

The results also correlate well with the results obtained by Rodgers and Marston (2010). These authors conducted an IX pilot trial at ASARCO in an attempt to recover copper and cobalt from their copper SX raffinate. Dow XUS 43578, the uniform, smaller PSD equivalent of Dow M4195, was loaded with 2.35 g/L cobalt and 1.2 g/L nickel, amongst other metals. The cobalt was eluted from the resin with 4 BV of 2% H_2SO_4, followed by nickel that was eluted with 2 BV of 20% H_2SO_4.

6.2.2 Effect of flow rate

The effect of flow rate on nickel and cobalt elution is shown in figures 6.9 and 6.10. Under the conditions tested the flow rate did not influence metal elution significantly and both the elution profiles for nickel and cobalt were essentially the same. Nickel and cobalt were eluted from Dow M4195 with 3 BV of 200 g/L H_2SO_4 at 60°C, irrespective of the flow rate. The elution peak for nickel, however, was slightly thinner and higher for 2 BV/h than it was for 10 BV/h. Rosato *et al.* (1984) also suggested that nickel elution can be minimized whilst effectively stripping cobalt by increasing the flow rate. They reported that most of the cobalt along with only 15% of the nickel can be eluted with 4 BV of 2.5% H_2SO_4 at a flow rate of 15-16 BV/hr.

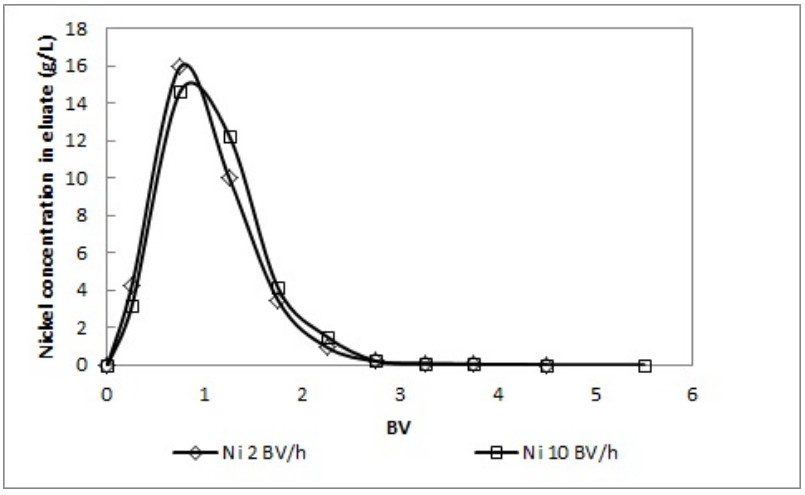

Figure 6.9: Effect of flow rate on nickel elution from Dow M4195

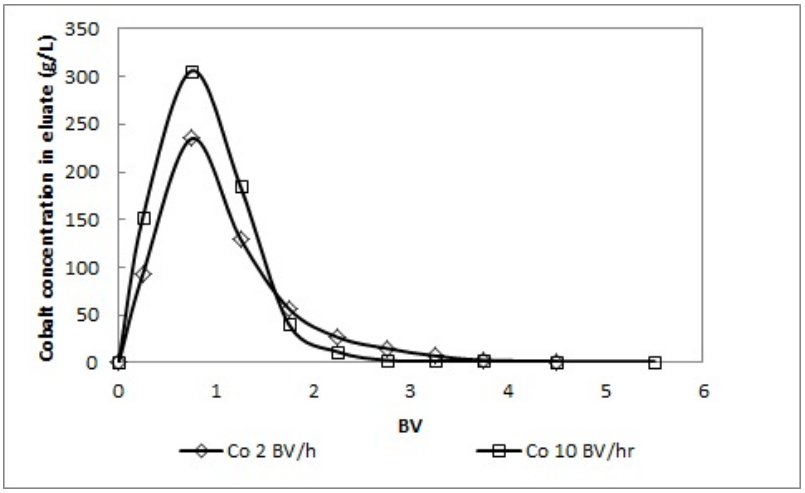

Figure 6.10: Effect of flow rate on cobalt elution from Dow M4195

6.2.3 Effect of temperature

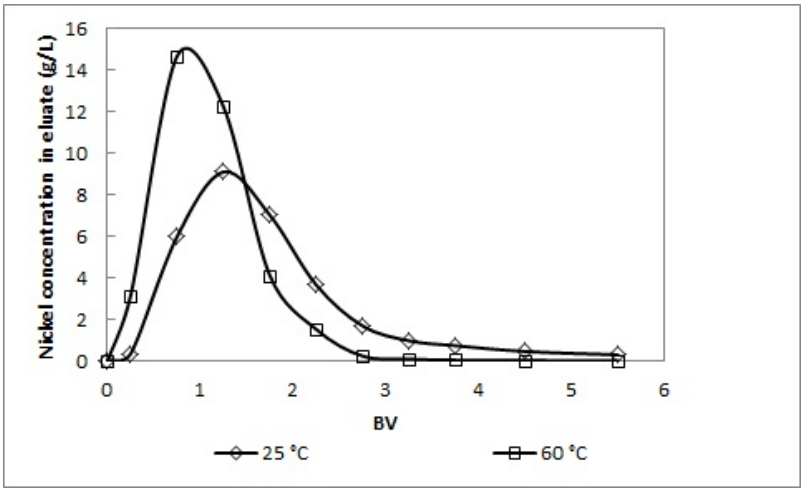

Figure 6.11: Effect of temperature on nickel elution from Dow M4195

Dow M4195 was eluted with 200 g/L H_2SO_4 at a flow rate of 10 BV/hr at 25°C and 60°C. The elution profiles for these experiments are shown in figures 6.11 and 6.12. The peak of the nickel elution profile shifted to the left and its height increased from 9 g/L to 15 g/L when the temperature was increased from 25°C to 60°C. Nickel was completely stripped with 3 BV of 200 g/L H_2SO_4 at 60°C while at 25°C 100% elution was only achieved with 4-6 BV of

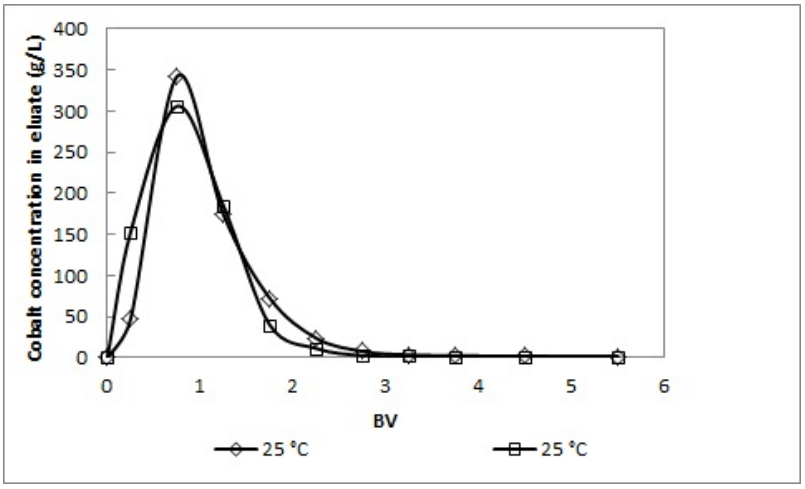

Figure 6.12: Effect of temperature on cobalt elution from Dow M4195

H_2SO_4, which is more in line with the results obtained by Rosato *et al.* (1984). The increase in temperature did not affect the elution of cobalt significantly.

Chapter 7

Flow sheet development

Two alternative flow sheets are proposed in this chapter for the recovery of the MOI based on the results obtained in the batch equilibrium and dynamic column sorption experiments. Both flow sheets are based on processing 36.5 BV of solution, as this was the point where copper was observed to break through the packed bed of Dow XUS43605 at a flow rate of 5 BV/h, initial solution pH of 4 and 60°C.

7.1 Flow sheet option 1

7.1.1 Solution purification

The bioleach solution exiting the heap bioleach at pH 0.8 - 1.2 and 60°C is treated with an SO_2/air mixture to selectively oxidize the ferrous iron in the solution to ferric iron, after which the ferric iron is precipitated out of the solution at pH 1-2 using calcium hydroxide (R-101 in figure 7.1). From literature it has been established that complete iron removal could be achieved using this approach with minimal losses of the MOI (Mouton *et al.*, 2007). After the solid/liquid separation step (screening), the solution pH is adjusted to 4 in V-101 prior to entering the IX circuit.

7.1.2 IX circuit

The IX circuit in this flow sheet consists of a single column packed with Dow XUS43605 (R-102A/B), followed by a lead-lag configuration of two columns, R-104A/B and R-106A/B, packed with Dow M4195 (A and B refer to process units in parallel to each other). A complete cycle consists of loading the desired metals onto the resins, followed by washing the excess feed from the resins with water. The loaded resins are then transported to the elution circuit where the metals are eluted and the resins are regenerated (converted back into the H^+-form). After washing excess eluant from the resins with water, they are returned to the loading circuit and the cycle repeats itself again. A PFD for this flow sheet is shown in figure 7.1 and the corresponding stream table is shown in table 7.1.

7.1.2.1 Copper adsorption and elution

The bioleach solution, at pH 4 and 60°C after iron removal and pH adjustment, is passed through the column containing Dow XUS43605 (R-102A) at a flow rate of 5 BV/h. At these operating conditions it was observed in column loading experiments that 100% copper and 14.4% nickel was adsorbed at copper breakthrough, which occurred at BV 36.5, therefore these recoveries were used to calculate the concentrations of copper and nickel on Dow XUS43605. As soon as copper breaks through the column, the feed is redirected to another column containing Dow XUS43605 (R-102B), and the loaded resin is transported to the copper elution column (R-103). Based on the elution results reported in chapter 6, 90% nickel could be removed along with 34% copper with 2 BV of 20 g/L H_2SO_4 (stream 19A). The remaining metals could then be stripped with 2 BV of 200 g/L H_2SO_4 (stream 19B). The resin, now fully regenerated, is returned to the loading circuit after having been washed with water.

The first eluate fraction (stream 19A) contains the majority of the nickel that was loaded on the resin, while the second fraction contains the majority of the copper.

Table 7.1: Stream table for PFD in figure 7.1

Stream number	1	8	9	10	11	16A	17A	18A	19A	19B	20A	20B	21A	21B
Flow rate (BV/h)	5	5	5	5	5	0.14	0.14	0.14	10	10	10	10	10	10
Temperature (°C)	60	60	60	60	60	60	60	60	60	60	60	60	60	60
pH	0.8-1.2	4	2	1-2	1-2				0-1	0-1	0-1	0-1	0-1	0-1
Species concentration (g/L)														
Cu^{2+}	0.69	0.69	0	0	0	-	-	-	4.28	8.31	-	-	-	-
Ni^{2+}	0.97	0.97	0.83	0.30	0	-	-	-	2.30	0.26	1.50	4.61	0.85	0.23
Co^{2+}	0.03	0.03	0.03	0.03	0	-	-	-	-	-	0.01	0	0.28	0
Fe^{2+} and Fe^{3+}	5.33	0	0	-	0	-	-	-	-	-	-	-	-	-
Zn^{2+}	0.02	0.02	0.01	0.01	0	-	-	-	-	-	0.02	0	0.12	0
Mn^{2+}	0.03	0.03	0.02	0.02	0.02	-	-	-	-	-	-	-	-	-
Al^{3+}	0.78	0.78	0.65	0.65	0.65	-	-	-	-	-	-	-	-	-
Mg^{2+}	1.05	1.05	0.88	0.88	0.88	-	-	-	-	-	-	-	-	-
Dow XUS43605 - Cu^{2+}	-	-	-	-	-	25.19	-	-	-	-	-	-	-	-
Dow XUS43605 - Ni^{2+}	-	-	-	-	-	5.11	-	-	-	-	-	-	-	-
Dow M4195 - Ni^{2+}	-	-	-	-	-	-	19.44	10.98	-	-	-	-	-	-
Dow M4195 - Co^{2+}	-	-	-	-	-	-	0.04	0.99	-	-	-	-	-	-
Dow M4195 - Zn^{2+}	-	-	-	-	-	-	0.07	0.42	-	-	-	-	-	-

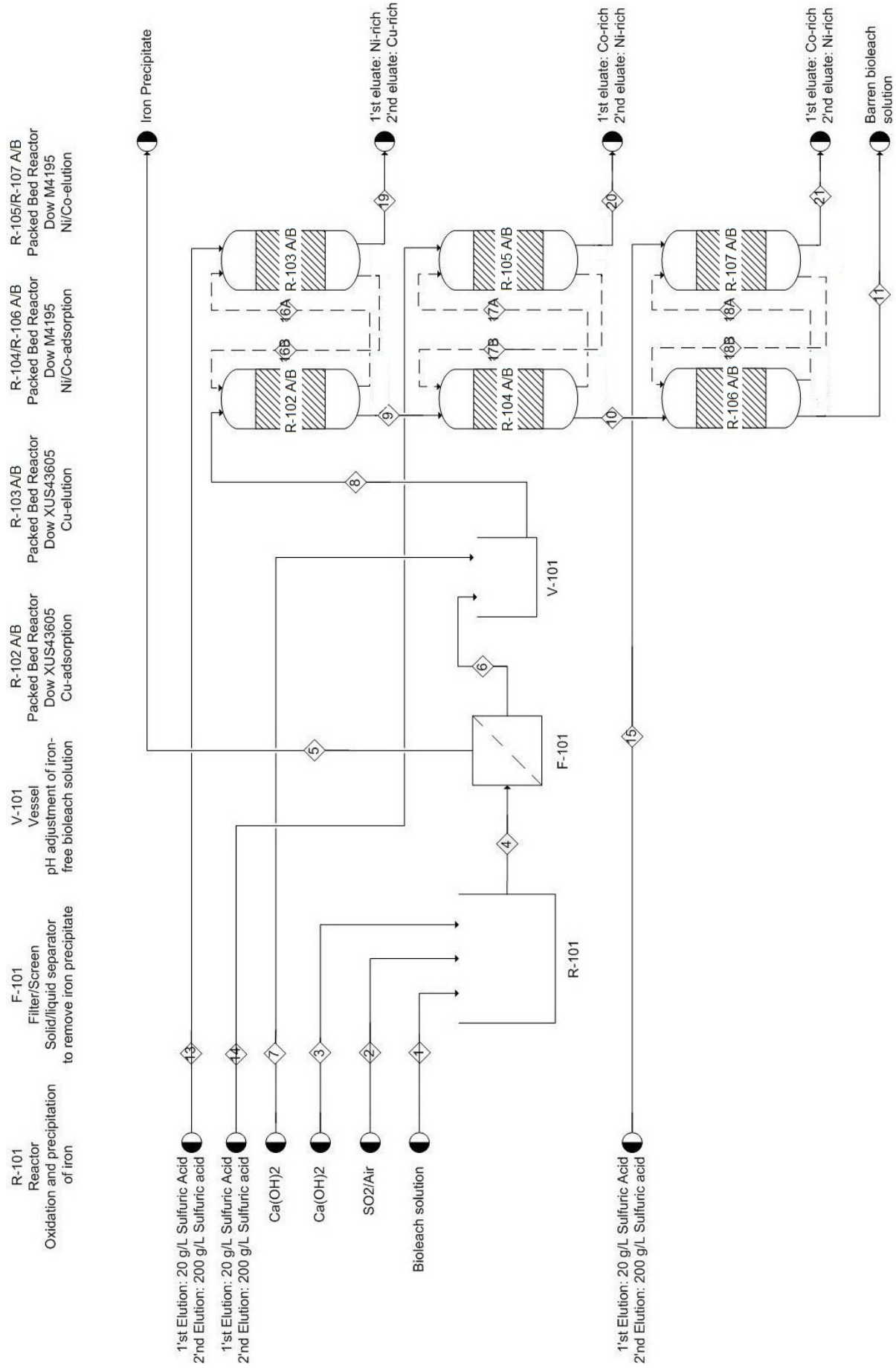

Figure 7.1: PFD for flow sheet option 1

7.1.2.2 Nickel and cobalt adsorption and elution

The copper-free bioleach solution exiting R-102 (stream 9) is treated in a lead-lag column configuration packed with Dow M4195 to adsorb nickel and cobalt (R-104A/B and R-106A/B). It was observed that, at the pH of the stream (pH 2), the maximum nickel capacity of Dow M4195 is 22.72 g/L. From the column loading experiments, it was observed that after processing 36.5 BV of the solution at 5 BV/h, 60°C and a pH of 2, approximately 64% nickel, 4% cobalt and 15% zinc were adsorbed by Dow M4195. The concentrations of these species on Dow M4195 reported in table 7.1 were calculated from these recoveries. It was assumed that the remaining nickel, cobalt and zinc (because of the similar selectivities of Dow M4195 towards cobalt and zinc) exiting the first column will be completely recovered in the second column because the majority of the nickel was already extracted in the first column.

After having been washed with water to remove excess feed, the loaded resins from the two columns are transported to the nickel and cobalt elution section. Cobalt and zinc are eluted from both the lead and lag column resins with 3.5 BV of 20 g/L H_2SO_4, while only 27% nickel elutes at this acid strength. The remaining nickel is then eluted with 3.5 BV of 200 g/L H_2SO_4. Instead of performing a split elution to recover the nickel, cobalt and zinc in separate fractions from the loaded resin of the lead column, a single elution could be performed to yield a stream with a composition of 5.56 g/L nickel, 10 ppm Co and 21 ppm Zn.

7.2 Flow sheet option 2

The second flow sheet option is essentially the same as the first option, except that an intermediate pH adjustment is made to increase the pH of the effluent from the copper adsorption section from 2 to 4. The motivation for this additional process step is the 40% increase in the capacity of Dow M4195 for nickel for this pH increase, as was seen from the nickel equilibrium loading isotherms for Dow M4195 at these pH levels. As mentioned previously, the two flow sheets considered here are based on processing 36.5 BV of bioleach solution as this is the point where copper breakthrough occurs, but in reality the lead

and lag columns will be removed from operation at a later stage. Therefore it is desirable to operate at a higher pH to obtain a higher nickel loading on the resin in the lead column, and to increase the recovery of cobalt in the second column.

The PFD and stream table for this flow sheet option is shown in figure 7.2 and table 7.2. In figure 7.2 there is an additional vessel (V-102) included in the flow sheet to increase the pH of the effluent from R-102, prior to entering the nickel and cobalt recovery section. From table 7.2 it can be seen that the pH adjustment prior to nickel and cobalt recovery resulted in a 18.5% increase in nickel recovery in the first column and a 32.7% decrease in the recovery thereof in the second column. This is desirable as the nickel concentration in the first eluate fraction of the lead column is more concentrated than in the case of flow sheet option 2, and less nickel is lost to the cobalt-rich eluate of the lag column. Instead of the split elution proposed for the recovery of nickel and cobalt from the lead column, a single elution could be performed to yield a stream with 6.58 g/L Ni, 13 ppm Co and 28 ppm Zn, as it is not worthwhile to purify the stream any further.

The first eluate fraction of the lag column must undergo further separation to recover the cobalt from nickel and zinc.

Table 7.2: Stream table for PFD in figure 7.2

Stream number	**1**	**8**	**9**	**11**	**12**	**13**	**17A**	**18A**	**19A**	**20A**	**20B**	**21A**	**21B**	**22A**	**22B**
Flow rate (BV/h)	5	5	5	5	5	5	0.14	0.14	0.14	10	10	10	10	10	10
Temperature (°C)	60	60	60	60	60	60	60	60	60	60	60	60	60	60	60
pH	0.8-1.2	4	2	4	2	1-2				0-1	0-1	0-1	0-1	0-1	0-1
Species concentration (g/L)															
Cu2+	0.69	0.69	0	0	0	0	-	-	-	4.28	8.31	-	-	-	-
Ni	0.97	0.97	0.83	0.83	0.20	0	-	-	-	2.30	0.26	1.78	5.46	0.57	0.15
Co	0.03	0.03	0.028	0.03	0.027	0	-	-	-	-	-	0.01	0	0.28	0
Fe	5.33	0	0	0	-	0	-	-	-	-	-	-	-	-	-
Zn	0.02	0.02	0.013	0.01	0.011	0	-	-	-	-	-	0.03	0	0.11	0
Mn	0.03	0.03	0.02	0.02	0.02	0.02	-	-	-	-	-	-	-	-	-
Al	0.78	0.78	0.65	0.65	0.65	0.65	-	-	-	-	-	-	-	-	-
Mg	1.05	1.05	0.88	0.88	0.88	0.88	-	-	-	-	-	-	-	-	-
Dow XUS43605 - Cu	-	-	-	-	-	-	25.19	-	-	-	-	-	-	-	-
Dow XUS43605 - Ni	-	-	-	-	-	-	5.11	-	-	-	-	-	-	-	-
Dow M4195 - Ni	-	-	-	-	-	-	-	23.03	7.39	-	-	-	-	-	-
Dow M4195 - Co	-	-	-	-	-	-	-	0.05	0.98	-	-	-	-	-	-
Dow M4195 - Zn	-	-	-	-	-	-	-	0.10	0.39	-	-	-	-	-	-

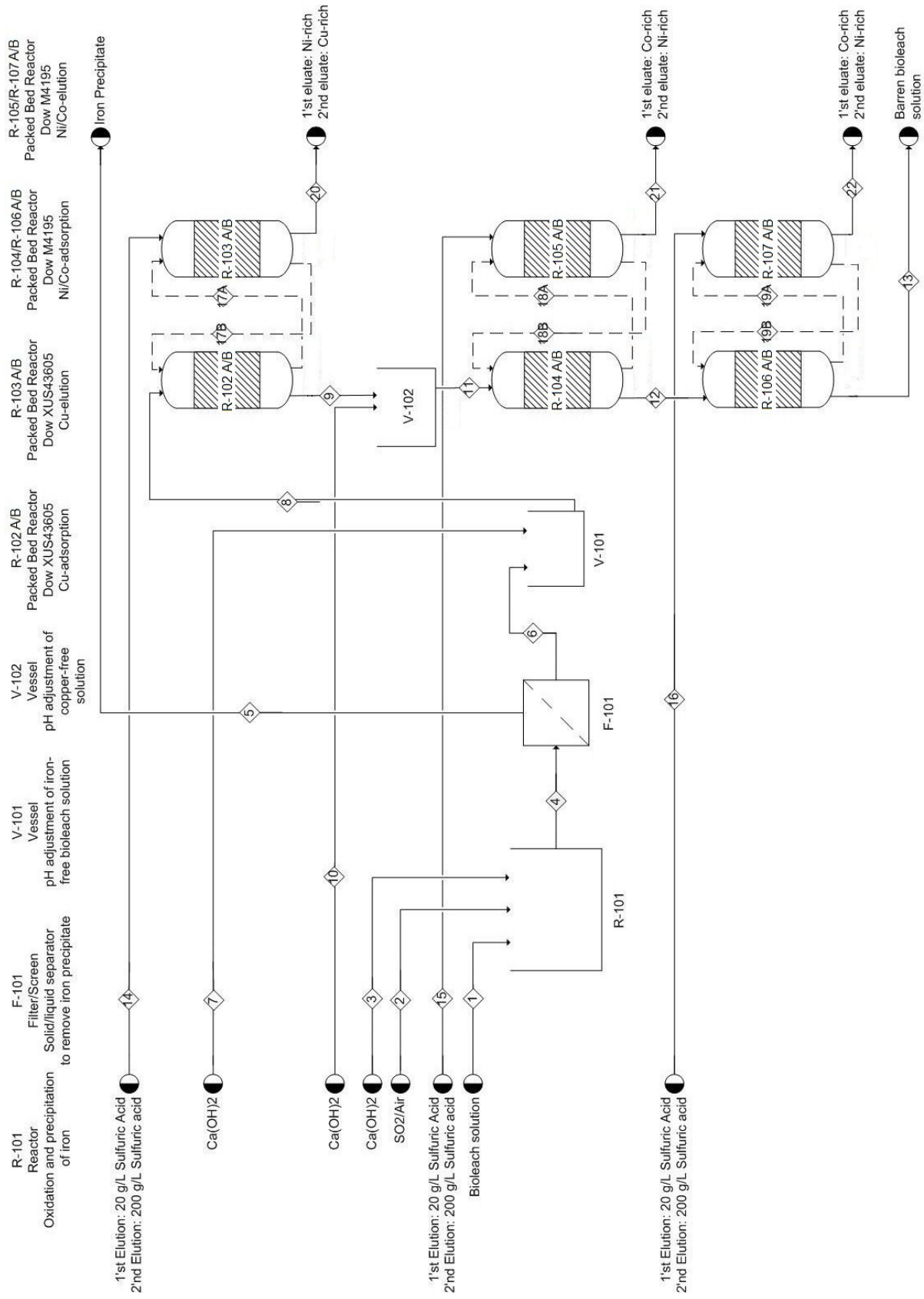

Figure 7.2: PFD for flow sheet option 2

Therefore, the overall recoveries of copper, nickel, cobalt and zinc for both flow sheets are 100%. This is because none of the MOI ever breaks through the IX circuit (MOI concentration in the effluent from the IX circuit maintained at zero). Of the 100% nickel that is loaded onto the resins in the IX circuit, 14% nickel is lost to the copper eluate for both flow sheets, while the nickel lost to the cobalt rich eluate of the lag column (R-107) is reduced from 8.3% for flow sheet option 1 to 5.6% for flow sheet option 2. By reducing the flow rate at which the process is carried out, these losses can be reduced. Also, by modifying flow sheet 2 and carrying out the copper recovery with Dow XUS43605 at a lower pH (pH 2 or 3), nickel losses to the copper eluate could be minimized as the resin's selectivity towards nickel is lower at lower solution pH values.

Chapter 8

Conclusion

The objectives of the project, as listed in section 1.4, were achieved. The conclusions are discussed at the hand of these objectives.

8.1 Select the appropriate resins for the selective recovery of the MOI

Five resins had been selected, based on published literature and on recommendations made by resin manufacturers, to be screened based on their suitability for the selective recovery of the MOI. These resins included Dow M4195 (bis-PA), Dow XUS43605 (HPPA), Amberlite IRC748 (IDA), Purolite S930Plus (IDA) and Purolite S930 (A/C).

8.2 Screen the selected resins based on selectivity towards the MOI

Screening tests were conducted in order to determine which resins are the most selective towards the MOI. It was found that Dow XUS43605 and Dow M4195 were the best options for the selective recovery of copper over other metals in the solution. α_{Fe}^{Cu} was found to be 153 and 26.6 for Dow M4195 and Dow XUS43605 at pH 3, respectively, and increased to 1492 and 226 when the pH increased to a value of 4. For Amberlite IRC748, Purolite S930 and Purolite

S991 iron rejection at both pH 3 and 4 was much poorer than for Dow M4195 and Dow XUS43605. α_{Fe}^{Cu} for these resins was less than 1 at pH 3 and less than 90 at pH 4. With respect to nickel and cobalt recovery, Dow M4195 showed to be the only resin able to selectively recover nickel and cobalt over iron, where α_{Fe}^{Ni} and α_{Fe}^{Co} were observed to be 9.73 and 3.86, respectively, at pH 4. Therefore, based on the screening test results, Dow XUS43605 and Dow M4195 was selected to be subjected to further tests. Amberlite IRC748 was co-selected as literature had stated that this resin elutes more effectively than Purolite S930Plus.

8.3 Determine kinetic and equilibrium parameters

Metal extraction kinetics tests and batch equilibrium tests were conducted with the resins that were selected based on the results of the screening tests. The initial rate of copper and nickel loading onto Dow M4195, Amberlite IRC748 and Dow XUS43605 was modeled following a second-order approach-to-equilibrium approach, and the rate constants determined from these models were used to compare metal uptake rates of the different resins. As ion exchange and adsorption are generally limited by intra-particle mass transfer, Dow XUS43605, which has the smallest average particle size (320μm), was observed to attain equilibrium the fastest, followed by Amberlite IRC748 (with particle sizes ranging from 500μm to 650μm) and Dow M4195 (with particle sizes ranging from 300μm to 850μm).

The effect of temperature on metal uptake rate and equilibrium loading was also studied with Dow XUS43605 and Dow M4195. As expected, an increase in temperature from 25°C to 60°C lowered the distributions of copper (with Dow XUS43605) and nickel (with Dow M4195) from 210 to 165, and from 75.56 to 63.65, respectively, while the kinetics of both copper and nickel loading onto Dow XUS43605 and Dow M4195 increased for the increase in temperature. The increased metal loading conditions at elevated temperature could be explained by the decrease in solution viscosity and enhanced intra-particle mass transfer.

Metals' equilibrium concentrations on Dow XUS43605 and Dow M4195

were determined by contacting these resins with synthetic bioleach solution at resin to solution ratios of 1:5 to 1:120. Single component Freundlich and Langmuir isotherm models were fitted to the copper and nickel isotherm data. In both cases the Langmuir model provided a better fit for the equilibrium data. The equilibrium capacity of Dow XUS43605 was determined to be 26.04 g/L, while the maximum equilibrium loading of nickel on Dow M4195 increased from 22.72 g/L at pH 2 to 30.86 g/L at pH 4.

8.4 Investigate the effects of process parameters on dynamic column adsorption and elution

Breakthrough profiles for Dow M4195, Dow XUS43605 and Amberlite IRC748 showed that Dow XUS43605 was the best suited for the continuous recovery of copper and Dow M4195 was the best suited for the dynamic recovery of nickel and cobalt. These tests were conducted at 25°C, at a flow rate of 10 BV/h and initial solution pH values of 3 and 4. As expected, iron selectivity for Amberlite IRC748 was high at pH 3, and at pH 4 this resin's selectivity towards all other metals increased. The faster rate at which Dow XUS43605 attained equilibrium was demonstrated as approximately 80% of the resin capacity was utilized at copper breakthrough at this high flow rate, while the percentage capacity utilization of Dow M4195 and Amberlite IRC748 at copper breakthrough at 10 BV/h was in the order of 14% and 35%, respectively. These results were obtained at a solution pH of 3. At pH 4 the capacity utilization of Dow M4195 and Dow XUS43605 was the same, but for Amberlite IRC748 it increased to 46%.

In general the flow rate and temperature were the operating conditions that had the most significant influence on the MOI loadings on Dow XUS43605 and Dow M4195 at copper and nickel breakthrough. For an increase in temperature from 25°C to 60°C, the copper loading on Dow XUS43605 increased by 36%. The main factor that influenced the amount of nickel co-loading on Dow XUS43605 was found to be the initial solution pH; an increase in pH resulted

in an increased loading of nickel on Dow XUS43605.

In the dynamic recovery of nickel and cobalt the temperature and initial solution pH had the greatest effects as a result of the increased rate of metal adsorption of Dow M4195 at elevated temperatures and its increased capacity for the TMs at higher pH values. The effect of flow rate was also more pronounced for metal recovery with Dow M4195 than for Dow XUS43605 as a result of the resin's slower rate metal adsorption.

Dynamic column elution experiments were performed to elute metals from XUS43605 and Dow M4195. It was determined that copper eluted from Dow XUS43605 in 2, 3 and 10 BV using 20 g/L, 100 g/L and 200 g/L H_2SO_4, respectively, at a flow rate of 2 BV/h. Co-loaded nickel on Dow XUS43605 was fully eluted at the same conditions with 4 BV of 20 g/L H_2SO_4. These results suggested that a split elution is possible by optimizing the eluant concentration, but this was not done in this thesis.

Cobalt was fully eluted from Dow M4195 with 4 BV of 20 g/L H_2SO_4, while the percentage nickel elution at this point was 27%. Nickel was completely eluted from the resin with 3 BV of 200 g/L H_2SO_4, thus a split elution could also be performed to remove the majority of the cobalt with 3-4 BV of 20 g/L H_2SO_4 followed by 3 BV of 200 g/L H_2SO_4 to obtain a purer nickel-rich eluant.

8.5 Construct a workable flow sheet for the recovery of the MOI

Two flow sheets were proposed for the recovery of the MOI with IX. The column configuration proposed in the first flow sheet consisted of a single column packed with Dow XUS43605 (copper recovery section) followed directly by two columns (a lead-lag configuration) packed with Dow M4195 (nickel and cobalt recovery section). The second flow sheet only included a pH adjustment step between the copper recovery section and the nickel and cobalt recovery section. Overall recoveries of copper, nickel, cobalt and zinc for both flow sheets were 100%. 14% nickel was lost to the copper eluate for both flow sheets, while the nickel lost to the cobalt rich effluent of the lag column (R-107) was reduced from 8.3% for flow sheet option 1 to 5.6% for flow sheet

option 2. By reducing the flow rate at which the process is carried out, these losses could be reduced. Also, by modifying flow sheet 2 and carrying out the copper recovery with Dow XUS43605 at a lower pH (pH 2 or 3), nickel losses to the copper eluate could be minimized as the resin's selectivity towards nickel is lower at lower solution pH values.

Chapter 9

Future Work

The following recommendations are made regarding future work:

- Investigate the degree of iron oxidation and precipitation that is achievable from the bioleach solution as an assumption based on literature has been made regarding the degree of iron removal. It is suggested that the SO_2/air system discussed in chapter 1 is used for the oxidation of ferrous to ferric iron followed by precipitation of the ferric iron as a hydroxide salt.

- Construct metal equilibrium loading isotherms for Dow XUS43605 and Dow M4195 at 60°C as the bioleach exits the heap bioleach at this temperature and therefore the IX process will most probably be carried out at this temperature. Furthermore, it was established in this thesis that there is a significant increase in the metal uptake rates of Dow XUS43605 and Dow M4195 at elevated temperatures which was demonstrated to be advantageous in terms of MOI recovery. Also investigate metal adsorption kinetics at 60°C in more detail for these resins.

- Use a lead-lag column configuration for the recovery of nickel and cobalt with Dow M4195. This would approach real-life operation better than the single columns that were operated in this thesis.

- Run the copper guard bed (Dow XUS43605), and lead-lag column configuration for nickel and cobalt recovery (Dow M4195) in continuous mode.

- Perform split elutions with the recommended eluate concentrations to obtain purer copper-rich and nickel-rich eluates.
- Upscale the laboratory-scale recovery of copper with Dow XUS43605 and nickel and cobalt with Dow M4195 to a pilot plant scale.

List of References

Cotton, F. and Wilkinson, G. (1988). *Advanced Inorganic Chemistry*. 1st edn. Wiley.

Davies, J., Hockensmith, C., Kukushkina, V. and Kukushkin, Y. (1996). *Synthetic Coordination Chemistry*. World Scientific.

Deepatana, A., Tang, J. and Valix, M. (2006). Comparitive study of chelating ion exchange resins for metal recovery from bioleaching of nickel laterite ores. *Minerals Engineering*, vol. 19, pp. 1280–1289.

Diniz, C., Doyle, F. and Ciminelli, V. (2002). Effect of pH on the adsorption of selected heavy metal ions from concentrated chloride solutions by chelating resin dow m4195. *Separation Science and Technology*, vol. 37, pp. 3169–3185.

Dorfner, K. (1991). *Ion Exchange*, vol. 1. Walter De Gruyter.

Falk, G., Litz, C. and Taylor, R. (2000). Wastewater technology fact sheet, chemical precipitation. *EPA Report 832-F-00-018*, pp. 1–8.

Fleming, C. and Nicol, M. (1980). A comparitive study of kinetic models for the extraction of uranium by strong base anion exchange resin. *Journal of the South African Institute of Mining and Metallurgy*, vol. 80, no. 2, pp. 89–99.

Flett, D. (2004). Cobalt-nickel separation in hydrometallurgy: a review. *Chem. Sust. Develop.*, vol. 12, pp. 81–91.

Grinstead, R. (1984). Selective absorption of copper, nickel, cobalt and other transition metal ions from sulfuric acid solutions with the chelating ion exchange resin Dow XFS 4195. *Hydrometallurgy*, vol. 12, pp. 387–400.

Habashi, F. (1990). *A textbook of Hydrometallurgy*. 1st edn.

Hamdaoui (2009). Removal of copper(II) from aqueous phase using Purolite C100-MB cation exchange resin in fixed-bed column: modeling. *Hazardous Materials*, vol. 161, pp. 737–746.

Helfferrich, F. (1995). *Ion Exchange*. Dover Publications.

Ho, E. and Quan, C. (2007). Iron(II) oxidation by SO_2/O_2 for use in uranium leaching. *Hydrometallurgy*, vol. 85, pp. 183–192.

Irving, H. and Williams, R. (1953). The stability of transition metal complexes. *Chemical Society*, pp. 3192–3210.

Jay, B. (1998). Applications of ion exchange technology on copper hydrometallurgy. In: *ALTA Copper Hydrometallurgy Conference*, pp. 1–33.

Jeffers, T. and Harvey, M. (1985). Cobalt recovery from copper leach solutions. Tech. Rep., United States Bureau of Mines.

Koretsky, M. (2003). *Engineering and chemical thermodynamics*. 1st edn. Wiley.

Lin, L. and Juang, R. (2007). Ion exchange kinetics of copper and zinc from aqueous solutions with two chelating resins. *Chemical Engineering*, vol. 132, pp. 205–213.

Loan, M., Parkinson, G., Newman, M. and Farrow, G. (2002). Iron oxy-hydroxide crystallization in hydrometallurgical residue. *J. Crystal Growth*, vol. 235, pp. 482–488.

Mendez, F. and Martins, A. (2004). Selective sorption of nickel and cobalt from sulphate solutions using chelating resins. *Minerals Processing*, vol. 74, pp. 359–371.

Monhemius, J. (1981). Hydrometallurgical processing of complex materials. *Chem. Ind. (London)*, vol. 20, pp. 410–420.

Mouton, M., van Deventer, J. and Vaarno, J. (2007). Oxidative precipitation of iron and manganese by air/SO_2. In: *The Fourth Southern African Conference on Base Metals*, pp. 179–192.

Mwase, J. (2009). *Hydrometallurgical extraction of platinum group metals from a low grade ore concentrate*. Master's thesis, University of Cape Town.

Mwase, J., Petersen, J. and Eksteen, J. (2012). A conceptual flow sheet for heap leaching of platinum group metals (PGMs) from a low-grade ore concentrate. *Hydrometallurgy*, vol. 111-112, pp. 129–135.

Nicol, M. (2003). Ion exchange and adsorption in hydrometallurgy. Notes for a course presented for Anglo-American Research Laboratories.

Pavlides, A. and Wyethe, J. (2000). Ion exchange column design for separation of nickel traces from cobalt electrolyte. Tech. Rep., Bateman.

Pearson, R. (1963). Hard and soft acids and bases. *Journal of American Chemical Society*, vol. 85, pp. 3533–3539.

Petersen, J. and Dixon, D. (2002). Thermophylic heap leaching of a chalcopyrite concentrate. *Minerals Engineering*, vol. 15, no. 11, pp. 777–785.

Riveros, P. and Cooper, W. (1988). Kinetic aspects of the ion exchange extraction of gold, silver and base metal cyano-complexes. *Environmental Science and Technology*, vol. 16, pp. 852–857.

Rodgers, M., Marston, C. and Nedebeker, N. (2010). Cobalt recovery from copper solvent extraction raffinate using ion exchange resins. In: *SME Annual Meeting*, pp. 1–6.

Rosato, L., Harris, G. and Stanley, R. (1984). Separation of nickel from cobalt in sulphate medium by ion exchange. *Hydrometallurgy*, vol. 13, pp. 33–44.

Schouwstra, R. and Kinloch, E. (2000). A short geological review of the bushveld complex. *Platinum Metals Review*, vol. 44, no. 1, pp. 33–39.

Sirola, K. (2009 December). *Chelating Adsorbents in Purification of Hydrometallurgical Solutions*. Ph.D. thesis, Lappeenranta University of Technology, Acta Universitatis, Lappeenrantaesis, 360.

Sirola, K., Laatikainen, M. and Paatero, E. (2010*a*). Effect of temperature on sorption of metals by silica supported 2-(aminomethyl)pyridene. Part I: Binding equilibria. *Reactive and functional polymers*, vol. 70, pp. 48–55.

Sirola, K., Laatikainen, M. and Paatero, E. (2010*b*). Effect of temperature on sorption of metals by silica supported 2-(aminomethyl)pyridene. Part II: Sorption dynamics. *Reactive and functional polymers*, vol. 70, pp. 48–55.

Vallet, V., Wahlgren, U. and Grenthe, I. (2003). Chelate and effect thermodynamics of metal complex formation in solution: a quantum quality study. *Journal of American Chemical Society*, vol. 125, pp. 14941–14950.

Williams, R. (1952). The stability of complexes of group IIA metal ions. *Chemical Society*, pp. 3770–3778.

Zainol, Z. and Nicol, M. (2009). Comparitive study of chelating ion exchange resins for the recovery of nickel and cobalt from laterite leach tailings. *Hydrometallurgy*, vol. 96, pp. 283–287.

Zhang, W. and Muir, D. (2010). Oxidation of Fe(II) in a synthetic nickel laterite leach liquor with SO2/air. *Minerals Engineering*, vol. 23, pp. 40–44.

Zhang, W., Muir, D. and Singh, P. (2000). Fe(ii) oxidation by SO_2/O_2 in acidic media part II. effect of copper. *Hydrometallurgy*, vol. 58, pp. 117–125.

Appendices

Appendix A

pH dependence of adsorption constant

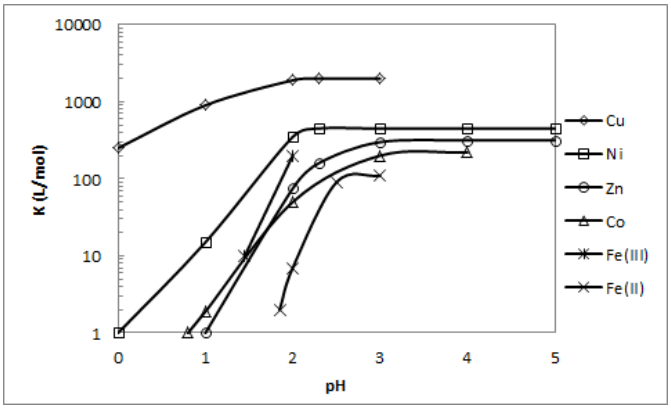

Figure 1: Effect of pH on the metal adsorption constant for various transition metals with Dow M4195

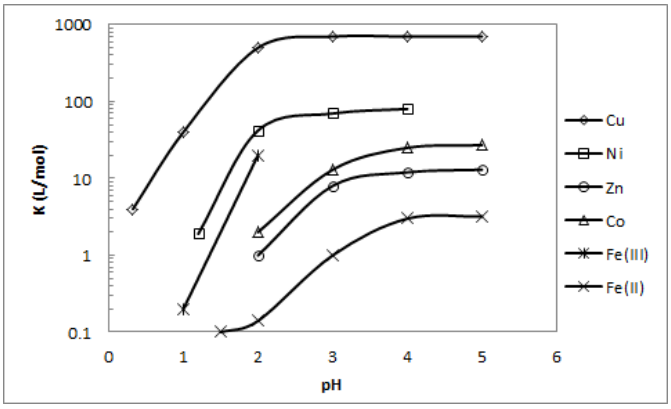

Figure 2: Effect of pH on the metal adsorption constant for various transition metals with Dow XUS43605

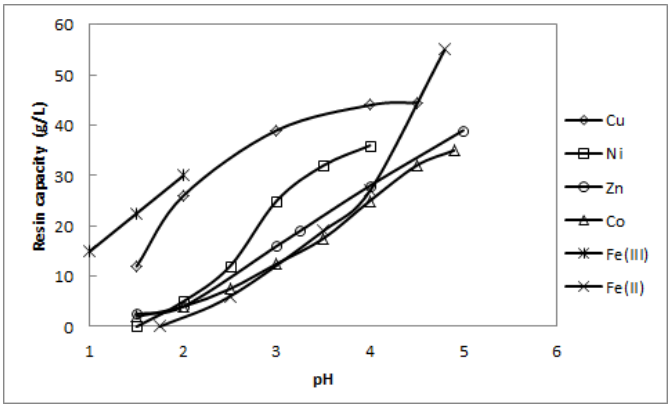

Figure 3: Effect of pH on the metal adsorption for various transition metals with Amberlite IRC748

Appendix B

Kinetics of copper extraction

Kinetics for Dow M4195

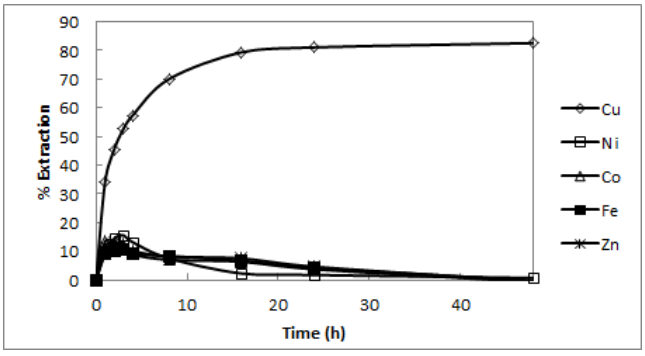

Figure 4: Metal extraction profile with Dow M4195 at pH 2

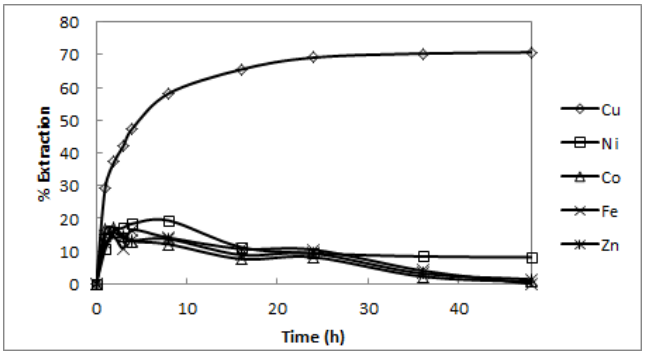

Figure 5: Metal extraction profile with Dow M4195 at pH 3

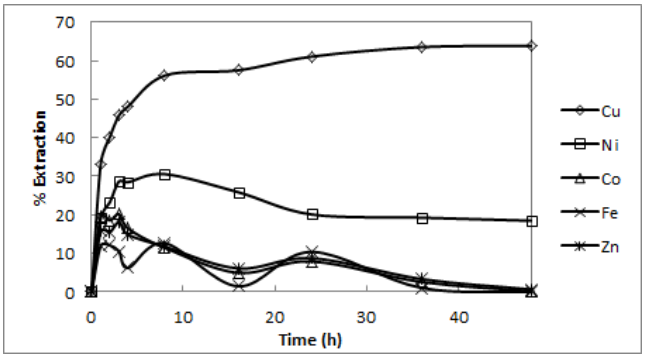

Figure 6: Metal extraction profile with Dow M4195 at pH 4

Kinetics for Amberlite IRC748

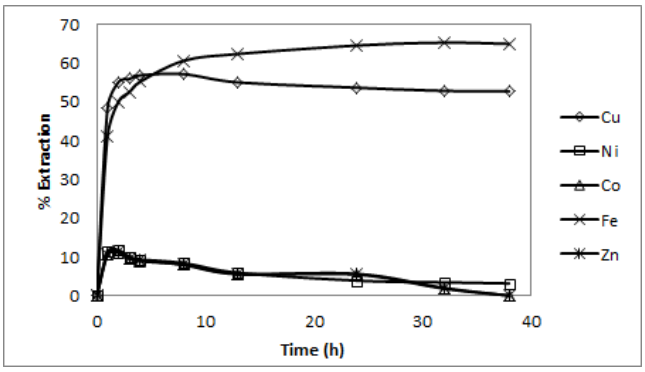

Figure 7: Metal extraction profile with Amberlite IRC748 at pH 2

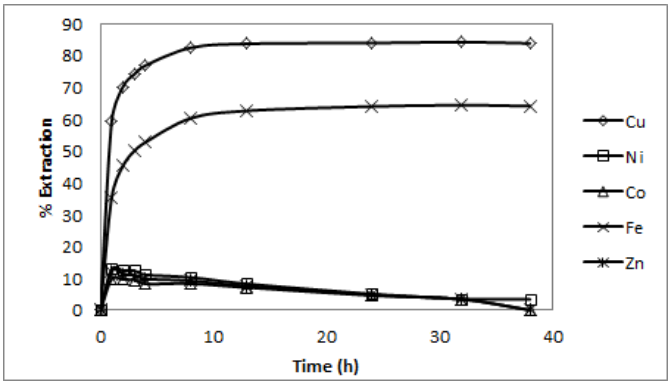

Figure 8: Metal extraction profile with Amberlite IRC748 at pH 3

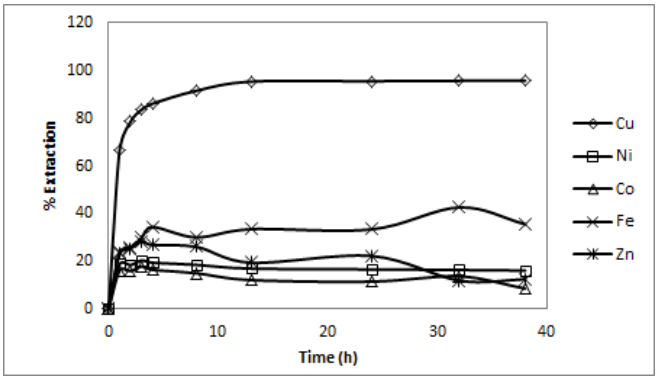

Figure 9: Metal extraction profile with Amberlite IRC748 at pH 4

Kinetics for XUS43605

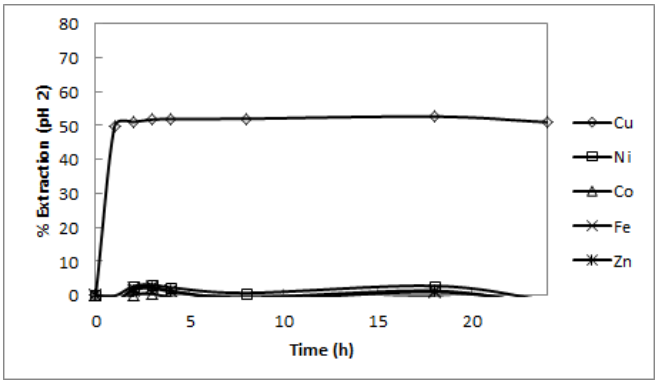

Figure 10: Metal extraction profile with XUS43605 at pH 2

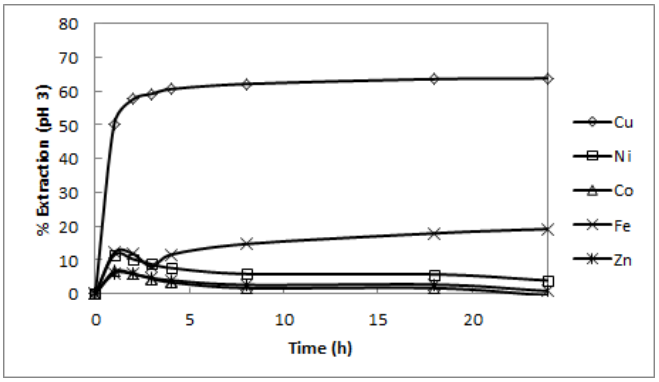

Figure 11: Metal extraction profile with XUS43605 at pH 3

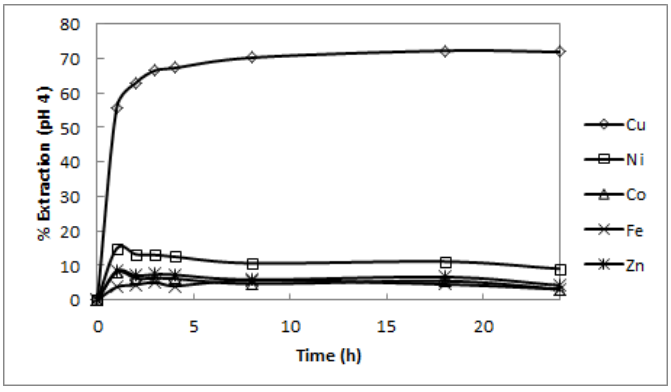

Figure 12: Metal extraction profile with XUS43605 at pH 4

Kinetics of nickel extraction

Kinetics for Dow M4195

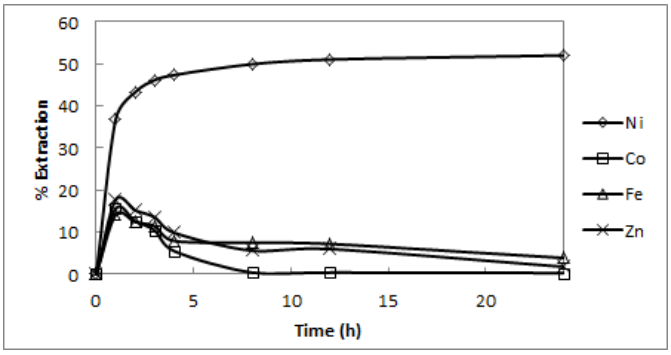

Figure 13: Metal extraction profile with Dow M4195 at pH 2

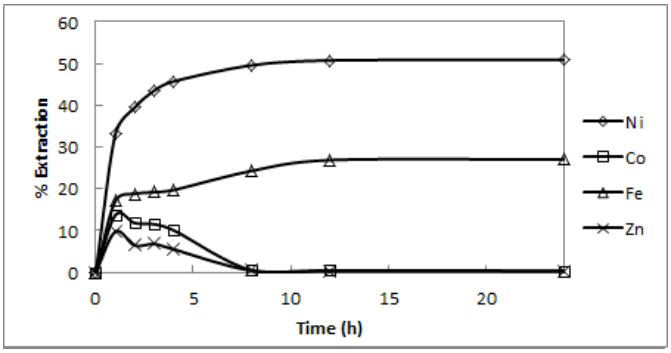

Figure 14: Metal extraction profile with Dow M4195 at pH 3

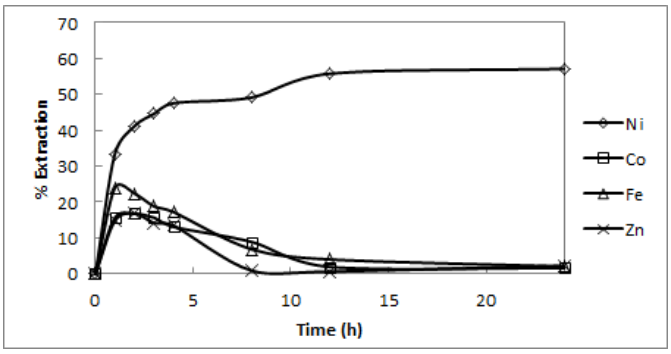

Figure 15: Metal extraction profile with Dow M4195 at pH 4

Kinetics for Amberlite IRC748

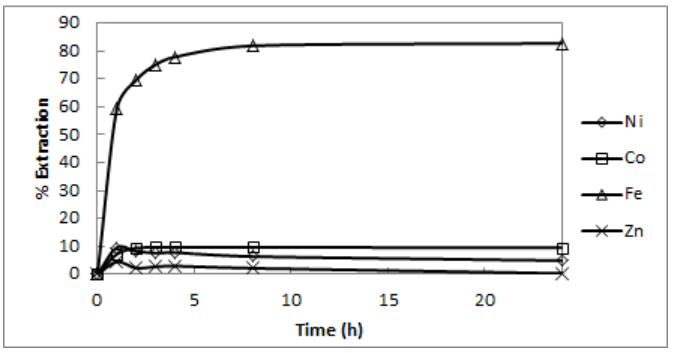

Figure 16: Metal extraction profile with Amberlite IRC748 at pH 2

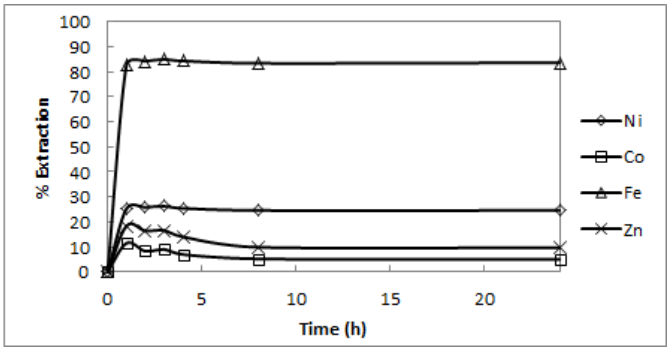

Figure 17: Metal extraction profile with Amberlite IRC748 at pH 3

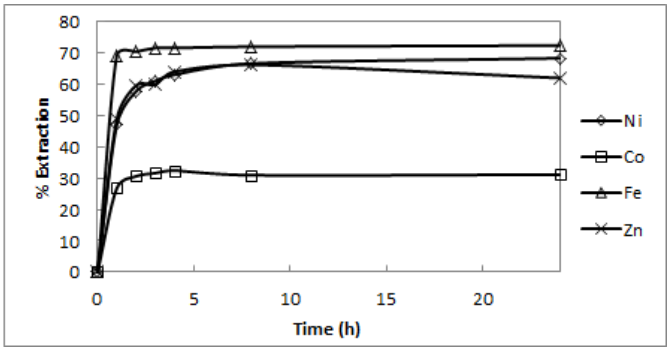

Figure 18: Metal extraction profile with Amberlite IRC748 at pH 4

Kinetics for Dow XUS43605

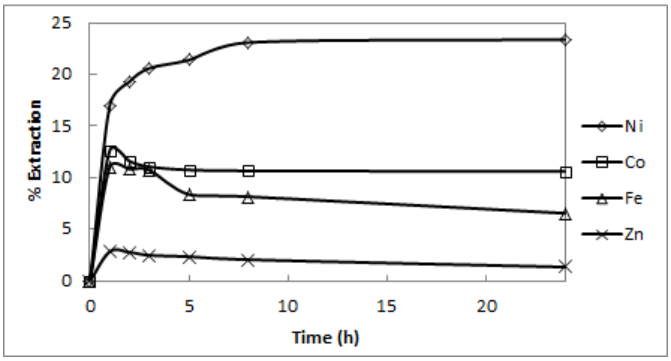

Figure 19: Metal extraction profile with Dow XUS43605 at pH 2

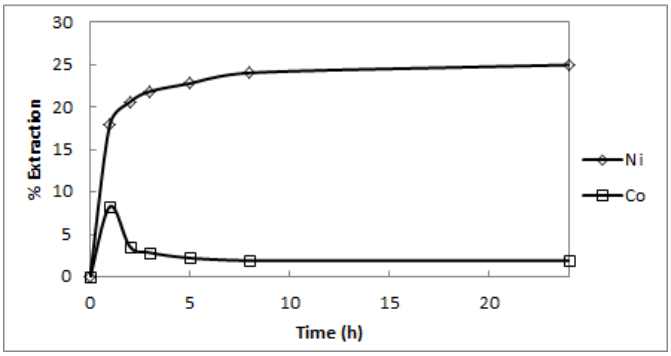

Figure 20: Metal extraction profile with Dow XUS43605 at pH 3

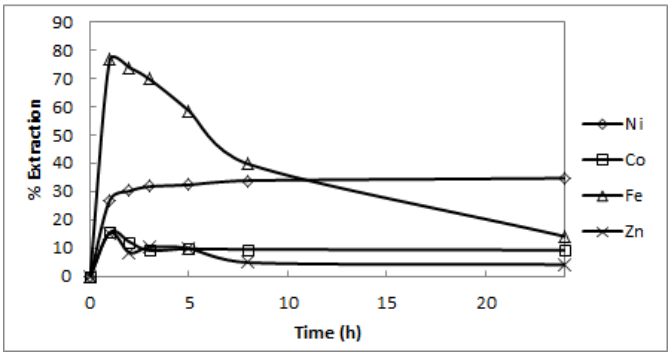

Figure 21: Metal extraction profile with Dow XUS43605 at pH 4

Appendix C

Column loading breakthrough profiles for experimental design

Solution A breakthrough profiles with Dow XUS43605

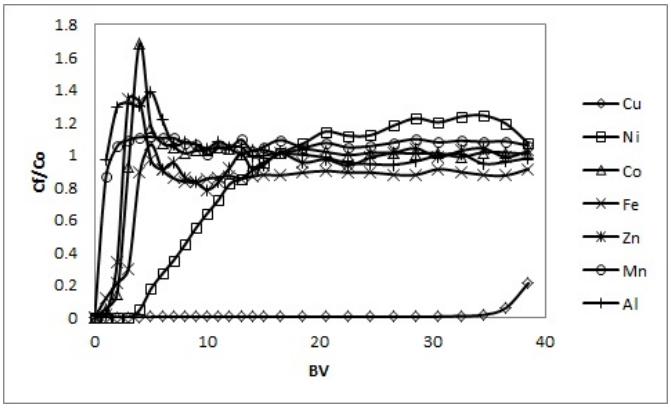

Figure 22: Metal breakthrough profiles for Dow XUS43605: Experiment 1

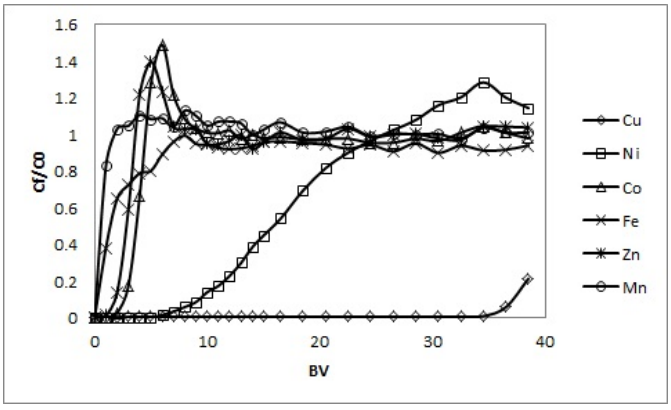

Figure 23: Metal breakthrough profiles for Dow XUS43605: Experiment 2

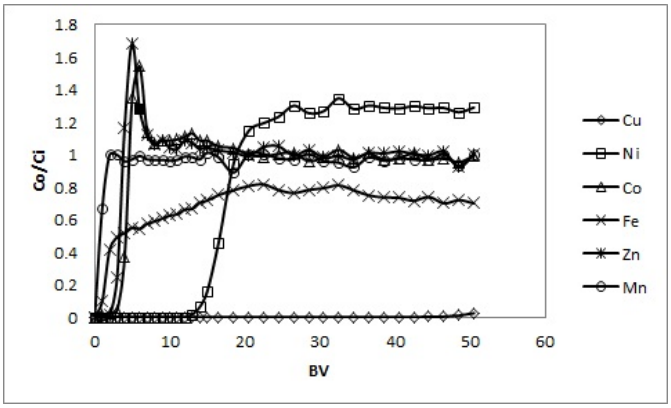

Figure 24: Metal breakthrough profiles for Dow XUS43605: Experiment 3

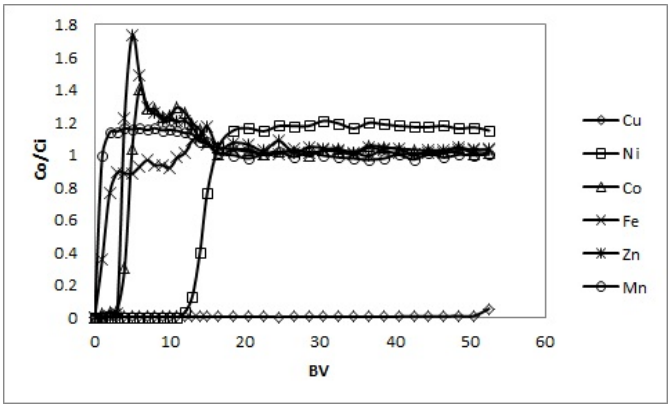

Figure 25: Metal breakthrough profiles for Dow XUS43605: Experiment 4

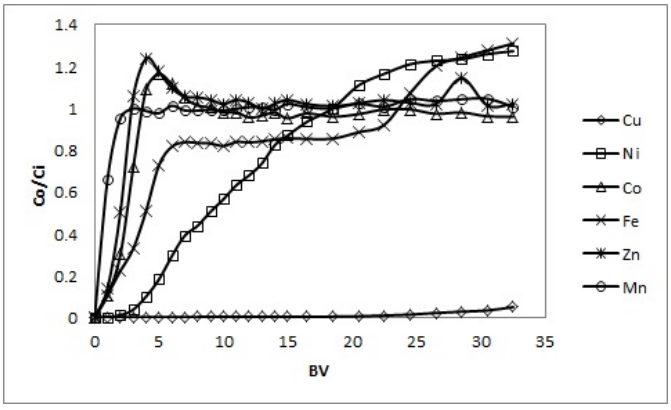

Figure 26: Metal breakthrough profiles for Dow XUS43605: Experiment 5

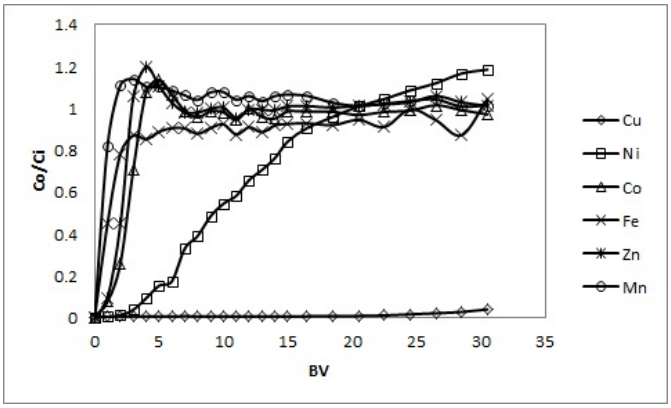

Figure 27: Metal breakthrough profiles for Dow XUS43605: Experiment 6

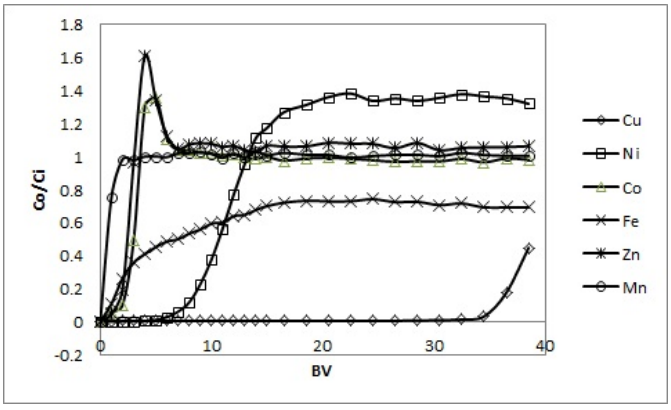

Figure 28: Metal breakthrough profiles for Dow XUS43605: Experiment 7

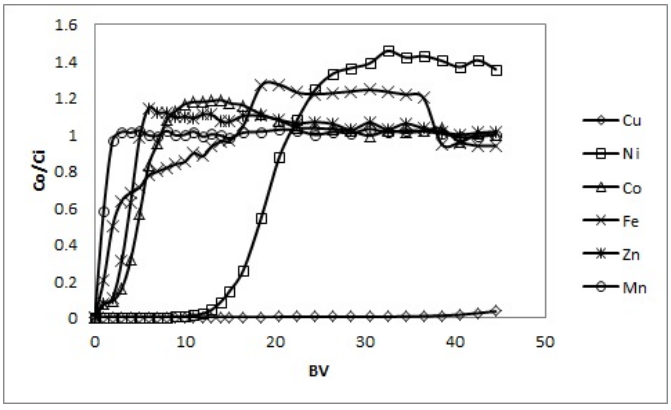

Figure 29: Metal breakthrough profiles for Dow XUS43605: Experiment 8

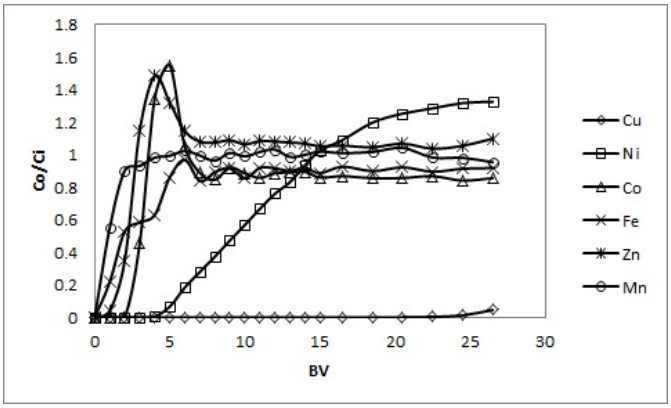

Figure 30: Metal breakthrough profiles for Dow XUS43605: Experiment 9

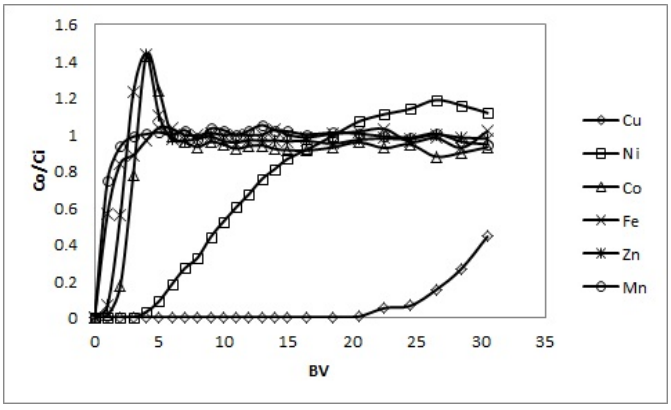

Figure 31: Metal breakthrough profiles for Dow XUS43605: Experiment 10

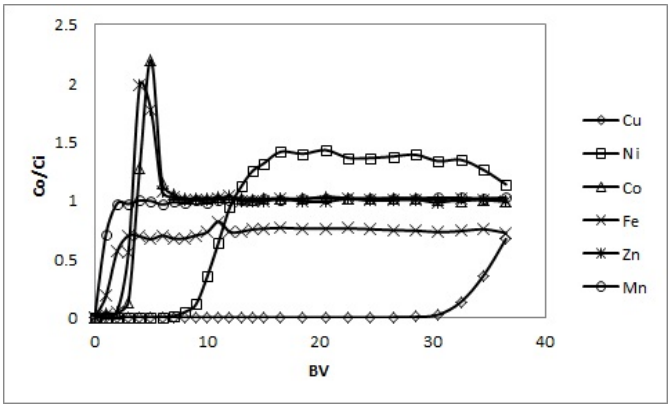

Figure 32: Metal breakthrough profiles for Dow XUS43605: Experiment 11

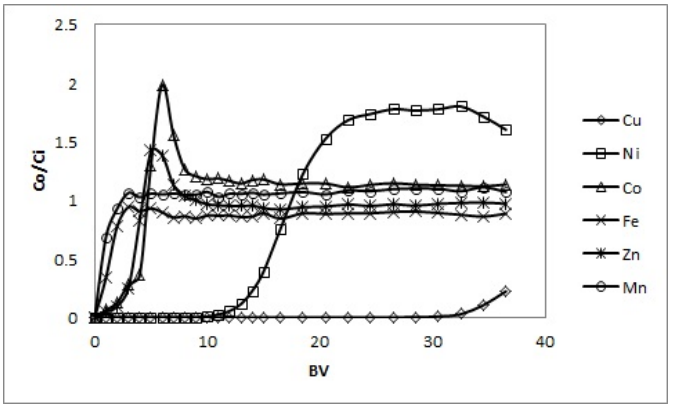

Figure 33: Metal breakthrough profiles for Dow XUS43605: Experiment 12

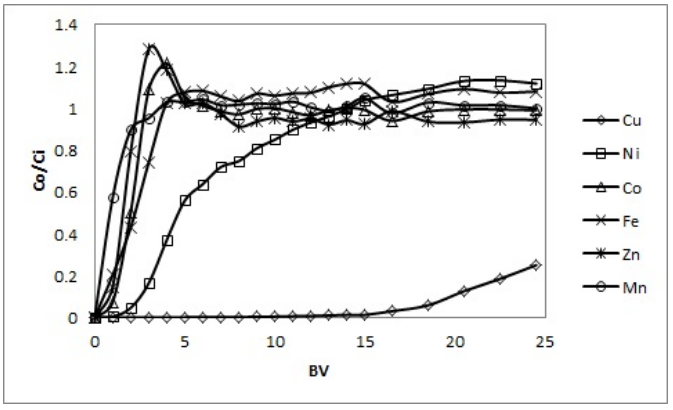

Figure 34: Metal breakthrough profiles for Dow XUS43605: Experiment 13

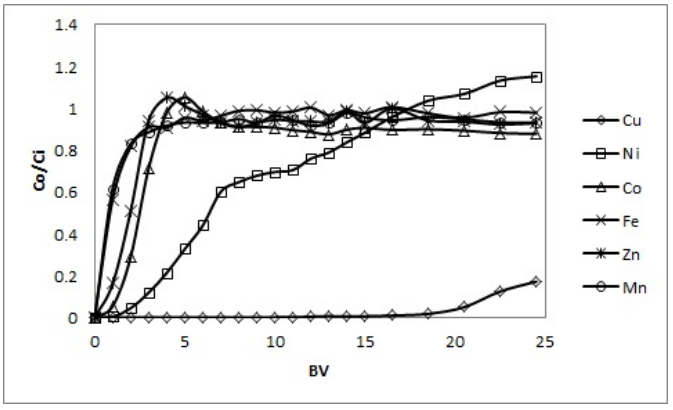

Figure 35: Metal breakthrough profiles for Dow XUS43605: Experiment 14

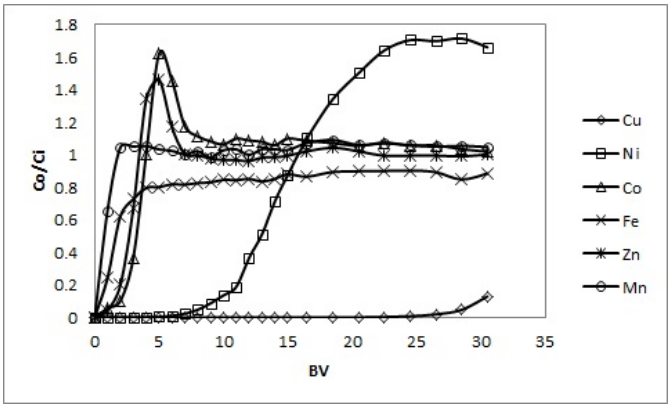

Figure 36: Metal breakthrough profiles for Dow XUS43605: Experiment 15

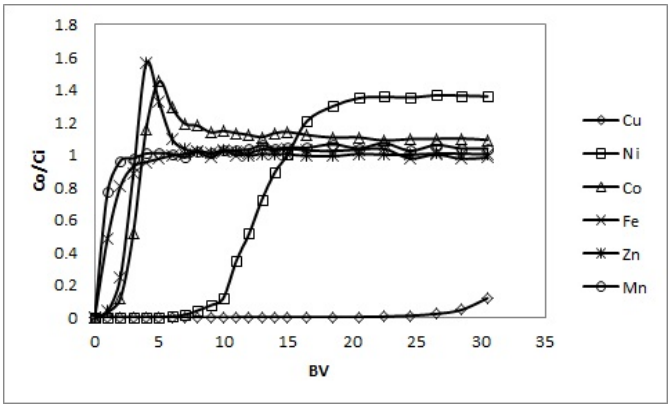

Figure 37: Metal breakthrough profiles for Dow XUS43605: Experiment 16

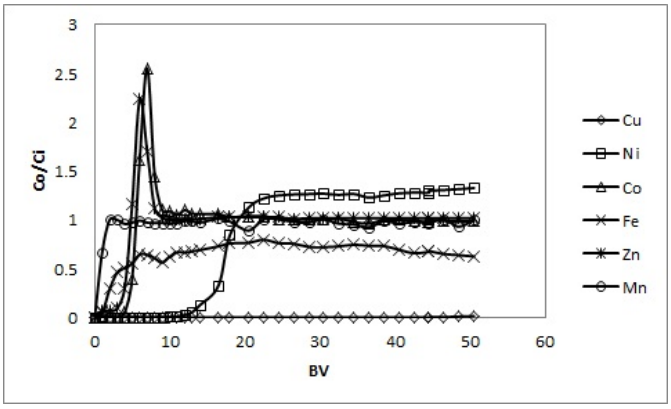

Figure 38: Metal breakthrough profiles for Dow XUS43605: Experiment 3 (repeat)

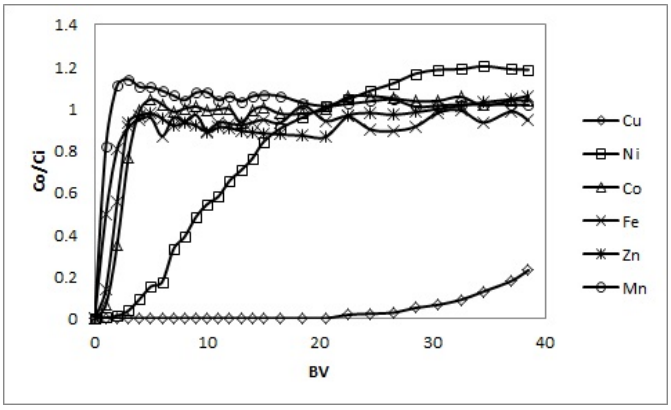

Figure 39: Metal breakthrough profiles for Dow XUS43605: Experiment 6 (repeat)

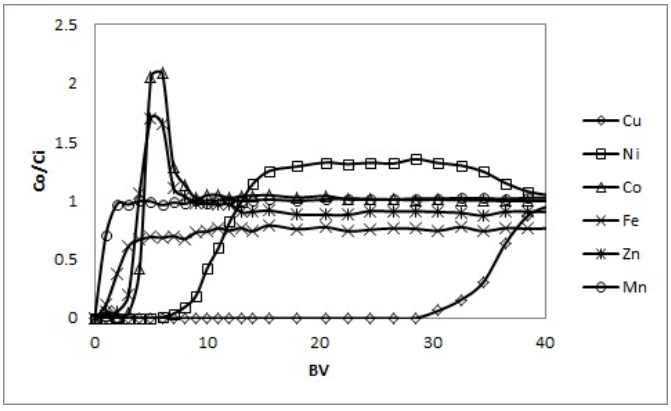

Figure 40: Metal breakthrough profiles for Dow XUS43605: Experiment 11 (repeat)

Solution B breakthrough profiles with Dow M4195

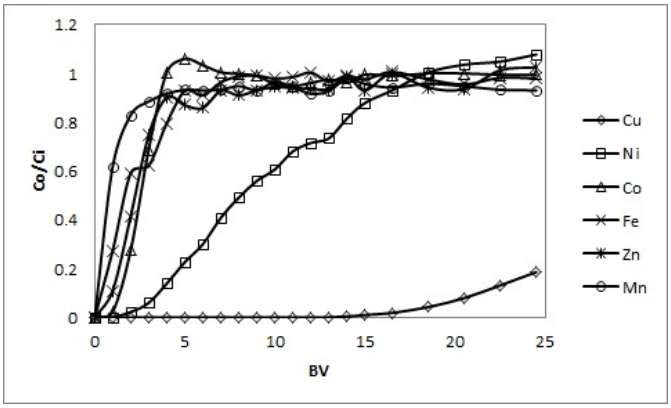

Figure 41: Metal breakthrough profiles for Dow XUS43605: Experiment 14 (repeat)

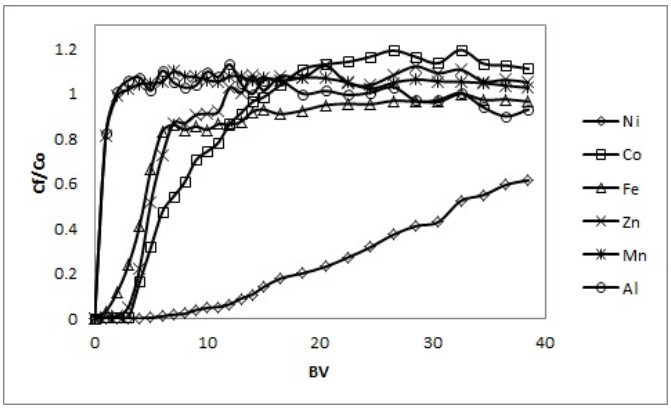

Figure 42: Metal breakthrough profiles for Dow M4195: Experiment 1

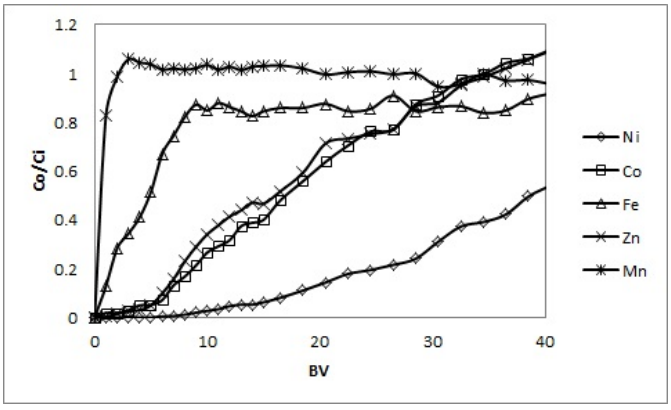

Figure 43: Metal breakthrough profiles for Dow M4195: Experiment 2

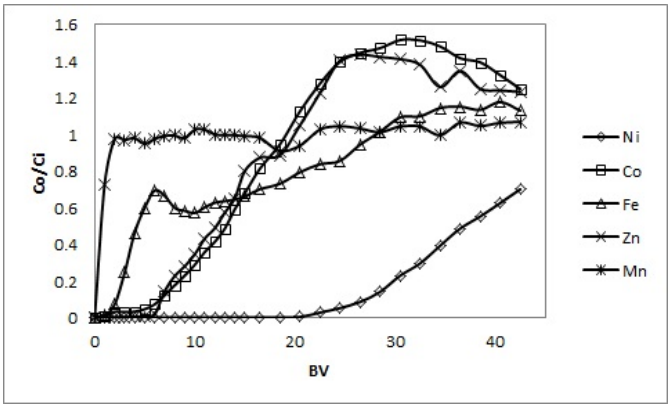

Figure 44: Metal breakthrough profiles for Dow M4195: Experiment 3

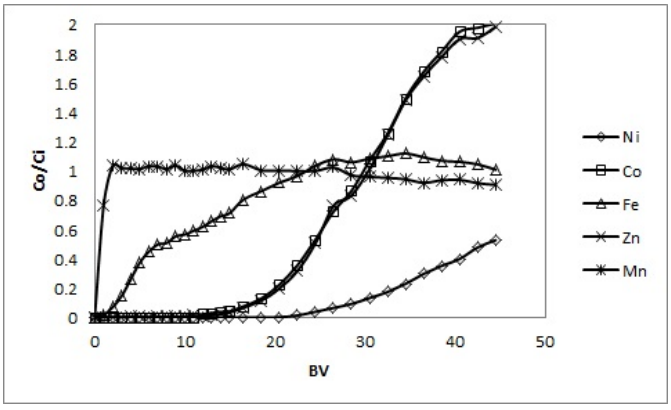

Figure 45: Metal breakthrough profiles for Dow M4195: Experiment 4

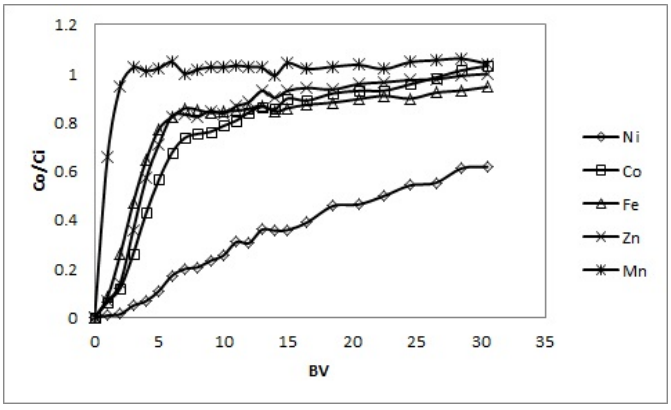

Figure 46: Metal breakthrough profiles for Dow M4195: Experiment 5

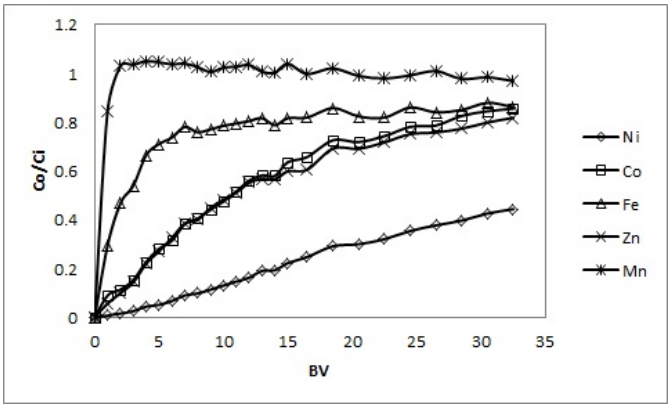

Figure 47: Metal breakthrough profiles for Dow M4195: Experiment 6

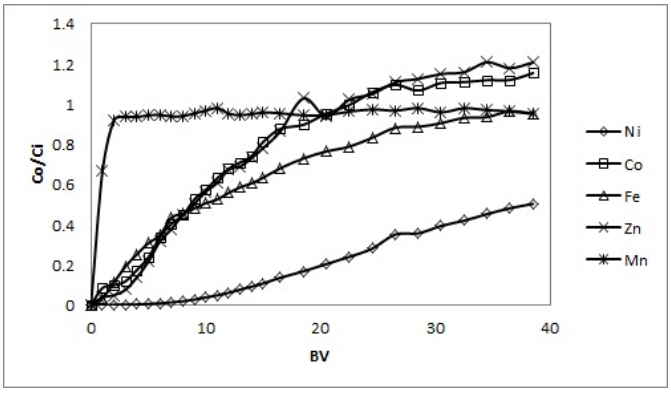

Figure 48: Metal breakthrough profiles for Dow M4195: Experiment 7

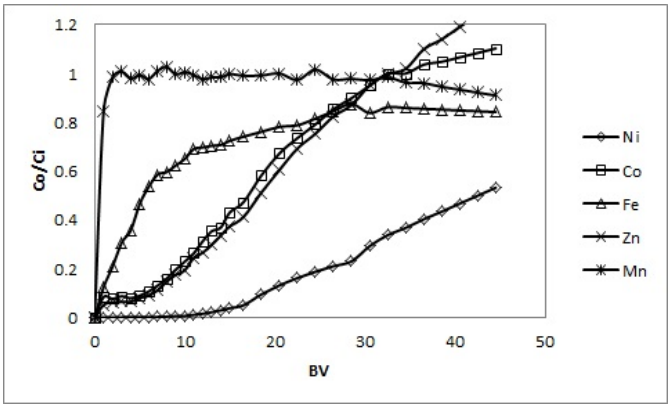

Figure 49: Metal breakthrough profiles for Dow M4195: Experiment 8

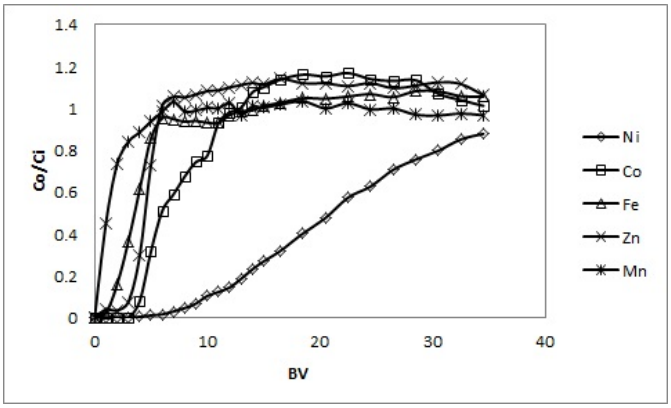

Figure 50: Metal breakthrough profiles for Dow M4195: Experiment 9

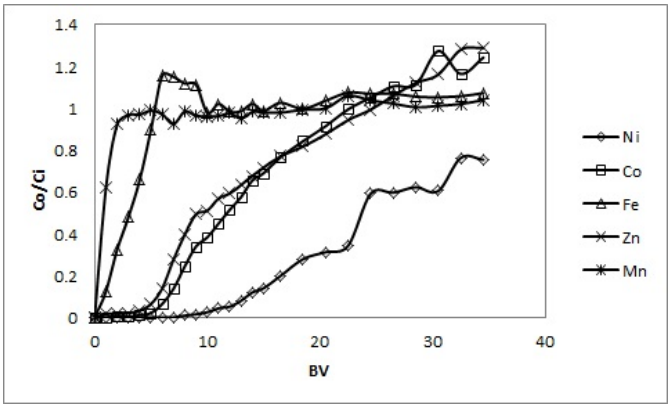

Figure 51: Metal breakthrough profiles for Dow M4195: Experiment 10

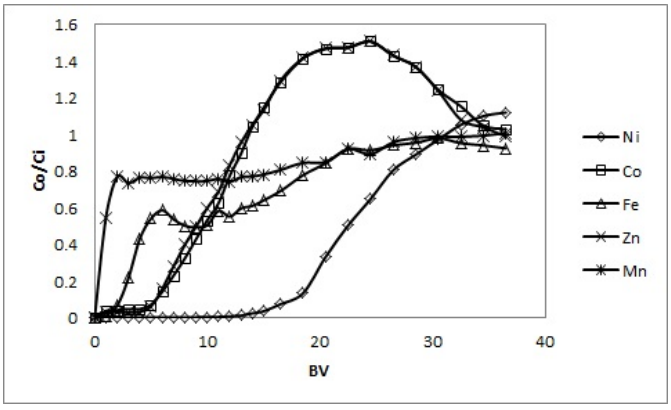

Figure 52: Metal breakthrough profiles for Dow M4195: Experiment 11

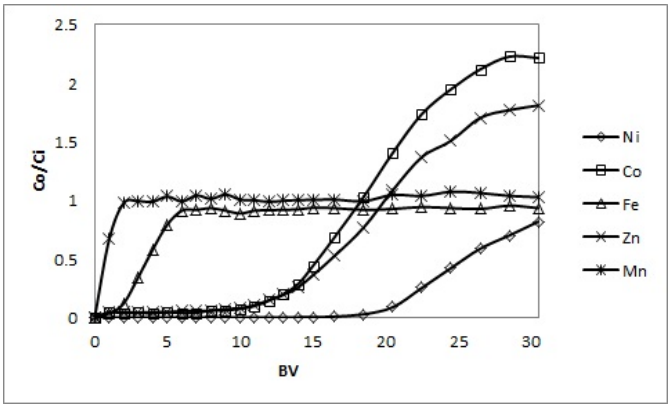

Figure 53: Metal breakthrough profiles for Dow M4195: Experiment 12

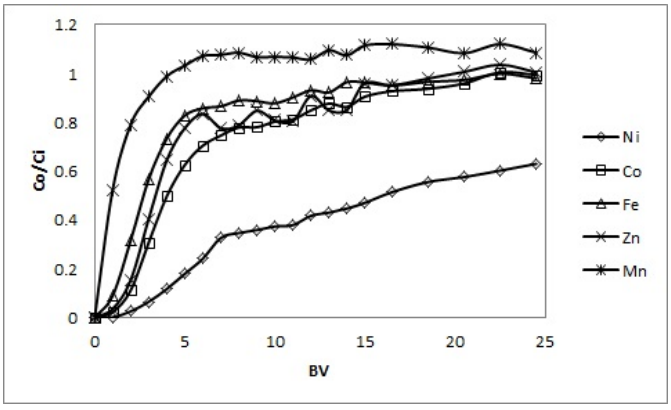

Figure 54: Metal breakthrough profiles for Dow M4195: Experiment 13

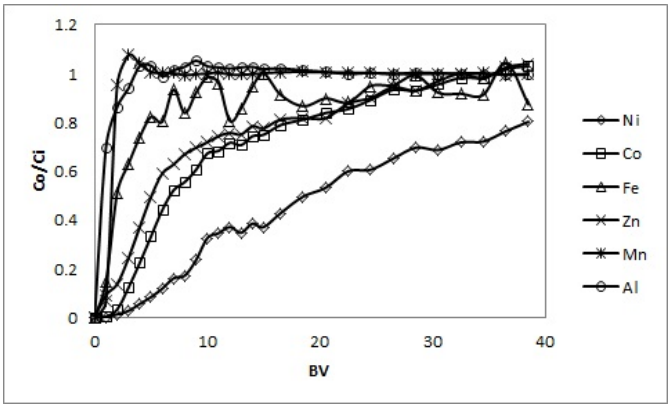

Figure 55: Metal breakthrough profiles for Dow M4195: Experiment 14

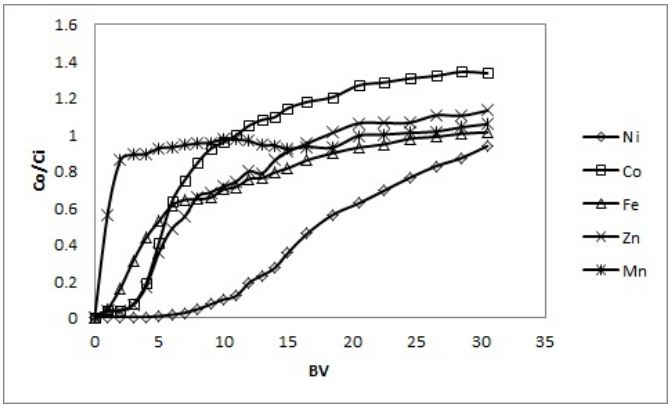

Figure 56: Metal breakthrough profiles for Dow M4195: Experiment 15

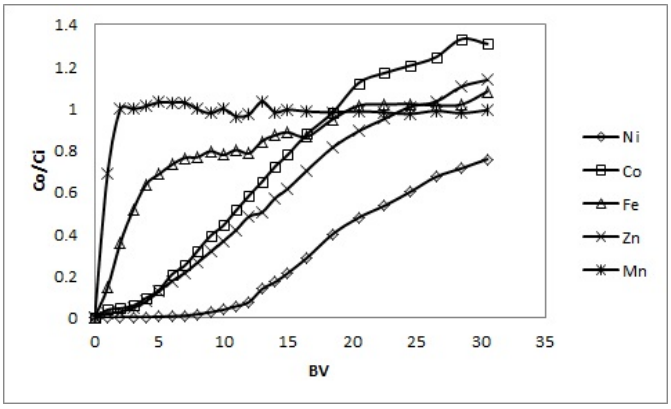

Figure 57: Metal breakthrough profiles for Dow M4195: Experiment 16

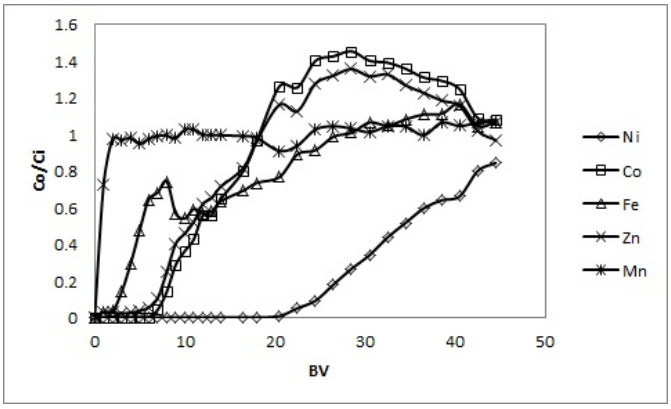

Figure 58: Metal breakthrough profiles for Dow M4195: Experiment 3 (repeat)

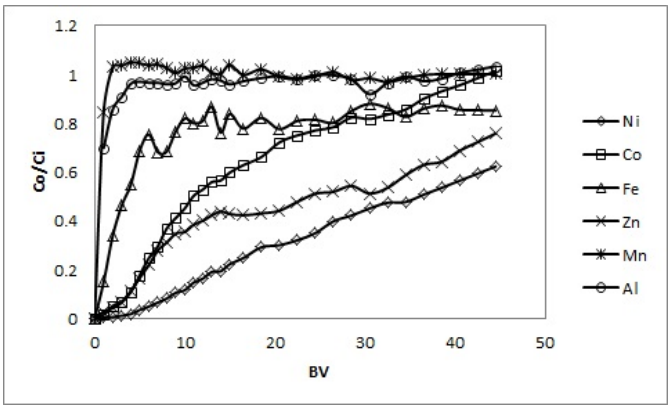

Figure 59: Metal breakthrough profiles for Dow M4195: Experiment 6 (repeat)

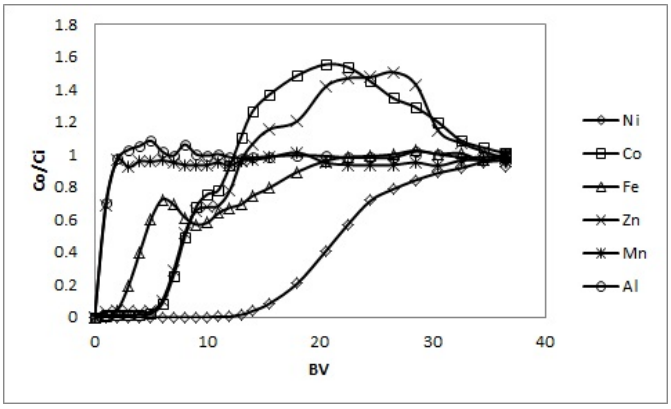

Figure 60: Metal breakthrough profiles for Dow M4195: Experiment 11 (repeat)

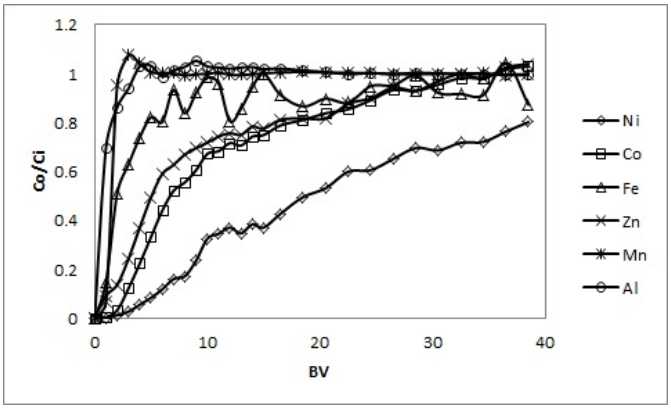

Figure 61: Metal breakthrough profiles for Dow M4195: Experiment 14 (repeat)